Garcia Center for Polymers at Engineered Interfaces

AT STONY BROOK UNIVERSITY

Summer 2018

"The program has no set time limits. Research is a lifelong experience and we hope to remain a resource to our students long after 'graduation'"

The Garcia Center for Polymers at Engineered Interfaces was founded in 1996 and is named after the late Queens College professor Narciso Garcia, who was a pioneer in the integration of education and research. The Center focuses on the integration of materials research with tissue engineering, biomaterials, drug delivery systems, sustainable energy, nanocomposites, and recently, additive manufacturing. The Center also supports innovation through entrepreneurship and has multiple collaborations with industry and national laboratories, both in the US and abroad. For information on the numerous programs that are available please see our website at: http://polymer.matscieng.stonybrook.edu

The research scholar program offers the opportunity for high school teachers, undergraduate, and high school students to perform research on the forefront of polymer science and technology together with the Garcia faculty and staff. Students work as part of focus research teams and are taught to make original contributions of interest to the greater scientific community. In addition to entering national high school STEM competitions, the students are encouraged to publish in refereed scientific journals, present their results at national and international conferences, and file for disclosures and patents to protect their intellectual property.

Our goal is to convey to the students the excitement we enjoy daily in research and provide for them a supportive network within the scientific community. Research is a lifelong experience and we hope to remain a resource to our students long after "graduation".

Miriam Rafailovich & Jonathan Sokolov August 8, 2018

Credits: Sahith Vadada and Kuan- Che Feng, AFM topographical image of PLA crystalline film spun cast on single crystal silicon.
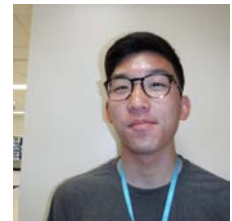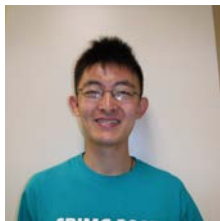
High School Students
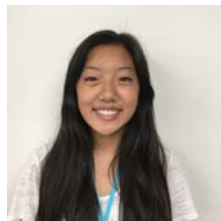
Auerbach, Yehoshua

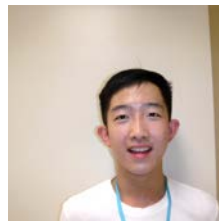**Blatt, Ashley**

Brahmbhatt, Isha
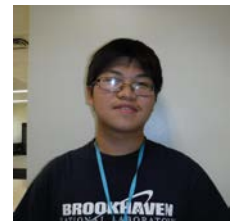
Chang, Benjamin

Chao, Daniel V

Chao, Elaine Y

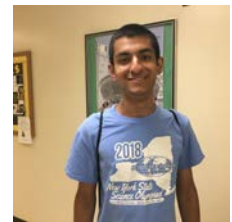**Chen, Guan Hao (Michael)**

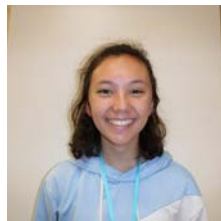**Chen, John**

Chen, Kevin

Chen, Thomas

Choi, Inyoung (Erica)

Chowdhury, Saajid

Deluxe, Antony J

Fontaine, Alice S

Gan, Alan Q

Goldschlag, Jonathan A

Hsu, Allison L

Hulyalkar, Miguel F
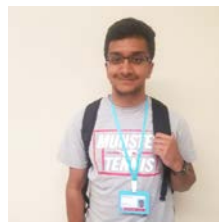
Iyer, Shreyas A

Jacobsen, Nicole B

Lipa, Isaias

High School Students
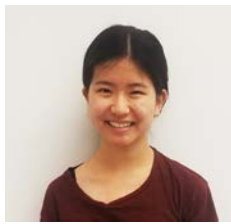
Jiang, Lan

Jindal, Varun

Kelly, Danielle M

Khan, Zaiff

Lam, Pik Hoi

Lee, Joon Young
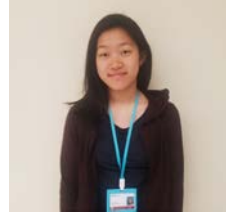
Li, Mindy Z

Limjoco, Ian J

Lin, Lucia
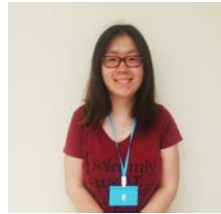
Liu, Grace
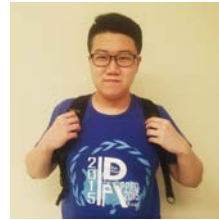
Liu, Zipei
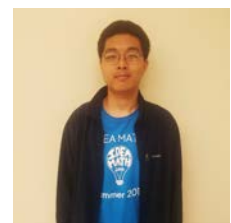
Lu, Evan C

Millstone, Eliana
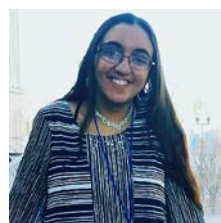
Murthy, Bhuvna R

Nitta, Frederick
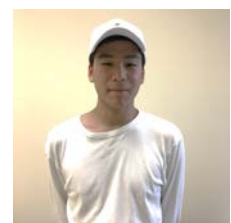
Oh, Brandon
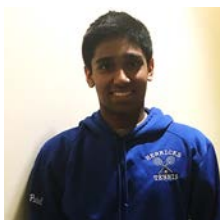
Patel, Rushikesh
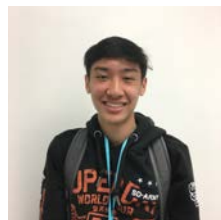
Phan, Byron M
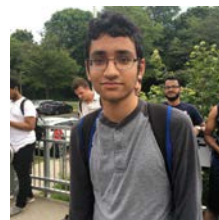
Pisipati, Anish V

Popova, Anastasia N

High School Students

Prasad, Anisa V

Prasad, Sirina V

Puri, Isha
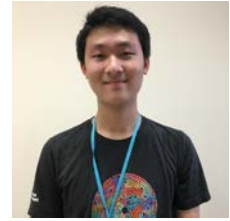
Qu, Matthew T

Radinsky, Avi

Rai-Gersappe, Diya
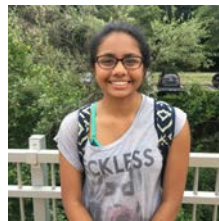
Rao, Kavya G

Sandhu, Bhawan K

Shine, Audrey

Schein, Tzipora C

Schneider, Gemma J

Shi, Zhining (Clara)
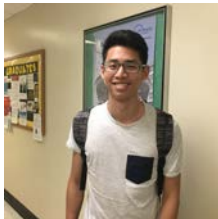
Shin-An, (Ethan) Ho

Singh, Anjali

Singh, Vedant

Sun, Aaron
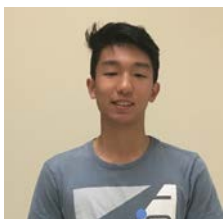
Tian, Albert

Todt, Andrew D

Tong, Christina Y
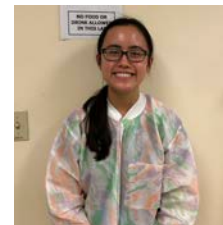
Tran, Kimberley P

High School Students

Upadhyay, Aum D

Urquiola, Elena

Vadada, Sahith

Vilkas, Joshua S

Wang Xiaoxin

Winkler, Ethan S
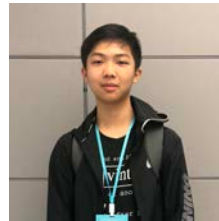
Wu, Kenton

Wu, Steven

Xu, Kevin J

Xu, Vicki

Yin, Ruilin
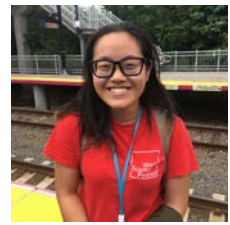
Ying, Samantha

Zeng , Caroline

Zhang, Michael S
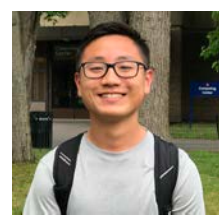
Zhang, Vincent

Zhao, Wenqi (Jennifer)
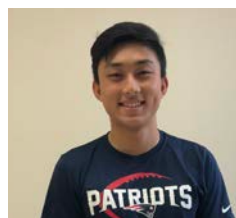
Zheng, Derek, N
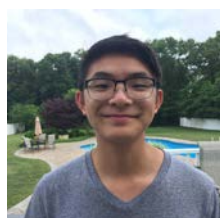
Zhou, Anson Y
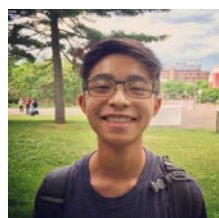
Zhou, Justin
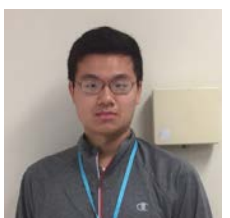
Zhu, Albert Y

Research Experience for Undergraduates

Albert, Deena B

Chan, Kenneth K
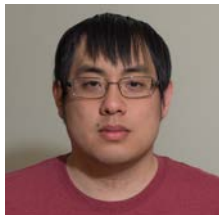
Gao, Ryan

Hofflich, Jessica
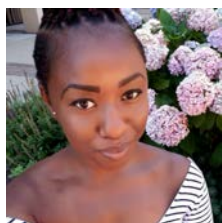
Jenkins, Delivrance

Labiak, Kaitlin C

Lo, Liana
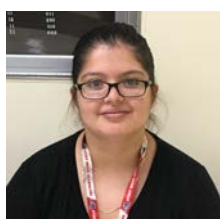
Mora, Anyerlin M

Moulton, Matthew

Orduna, Cecilia

Passariello, Diana

Shata, Ahmed

Sutaria, Jainil

Waqar, Kasim M
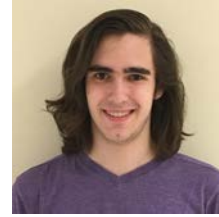
York, Matthew J

Zaidi, Mustafa

Zumba, Nicholas
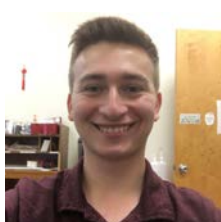
Ossip, Jonathan

Graduate Students

Budassi, Julia

Chuang, Ya-chen
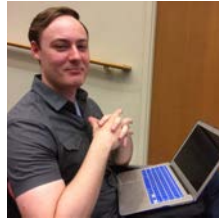
Clayton, Nicholas

Feng, Kuan-che
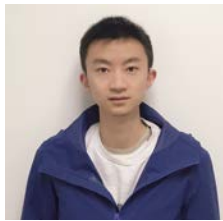
Li, Juyi

Li, Kao
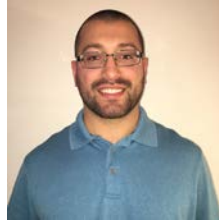
Ricotta, Vincent
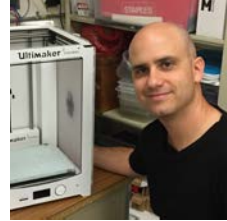
Shmueli, Yuval

Wang, Likun

Xue, Yuan
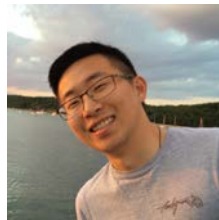
Yang, Fan

Yin, Yifan

Zhang, Linxi

Zhou, Yuchen
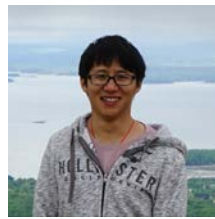
Zuo, Xianghao

Faculty Mentors

Davis, Raphael

Fiore, Susan

Galanakis, Dennis

Gersappe, Dilip

Jerome, John Luckner

Tuminello, Donna

Pinkas-Sarafova, Adriana

Phillips, Reed

Simon, Marcia

Walker, Stephen

Bliznakov, Stoyan

Tae Jin Kim

Research Experience for Teachers

Cuiffo, Mike
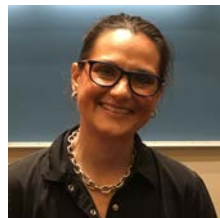
Grella, Rebecca

Isseroff, Rebecca
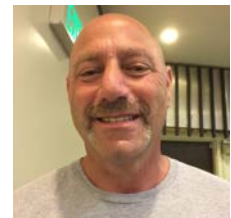
Weiss, Herb

It's Lit

On the Road…
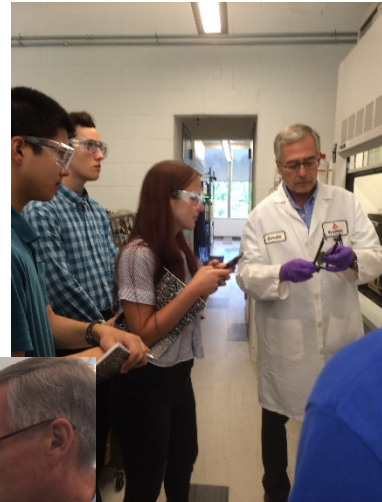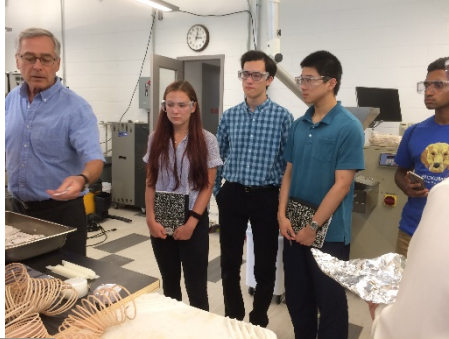
Lectures and Presentations

In the Lab!

Garcia Moments

GO anode is on the left. Transparent solution!

Came out well Really Impressive!
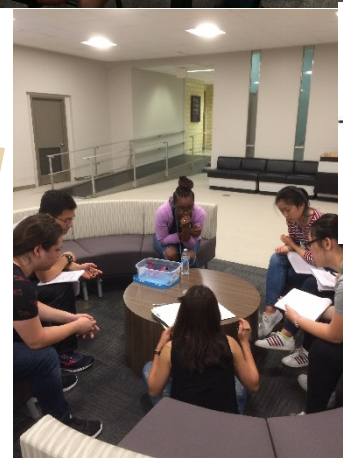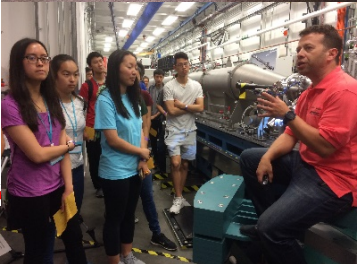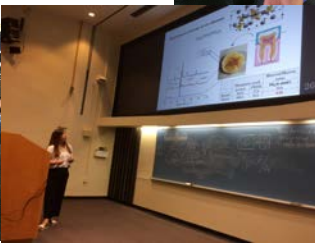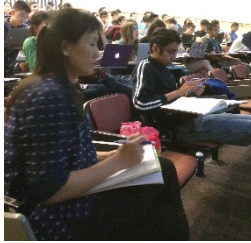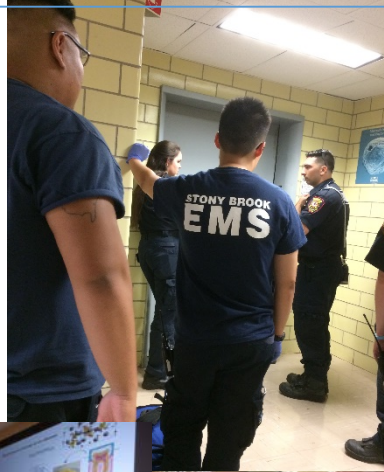
144p

720p

Bae: Come over
Me: I can't, Garcia is over
Bae: I'm determining the molecular weight of polystyrene through spin casting
Me:

Garcia: Polymers at Engineered Interfaces-2018
Summer Scholar Program Schedule of Activities

EVERY DAY STARTS WITH A GROUP MEETING

CHECK SCHEDULE DAILY!

	MONDAY	TUESDAY	WEDNESDAY	THURSDAY	FRIDAY
Week of 6/25	*6/25* **10:00am -10:15** **Judith Berhannan** Dean of Admissions **Welcome to Stony Brook** **10:15-10:50** Intro to Garcia - Miriam Rafailovich Grad and REU introduction **11:00am-1:30pm** ID cards at SAC and lunch at East Side Dining **1:30pm-2:15pm** **Madeline Augustine**, BOEING **2:15pm-4:00pm** **University Tour** 2 groups - bus tour to Dental school, Marine science bldg, and Energy center	*6/26* **10:00am** **General meeting** **10:15 am-11:00 am Michael Hadjiargyrou -** NYIT **11:00 – 11:30 pm** **Robert Harrison** **Theoretical Modelling** **11:30- 12:00 Vincent Ricotta, PhD** **Engineering Biosensors** **12:15pm-1:15pm** **Lunch** **1:15pm-4:00pm** **Facilities Tour:** **AFM** - Ya-Cen Chung **FTIR** - Harry He **LB trough** - Yuchen Zhou **3D printer** -Yuval Shmueli **Cell Lab** - Kuan-Che Feng **Rheology** –Jui Li **Electrospinning** - Kao LI, **Fuel cells** - Likun Wang **Hands on safety training specific to Garcia labs** - Linxi **Tensile** - Xianghao Zuo **Brands ender** - Yuan Xue **Spinner/ Oven Ellipsometer** - Jonathan Sokolov **Confocal microscope** - Julia **UV vis and DLS** - Fan Yang	*6/27* **10:00am - 10:15** **General meeting** **10:15am- 12:45** **Mandatory Lab Safety Training w/ EH&S** **12:45pm-1:45pm** **Lunch** **1:45 pm-2:30 pm** **Richard Clark** Dermatology, SBU **2:30pm–3:15 pm** **Steffen Mueller, Ph.D.** President & CSO Codagenix Inc. **3:15-4:00 pm** **Sherif Abdelaziz** Civil Engineering, SBU	*6/28* **10:00am** **General meeting** **10:30am-12:30pm** **Library Resources and Intro to Excel Courses** (2 Groups) **(Please have your laptop with you)** **12:30 pm-1:15pm** **Lunch** **1:15 pm-2:00 pm** **Kaustabh Ghosh, Ph.D** **2:00-2:30 pm** **Dr. Linxi Zhang** Engineering scaffolds for mineralization **2:30-2:50 PM** **Dr. Reed Philips** Energy Systems **2:50-4:00pm** **Ms. Rebecca Isseroff,** Lawrence HS Science Research Coordinator (i) Magic of Graphene (ii) Keeping a Laboratory Notebook **(iii)box presentation**	*6/29* **10:00am** **General meeting** **10:05am-11:05 am** Lab Safety and Facilities Quiz **11:05-11:50 am** **Gary Halada** Nanoscale characterization SBU **PIZZA (Hunkis)** **12:00- 12:30** **Herb Weiss** ISEF Ethics regulations **12:30- 1:00 pm** **Jainil Sutaria** Hybrid hydrogels **1:00-2:00** **Jonathan Sokolov** DNA Research at SBU

	7/2	7/3	7/4	7/5	7/6

Week of 7/2
 	
HOMEWORK for 7/2
Prepare ppt for journal club.
a. Choose a research paper of interest to you.
b. Prepare a 5 minute Power Point presentation summarizing the paper.
Slides:
1. your name, school, title of paper, reference
2. Hypothesis
d3.Materials/Methods
4. Results and Discussion
5. Conclusion and tevaluation
	10:00-10:15 am
	General Meeting
	
	10:15 -11:00 am
	Frederick E. Grine
	SBU
	
	11:00-11:45 am
	Dilip Gersappe
	SBU
	Theory and Modeling
	
	11:45 am – 12:00 pm
	Yuval Shmueli: FDM printing
	
	12:00-12:15 **Yuchen Zhou:** Perovskite Solar Cells
	
	12:30-1:15 pm Lunch
	
	1:15 -2:00 pm
	
	Marcia Simon: Biology of cells on surfaces/projects
	
	2:15 – 3:00 pm
	Stan Wong Catalysis and Nanotechnology
	
	3:00-3:50 PM
	Chang- Yong Nam Atomic Layer Deposition
		10:00am
		General Meeting
		
		GROUP PICTURE outside of lecture hall 102 light engineering
		
		10:30 am-1:00 pm
		Divide into groups for Journal Club Student Presentations
		
		1:00-2:00 Lunch
		(Lab safety Quiz make up exam in room 173 Light Engineering)
		
		2:00-2:30:
		
		Sherif Abdelazziz Biodegradable Polymers in civil engineering
		
		2:30 - 3:15 pm
		Dr. Steven Schwarz - Department of Physics, 2 Queens College
		Said
		3:15- 4:00 pm
		
		Dennis Galanakis, MD
		The story of Blood
		Stony Brook University
		
		REMEMBER: appropriate laboratory dress on Thursday.
			Happy 4th of July	**Proper Laboratory Attire**
				10:00am
				General Meeting
				Statistics part I
				Dr. Miriam Rafailovich
				
				Distribution of boxes
				10:30 -4:00
				Group Experiment: Polymer Thin Film Processing:
				     Recycling,
				     Rheology,
				     Determination of Mw
				     Si Single Xtals
				     Lab Data Analysis
				Dr. Jonathan Sokolov
				 The ellipsometer: coherent and incoherent light--a hands on experience
				
				Proper Laboratory Attire
					10:00am
					General Meeting
					Data Analysis and Statistics Part II
					Dr. Miriam Rafailovich
					
					10:30 am-2:00pm
					Group Experiment Cont: Polymer Thin Film Processing:
					     Recycling
					     Rheology
					     Determination of Mw
					     Si Single Xtals
					     Lab Data Analysis
					Dr. Jonathan Sokolov
					 The ellipsometer: coherent and incoherent light--a hands on experience
					3:00pm-4:00pm
					Preparation of group ppt and lab reports.
					General meeting
					
					11:30am
					Pizza Lunch

	7/9	7/10	7/11	7/12	7/13

Week of ` 7/9
 	
Homework
Each student must submit a lab report by
Midnight
on
Monday Morning.
 	
Remember to give proper acknowledgements to your group partners, REUs, Grads.
	10:00am
	General meeting
	
	10:15 am-11:00 am
	Gordon Taylor:
	   RAMAN
	   Spectroscopy
	
	11:00 am-11:45 am
	 Steve Walker:
	Microbiology
	i
	11:45-12:30 pm
	Lunch
	
	12:30-2:00
	Student presentation on Spin Casting Lab
	
	2:15 pm-3:00 pm
	Graduate student
	   presentations--
	Yuan Xu/ Xianghao composites
	Juyi--hydrogels
	Ya-Chen--DPSC
	   Andrew
	   nanoparticles
	
	Selection of Projects I
		10:00am
		General meeting
		
		10:15-11:00 am
		SOP Writing
		Ying Liu(EHS)
		
		11:00- 11:15 pm
		Harry Shan He--electrospun fibers for trapping chemical free trapping of insects
		
		11:15-11:30 Lev Neymotin Laser Lithography
		
		11:30-12:30 Selection of projects II
		
		12:30pm-1:30 pm Lunch
		
		1:30- 2:30 pm
		Selection of projects III
		
		2:30-4:00pm
		Writing and submission of SOPs with student signatures
		Official date for ISEF/Regeneron project
		paper work
			10:00am
			General meeting
			
			10:15 am
			WORK!
			12:30pm: Lunch
			1:30pm
			WORK!
			
			Proper Laboratory Attire
				10:00am
				General meeting
				10:30am
				WORK!
				12:30pm: Lunch
				1:30pm
				WORK!
					10:00-10:10 am:
					General meeting
					
					10:10-11:00
					
					 Student talk 1: Cellulose hydrogen fuel cell group
					
					 Student talk II: 3-D printing /ALD/DPSC scaffolds
					
					11:00 Hunki Pizza
					
					Lab work
					
					 2:00pm
					End of Day

Week of	**7/16** **10:00am**	**7/17** **10:00am**	**7/18** **10:00am**	**7/19** **10:00am**	**7/20** **10:00am**

7/16	General meeting: Science moment: 10:30am WORK! 12:30pm: Lunch 1:30pm WORK! **Proper Laboratory Attire**	General meeting **Science moment: Dr. Ping Liu DFT Calculations** 10:30am WORK! 12:30pm: Lunch 1:30pm WORK! **Proper Laboratory Attire**	General meeting 10:30am WORK! 12:30pm: Lunch 1:30pm WORK! **Proper Laboratory Attire**	General meeting 10:30am WORK! 12:30pm: Lunch 1:30pm WORK! **FUEL CELLS vs Everyone else** **Proper Laboratory Attire**	General meeting **Science moment: Dr. Karen-Chen Wiegart--** Visiting the BNL National Synchrotron Light Source Student presentations: III Nanocomposites group Student presentations IV: TBD 11:00 PIzza Laboratory work **Proper Laboratory Attire at all times** 2:00 Have a good weekend **REMINDER: (a)Bring instruments for music practice with Dr. John Jerome** **(b) Have you submitted your slip for the canoe trip?**
Week of 7/23	7/23 10:00am **Science moment:** **Dr. Rebecca Grella --** **Plastics and the environment** **General meeting** **WORK!** **12:30pm: Lunch** **Proper Laboratory Attire**	7/24 10:00am **General meeting** **Trip to VJ Technology for 3-D PLA printing group** **WORK!** **12:30pm: Lunch** **Proper Laboratory Attire**	7/25 10:00am **General Meeting** **WORK!** **12:30pm: Lunch** **Proper Laboratory Attire**	7/26 10:00am **General Meeting** **12:30 pm Lunch** **Proper Laboratory Attire**	7/27 10:00am **General meeting** **Student talks** **Fibrinogen** **Nanocomposites (2 groups)** **Stem Cell Education Nanoparticles and stem cell differentiation** **Pizza Lunch** **2:00pm** **End of Day** **Proper Laboratory Attire**

	7/30	7/31	8/1	8/2	8/3
July 29th BNL trip: Summer Sundays Buses leave dorm at 9:00 AM Sharp Special Tour by Dr. Wiegart **July 29** **Brilliant Light, Dazzling Discoveries** Visit the National Synchrotron Light Source II. Week of 7/30	**10:00am** **Rescheduled Canoe trip** **Board buses for canoe trip at 10:00 am sharp. Tide at 11:00** **NISSEQUOGUE River Canoe & Kayak Rentals Inc.** 631 979-8244 **Water, Pizza, Lunch at dock** **Never Happened!!!!** **3:30 BASEBALL GAME!!** **Labs closed till 3:30 PM**	**10:00am** **General meeting** **10:30am WORK!** **12:30pm: Lunch** **1:30pm WORK!** **3:30pm Student presentations/ice cream** **Proper Laboratory Attire** **4:00 Student presentations Hydrogen fuel cell groups**	**10:00am** **General meeting** Do you want to be a dentist/ Applying to dental schools. **Dr. Debbie Cinotti, DDS** Chair of General Dentistry **10:30am WORK!** **12:30pm: Lunch** **1:30pm WORK!** **3:30pm Student presentations/ice cream:** **The 3 Theory Projects** **Proper Laboratory Attire**	**10:00am** **General meeting** **10:30am WORK!** **12:30pm: Lunch** **4:30pm student presentations/ice cream** **Juyi's** Hydrogel Groups and Bioprinting **Proper Laboratory Attire** **Evening Dinner/Fishing Trip with the Osprey on the Long Island Sound (Port Jefferson Harbor) 6:30-8:30 PM**	**10:00am** **General meeting** **Student presentations** **BBQ: bring your fish!** **Musical Rehearsal** **2:00 End of Day** **Proper Laboratory Attire**
Abstracts 1. **One page**, (one inch margins, min. 11 pt font.) 2. One or more Figures with fig. captions 3. Two or more references from peer reviewed sources. Due Sunday at **8:30 PM**	8/6 **10:00am** **General meeting** **student talks** Biosensor group Graphene Oxide/Isseroff group 3D printing/Yuval group I **Trip to ICL Chemical Ardsley, NY for groups using RDP** **12:30pm Lunch** **1:30pm WORK!** **Proper Laboratory Attire**	8/7 **10:00am** **General meeting** Farzahd group Yuval 3D printing group II **12:30pm Lunch** **Prepare viewgraph for final presentation with your grad supervisors** **REUs: Prepare ppt presentation for symposium** **4:30 Fan Yang's group Adriana 3D printing** **Proper Laboratory Attire**	8/8 **Garcia MRSEC** Polymers at Engineered Interfaces **SYMPOSIUM** **Garcia Program Symposium by Students** Guest Lecturer: Prof. Peter Brink *Swimming with the Sharks Aggressive New Therapies for Cancer* Musical Program arranged by Prof. John Luckner Jerome **SAC Ballroom A Stony Brook** **10:00 am - 2:00 pm**	Note to students: **Research continues...** If you can continue coming back to the lab please leave your boxes in their proper shelves. Leave chemicals and solutions in the boxes. **If you are not coming back**-- take your lab notebook, goggles, box/art work etc. They are yours!! Return all chemicals and solutions to your graduate student supervisors. (Or leave in box with your name)	**Symposium:** Please come at 9:30 for coffee and great music. Program starts promptly at 10:00 Business formal attire please. **Garcia Center for Polymers at Engineered Interfaces** AT STONY BROOK UNIVERSITY 2018

Garcia Center for Polymers at Engineered Interfaces

AT STONY BROOK UNIVERSITY
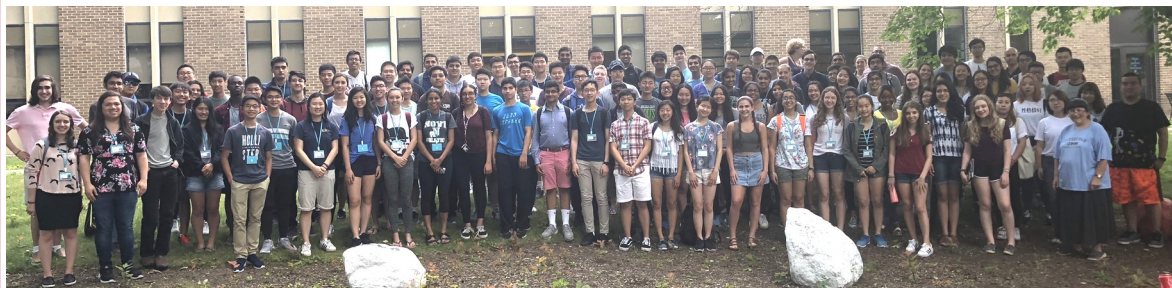
Annual Summer Scholar
Research Symposium & Musicale
August 8th, 2018
10:00am — 2:00pm
Student Activity Center
Ballroom A
Buffet Luncheon: Wing Wan of West Hempstead
Opening Speaker
Prof. Peter Brink

SWIMMING WITH SHARKS AND LEARNING ABOUT CANCER

RSVP ADRIANA.PINKAS-SARAFOVA@STONYBROOKMEDICINE.EDU
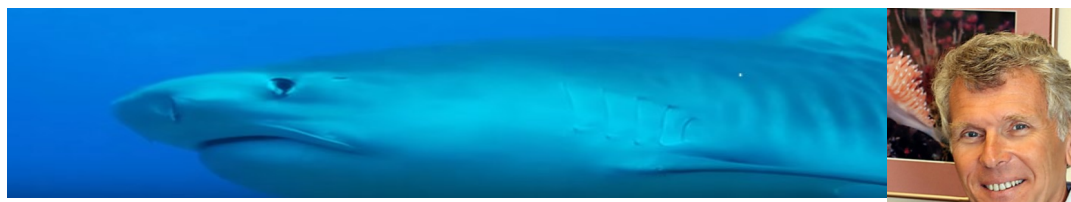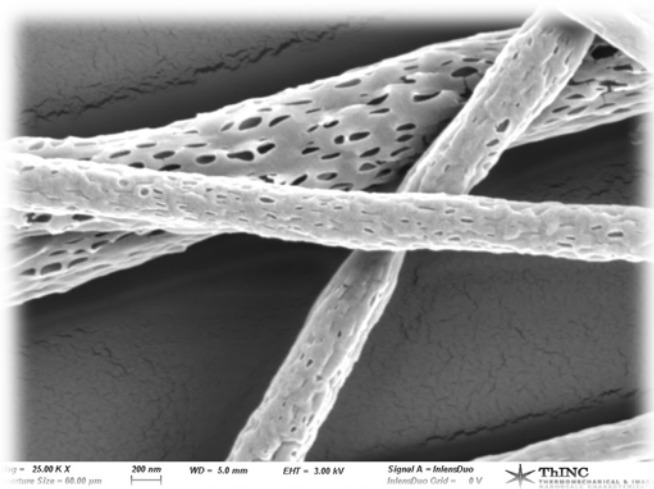
Garcia Summer 2018 Symposium

Credits: Linxi Zhang—SEM of PLA electrospun fiber.

SAC Ballroom A

9:30 AM – 10:00 AM	Breakfast Musical Presentation Arranged by Professor John Luckner Jerome and Garcia Students
10:00 AM	Professor Peter Brink – *Swimming with Sharks and Learning About Cancer*
10:10 AM – 10:20 AM	**Biosensors** Chairs: Deena Albert, Queens College of the City University of New York Kaitlin Labiak, University of Michigan
	Microfluidic Delivery of Enzymes for Ordered DNA Fragmentation Alan Gan, East Brunswick High School, East Brunswick, NJ
	Developing Potentiometric Biosensors Based on Surface Molecular Imprinting Utilizing Surface Roughness for The Detection of Bio-Macromolecules Yehoshua Auerbach, Lawrence High School, Cedarhurst, NY Miguel Hulyalkar, Southside High School, Rockville Center, NY Andrew Todt, Lake Oswego High School, Lake Oswego, OR
	A Pilot Study of the Analysis of Facial Motion using Digital Image Spectroscopy Following Acoustic Neuroma Surgery Ian Limjoco, Sachem East High School, Farmingville NY

	Diya Rai-Gersappe, Huntington High School, Huntington, NY Avi Radinsky, Davis Renov Stahler Yeshiva High School For Boys, Woodmere, NY
10:20 AM – 10:35 AM	**Hydrogels** Chair: Jainil Sutaria, Stanford University, Stanford, CA
	Optimizing Gelatin-Based Hydrogels for Use in 3D Bioprinting of Human Dermal Fibroblasts Elaine Chao, Northwood High School, Irvine, CA Eliana Millstone, Stella K Abraham High School for Girls, Hewlett, NY Kenton Wu, The Wheatlew School, Old Westbury, NY
	Synthesizing and Characterizing Novel Gelatin and Poloxamer PF127, PF108, PF98 Hybrid Hydrogels Erica Choi, St. Paul's School, Concord, NH Christina Tong, Fairview High School, Boulder, CO
	Analyzing the In Vitro *Viability of Novel Gelatin-Pluronic ® F127 Hybrid Hydrogels as Cell Barrier Membranes* Kevin Chen, Mira Costa High School, Manhattan Beach, CA Joon Young Lee, Seoul International School, Seongnam City, South Korea Aaron Sun, Ed W Clark High School, Las Vegas, NV
	Modeling the Diffusion of Drugs Through Hydrogels For Applications in Drug Delivery Isha Puri, Horace Greeley High School, Chappaqua, NY Zhining Shi, The Hockaday School, Dallas, TX
	Lattice Boltzmann Modeling of Fluid Flow Dynamics in Metal-Organic Frameworks Shreyas Iyer, Munster High School, Munster, IN
10:35 AM – 10:50 AM	**Cellular/Bacterial Interactions** Chair: Anyerlin Mora
	Characterization of Antibiofilm Activity of Silver Nanoparticles Deposited in Situ on 3D Printed Polylactic Acid Implant Models Anastasia Popova, Hackley School, Tarrytown, NY Isha Brahmbhatt, Ardsley High School, Ardsley, NY
	Bactericidal Efficacy and Cytotoxic Effects of Newly Developed Calcium Hydroxide Antibacterial Compound (CASA)

	Anish Pisipati, Half Hollow Hills High School East, Dix Hills, NY Isaias Lipa, Brentwood High School, Brentwood, NY
	Naturally Occuring Fibrinogen Chain Variant γ′ Associated with Decreased Risk for Staphylococcus Aureus *Bacteremia* Anson Zhou, Patchogue-Medford High School, Medford, NY
	Investigating the Nanotoxicity of Titanium Dioxide via Fibroblast Growth and Infection with Staphylococcus Aureus Justin Zhou, Patchogue-Medford High School, Medford, NY Vincent Zhang, Sachem High School East, Farmingville, NY Ethan Winkler, Hebrew Academy of the Five Towns and Rockaway, Cedarhust, NY Jonathan Goldschlag, Hebrew Academy of the Five Towns and Rockaway, Cedarhust, NY
10:50 AM – 11:10 AM	**Fuel Cells** Chairs: Matthew Moulton, Cooper Union, New York, NY Kenneth Chan, Boston University, Boston, MA
	Coating Nafion 117 Membranes with Graphene Oxide using Various Surface Pressures to Increase Performance of Proton Exchange Membrane Fuel Cells Lucia Lin, Townsend Harris High School, Flushing, NY Kimberley Tran, Clayton High School, St. Louis, MO
	Alteration of the Surface Structure of the Nafion Membrane to Increase PEMFC Efficiency Evan Lu, Clear Lake High School, Houston, TX Brandon Oh, Seoul International School, Seoul, South Korea Matthew Qu, Wayzata High School, Plymouth, MN Michael Zhang, Saratoga High School, Saratoga, CA
	Varying Graphene Oxide Deposition Mass in Polymer Electrolyte Membrane Fuel Cells to Optimize Fuel Cell Performance and Durability Saajid Chowdhury, MacArthur High School, Levittown, NY Kevin Xu, Ward Melville High School, East Setauket, NY
	Application of Electrospinning Deposition to Enhance Single and Triple MEA Performance in Polymer Electrolyte Membrane Fuel Cells Zipei Liu, Shenzhen Middle School, Shenzhen, China Guan Hao Chen, St. George's School, Vancouver, Canada Audrey Shine, Plainview Old-Bethpage JFK High School, Plainview, NY Danielle Kelly, Friends Academy, Locust Valley, NY

	Utilizing ALD-Coated Titanium Dioxide as a Gold Nanoparticle Catalyst Support in Electrodes to Increase Efficiency Proton Exchange Membrane Fuel Cells Alice Fontaine, Thomas Jefferson High School for Science and Technology, Alexandria, VA Allison Hsu, Syosset High School, Syosset, NY Anjali Singh, Novi High School, Novi, MI
11:10 AM – 11:30 AM	**Dental Pulp Stem Cells** Chairs: Jessica Hofflich, Stony Brook University, Stony Brook, NY Nicholas Zumba, Columbia University, New York, NY Delivrance Jenkins, Suffolk Community College, Brentwood, NY
	Investigating the Effects of ALD-Coated Titanium Dioxide on Dental Pulp Stem Cell Response to 3D-Printed PLA Scaffolds Benjamin Chang, Woodbridge High School, Irvine, CA Antony Deluxe, Wheatley High School, Old Westbury, NY Ethan Ho, Northfield Mount Hermon School, Gill, MA Bhuvna Murthy, Huron High School, Ann Arbor, MI Rushi Patel, Herricks High School, New Hyde Park, NY Wenqi Zhao, Milton Academy, Milton, MA
	Evaluating the Effects of Graphene-Loaded Polylactic Acid Electrospun Fibers and Spun-cast Thin Films on the Proliferation and Differentiation of Dental Pulp Stem Cells Sahith Vadada, Herricks High School, New Hyde Park, NY Kavya Rao, Half Hollow Hills East, Dix Hills, NY Ashley Blatt, Half Hollow Hills East, Dix Hills, NY
	Investigating the Effects of Substrate Mechanical Patterns on Proliferation and Differentiation of Dental Pulp Stem Cells Albert Zhu, Our Lady of Lourdes High School, Poughkeepsie, NY Grace Liu, Bayview Secondary School, Richmond Hill, Ontario, Canada
	The Effects of TiO$_2$ Nanoparticles on the Proliferation and Differentiation of Dental Pulp Stem Cells Mindy Li, Princeton High School, Princeton, NJ Samantha Ying, South Side High School, Rockville Centre, NY
	Utilization of P4VP, Graphene, and Polyornithine to Potentially Differentiate Dental Pulp Stem Cells into Functional Neurons

	John Chen, Lawrence High School, Cedarhurst, NY Zaiff Khan, Lawrence High School, Cedarhurst, NY
	The Effect of the Surface Characteristics of 316L Stainless Steel on Cell-Substrate Interaction and its Implications for Biomedical Applications Gemma Schneider, Roslyn High School, Roslyn, NY
11:30 AM – 11:40 AM	**Environmental Protection** Chair: Ryan Gao, Stony Brook University, Stony Brook, NY
	A Novel Fire Retardant Solution to Mitigate the Onset of Wildfires Pik Hoi Lam, Wilson Area High School, Easton, PA Nicole Jacobsen, Plainedge High School, Massapequa, NY Joshua Vilkas, Hebrew Academy of Nassau County High School, Uniondale, NY
	The Effect of Graphene Oxide on Pheromone Evaporation in Cimex Lectularius *Traps* Bhawan Sandhu, Lawrence High School, Cedarhurst, NY Tzipora Schein, Hebrew Academy of the Five Towns and Rockaway, Cedarhurst, NY
11:40 AM - 11:50AM	**Nanocomposites** Chairs: Mustafa Zaidi, Stony Brook University, Stony Brook, NY Kasim Waqar, Columbia University, New York, NY
	Enhancing Mechanical Properties of Biodegradable PLA Using Ternary Polymer Blends Ruilin Yin, St. Anthony's High School, South Huntington, NY Elena Urquiola, Hunter College High School, New York City, NY
	Enhancing Thermal Conductivity of Polylactic Acid and Polybutylene Adipate Terephthalate Blends with Boron Nitride and Graphene Frederick Nitta, Henry M. Gunn High School, Palo Alto, CA Vicki Xu, Mission San Jose High School, Fremont, CA
	Creating Flame Retardant and Biodegradable Polymer Blends for Industrial Use Albert Tian, Ward Melville High School, East Setauket, NY Varun Jindal, Ward Melville High School, East Setauket, NY
11:50 AM- 12:00PM	**Perovskite Solar Cells** Chairs: Cecilia Orduña, Columbia University, New York, NY Liana Lo, Cornell University, Ithaca, NY

|	
	Optimization of Organic-Inorganic Halide Perovskite Solar Cells via a Novel Polycaprolactone Additive Pathway Anisa Prasad, Staples High School, Westport, CT Sirina Prasad, Staples High School, Westport, CT
	Improvement of Perovskite Solar Cell Efficiency Through Polylactic Acid Additive Induced Boundary Passivation Thomas Chen, Mission San Jose High School, Fremont, CA Aum Upadhyay, Interlake High School, Bellevue, WA Byron Phan, Hunter College High School, New York, NY
12:00PM-12:10PM	**3-D Printing** Chairs: Matthew York, Case Western University, Cleveland, OH Ahmed Shata, Stony Brook University, Stony Brook, NY
	Characterization of Electrical and Mechanical Properties of Thermoplastic Poly(Lactic Acid) Filaments Infused with Graphene Nanoplatelets through Fused Deposition Modeling Techniques Xiaoxin Wang, Padua Franciscan High School, Parma, OH Steven Wu, Clear Lake High School, Houston, TX Derek Zheng, Monta Vista High School, Cupertino, CA
	Evaluating the Effects of Material Composition on Molded and 3D Printed Samples Vedant Singh, The Wheatley School, Old Westbury, NY Daniel Chao, Hunter College High School, New York, NY
	Optimizing 3D Printing of PLA Filaments Through Lattice-Boltzmann Modeling and Graphene Nanocomposite Integration Lan Jiang, University High School, Irvine, CA Caroline Zeng, Wayzata High School, Plymouth, MN
12:15	*Buffet Luncheon Catered by WingWan of West Hempstead*

Session 1: Biosensors

Chairs:
Fan Yang & Julia Budassi
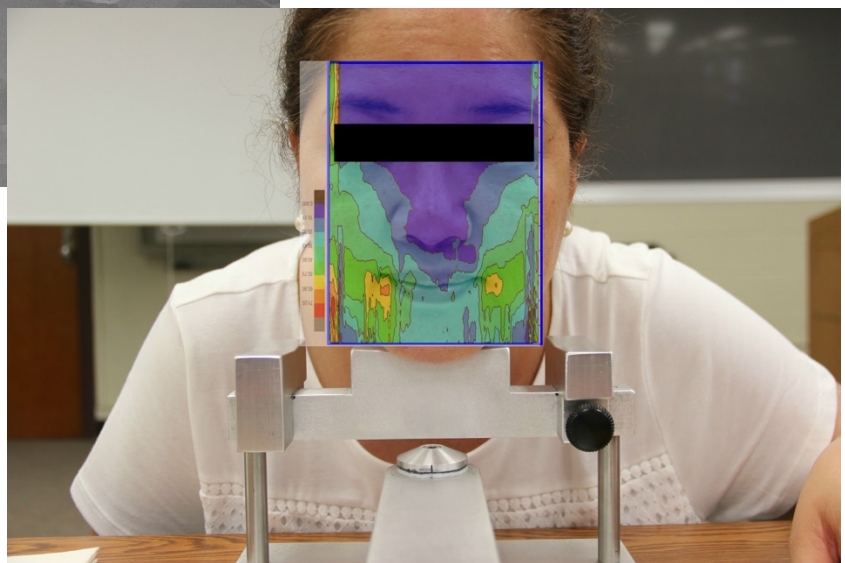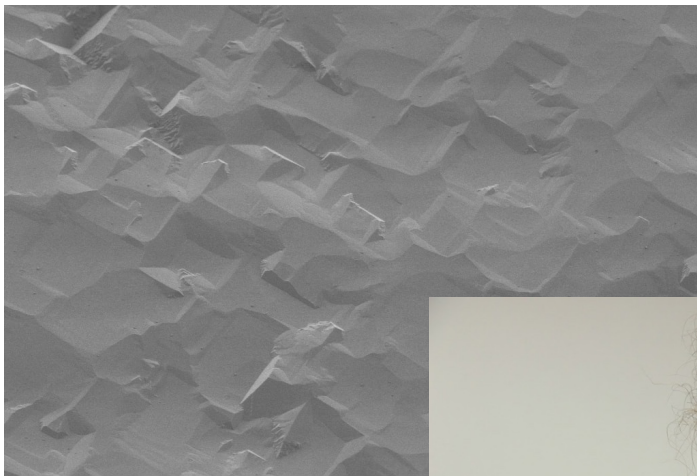
Microfluidic Delivery of Enzymes for Ordered DNA Fragmentation

Alan Gan[1] , Julia Budassi[2], Jonathan Sokolov[2]

[1]East Brunswick High School, East Brunswick, NJ 08816; [2] Department of Materials Science & Engineering, Stony Brook University, Stony Brook, NY 11790

Next generation sequencing, with all its improvements over older and less efficient and cost-effective methods of genome sequencing, remains unoptimized due to the neglect of preserving the order of the fragmented DNA[1] . This greatly complicates the reassembly process. A possible method of preserving order involves the cutting of linearized parallel strands of DNA adhered to and immobilized on a polymethyl methacrylate (PMMA) coated surface. The PMMA coated surface is lowered into a DNA solution and then raised slowly. The DNA is pulled upwards and stretched into a line as the meniscus follows the surface[2] . A polydimethylsiloxane (PDMS) stamp with microfluidic channels running in a perpendicular direction to the strands of DNA is placed on the surface. Flowing a solution of an enzyme that cuts DNA (DNase I) through the channels will cleave the DNA wherever it is exposed to the channels while preserving the sequence order and therefore simplifying the sequencing process.
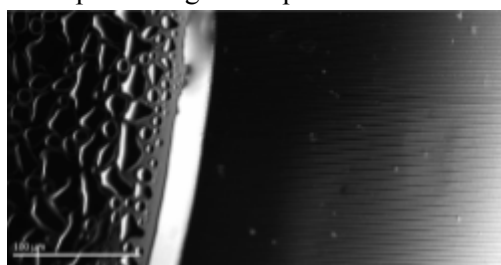
Figure 1: 10X magnified channel edge with fluorescent BSA, reservoir on left
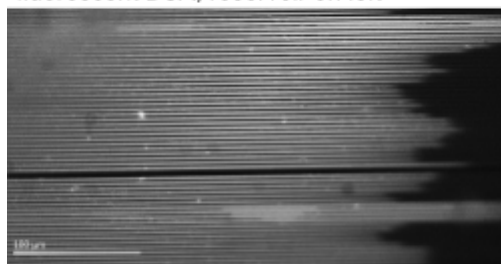
Figure 2: 10X magnified end of filled channels in a stamp

A problem with this method is that the DNase I enzyme is strongly attracted to the PDMS stamp used in the filling process, hindering its ability to travel the full length of the stamp. A coating to which DNase does not absorb must be applied to the inside of the channels first. Bovine serum albumin (BSA) in a solution can be used for this purpose. An experiment was conducted to test how far BSA would travel through the microfluidic channels when allowed to diffuse for variable amounts of time. The stamps that were created were cured from a mixture of PDMS and a curing solution at 60-70 C. They were poured onto a "master" pattern which is a silicon wafer etched with the negative replica of the desired microfluidic channels. After the PDMS is cured, it is cut into a stamp shape and a reservoir which holds the buffer, BSA solution, and DNase I solution is glued on with more liquid PDMS and left to cure. 150 µL of 1X buffer is pipetted into the reservoir and the entire stamp is left inside a lower pressure vacuum of approximately 115 torr for 15 minutes to promote filling of the channels. After returning to atmospheric pressure, the stamps are left on a 40 C hot plate with an additional 7.5 µL of BSA, which is added and mixed with a pipette.

For this experiment, PMMA was coated onto a cleaned #2 glass coverslip (thickness from 0.17 mm to 0.25 mm) so that microscopy could be used to examine the samples without removal of the stamp. A fluorescent BSA was used so that the distance the BSA traveled could be determined under a microscope. The samples were left on the heat for 6, 12, 24, 30, and 60 minutes. Each

Figure 3: Time vs. Travel Distance for tested run times

samples' reservoir is drained of the buffer and BSA, and examined. The distance the BSA traveled was measured by finding the coordinates of the beginning of the channels (Fig. 1) and subtracting it from the coordinates of where most of the channels end (Fig. 2). Additional testing includes adding more data points to increase accuracy as well as varying channel size to determine its effect on the diffusion rate of BSA.

[1]Mardis, E. (2008). Next-Generation DNA Sequencing Methods. Retrieved from http://www.annualreviews.org/doi/10.1146/annurev.genom.9.081307.164359
[2]Michalet, X. (1997). Dynamic Molecular Combing: Stretching the Whole Human Genome for High-Resolution Studies. *Science, 277* (5331), 1518-1523. doi: 10.1126/science.277.5331.1518

Developing Potentiometric Biosensors Based on Surface Molecular Imprinting Utilizing Surface Roughness for The Detection of Bio-macromolecules

Yehoshua Auerbach[1], Nick Clayton[2], Miguel Hulyalkar[3], Dr. Miriam Rafailovich[2],
Dr. Vincent Ricotta[2], Andrew Todt[4]

[1]Lawrence High School, Cedarhurst, NY; [2]Stony Brook University, Stony Brook, NY;
[3]South Side High School, Rockville Center, NY; [4] Lake Oswego High School, Lake Oswego, OR

The development of fast, inexpensive biosensors holds significance in both medical and biochemical fields of study and industry as they are non-invasive and accurate tools to detect bio-macromolecules. While it is possible to detect flaviviruses like Zika or Dengue virus via antibody- or RNA-based methods, biosensors utilize surface molecular imprinting to differentiate bio-macromolecules of similar size and shape with high selectivity and sensitivity. These biosensors are extremely versatile and can be tailored to identify a large range of molecules, which can lend itself for use in analyses of processes including stem cell differentiation.

A scanning electron microscope (SEM) was used to analyze the surface roughness of both polished (smooth) and unpolished (rough) Ti/Au-coated Si chips (**Fig.1**). Biosensor chips were fabricated using both smooth and rough Si wafers coated with 3 nm Ti and 50 nm Au, then diced into 8×20 mm chips. The chips were masked with adhesive PTFE tape hole punched with 6 mm holes and were imprinted in 19/1 (v/v) of known concentrations of analytes in 1X dPBS/100 uM 11-mercapto-1-undecanol in dimethyl sulfoxide. Analytes were imprinting at the following concentrations: EhV-163 with a final imprint concentration of 10^2 P/mL; S17 fibrin-depleted fibrinogen at 3 µg/mL and 30 µg/mL; 50P fibrin-rich fibrinogen at 2.3 µg/mL and 23 µg/mL, then washed with 3M NaCl overnight. Re-adsorption of the target analytes to the washed chips were measured in real-time potentiometrically; after 20 minutes of stabilization in 1X dPBS, serial dilutions of target analyte was added every 5 minutes in 100 µL aliquots, successively increasing in concentration 10-fold. Various tests of EhV-163 were performed, including testing washing methods using ethanol, DI H_2O, and Tween-20. The smooth imprints yielded no voltage response, as expected as its vertical roughness of about 3.5 nm[1], and cavity length in the range of 6 nm[1], is not in the size range of the ~150 nm EhV-163[2]. The rough EhV-163 imprints gave highly erratic responses, leading us to test instead with fibrinogen. Because of the low imprint concentration, these sensors were not very sensitive and only had a notable drop in open circuit potential (OCP) after additions of 230 µg/mL for 50P (**Fig. 2a**) and 300 µg/mL for S17 (**Fig. 2b**). However, the S17 imprints gave a larger average final addition response of -25.7mV, compared to the 50P's -11.8mV average. Attempting to increase the sensitivity of the fibrinogen biosensors, they were imprinted again at 10-fold lower concentration. This did not noticeably affect
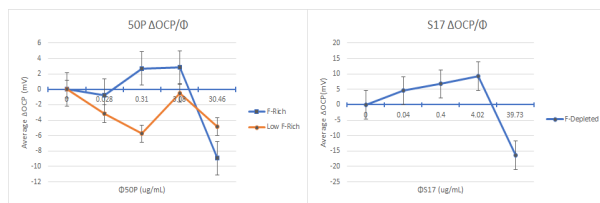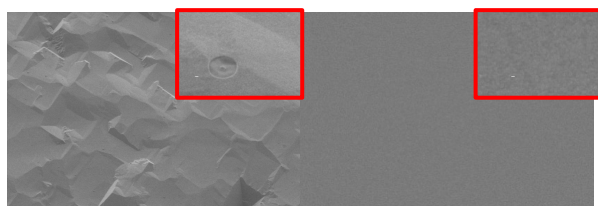
Figure 1: SEM of rough Ti/Au at **a)**5KX and **b)**50KX, and of smooth Ti/Au at **c)**5KX and **d)**50KX
Figure 2: a)50P/50P low-conc. and **b)**S17 average voltage response over concentration.

the sensitivity of the 50P sensors, only yielding an average of -4.1 mV final response (**Fig. 2a**), but we hypothesize that the low-concentration S17 sensors will yield better results, as they lack the disordered clusters of soluble fibrin which are present in 50P solutions. Our future work will focus on using imprinted biosensors to detect stem cell differentiation through detecting the presence of alkaline phosphatase and osteocalcin in growth medium, as well as on completing low-concentration fibrinogen testing.

[1] Analyst, 2016,141, 5607-5617; [2] Nissimov, Jozef I. (2013) Ecological and functional biodiversity in a marine algal-virus system: genotypes, phenotypes and their ecological significance. PhD thesis, University of Nottingham.

A Pilot Study of the Analysis of Facial Motion using Digital Image Spectroscopy following Acoustic Neuroma Surgery

Deena Albert[1] Ian Limjoco[2] Diya Rai-Gersappe[3] Avi Radinsky[4] Fan Yang[5] Miriam Rafailovich[6]

[1] CUNY Queens College Flushing NY, [2] Sachem East High School, Farmingville NY, [3] Huntington High School, Huntington, NY, [4] Davis Renov Stahler Yeshiva High School For Boys, Woodmere, NY, [5] Department of Material Science & Engineering, Stony Brook University, Stony Brook, NY, [6] Department of Materials Science & Engineering, Stony Brook University, Stony Brook, NY

Vestibular schwannoma (VS), also known as acoustic neuroma, is a benign brain tumor that develops along the cranial nerves running from the inner ear to the brain, affecting the facial nerve (cranial nerve VII) and the vestibulocochlear nerve (cranial nerve VIII)[1]. While the most common diagnostic methods of VS include MRI or CT scan, these methods prove to be expensive and time-consuming. The purpose of this study is to determine the extent to which VS influences facial nerve function by using digital photography. Digital Speckle Correlation (DISC) is an imaging technique that calculates facial motion from two pictures taken in rapid succession [2,3]. In contrast to MRI and CT scans that analyze the internal nerve network of the head through electromagnetic frequencies, DISC inspects only the external skin structure, providing insight to the progression of the VS tumor via optical examination of facial morphology. DISC can furthermore be applied to patients that undertook a surgical resection, a gamma knife procedure, or no operation to compare the effects of each treatment method on VS progression and facial nerve functionality. In order to compare the facial structure of the participants, a brief medical history, list of medications currently being taken, and an abbreviated cranial nerve exam were performed and recorded from the patients who had VS (n= 35) and the control group, who had no cranial nerve deficits (n= 36).
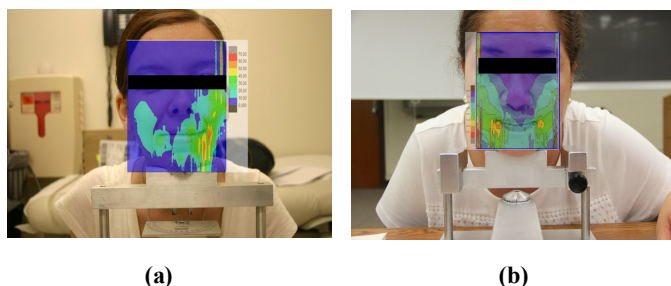
Figure 1. Picture of VS patient (a) and control participant (b) with contour overlay where the level of facial muscle movement from low to high activity is graduated from blue to red,

(a)   (b)
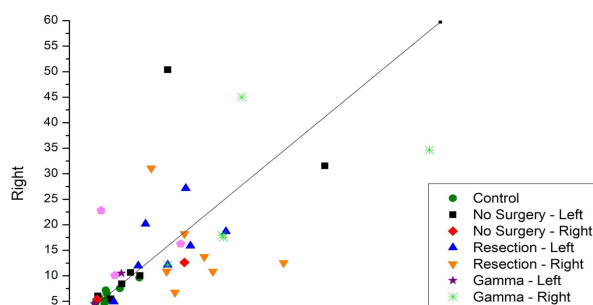
Figure 2. Graph depicting the amount of muscle movement in pixels on the left versus the right sides of the face. The line illustrates perfect symmetry.

For each participant, two pictures were taken: one expressionless and one slightly smiling. When comparing DISC-analyzed photographs of control participants to those of patients with VS, the results indicated that patients with VS had asymmetrical facial musculature, whereas control patients featured more symmetrical facial muscular structures. As seen in Figure 1.a, the patient with VS displays much higher muscle movement on the left side of their face whereas the control subject in Figure 1.b portrays a more equal amount of facial movement on both hemispheres of the face. As shown in Figure 2, we can conclude that DISC can successfully correlate severe VS progression to a detectable level of asymmetry that may not necessarily be observable to the human eye. Future applications of this study may be tested on the recovery speed of brain surgery patients via analysis of facial nerve repair changes and stroke victim aid in damage assessment.

1. Bhatanagar D., Susan F., Miriam R. Raphael D. Journal of Neuroscience and Neuroengineering Volume 3, Number 1(2014). An Analysis of Facial Nerve Function in Patients with Vestibular Schwannomas Using Digital Image Speckle Correlation.
2. Bhatnagar, D., Conkling, N., Rafailovich, M., Phillips, B. T., Bui, D. T., Khan, S. U., & Dagum, A. B. Journal of Skin Research and Technology Volume 19 Pg. 220-229(2013). An in vivo analysis of the effect and duration of treatment with botulinum toxin type A using digital image speckle correlation.
3. Pamudurthy, S., Guan, E., Mueller, K., & Rafailovich, M. Book Series: Lecture Notes in Computer Science Volume 3546 Pg.1010-1018 (2005). Dynamic Approach for Face Recognition Using Digital Image Skin Correlation.

Session 2: Hydrogels

Chairs:
Juyi Li & Hongyu Li
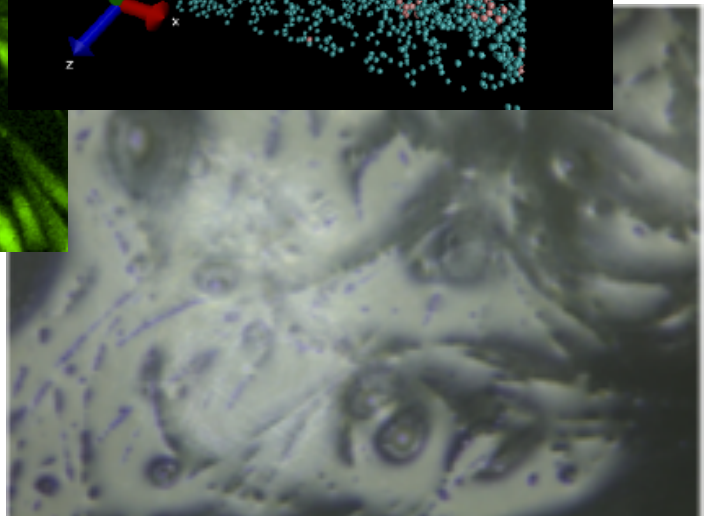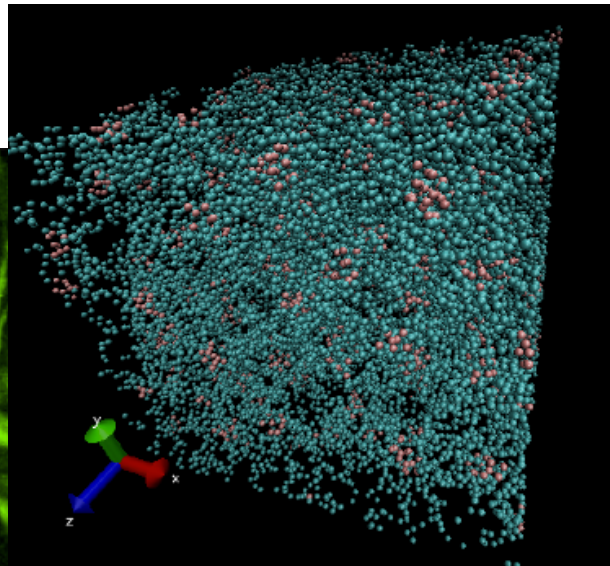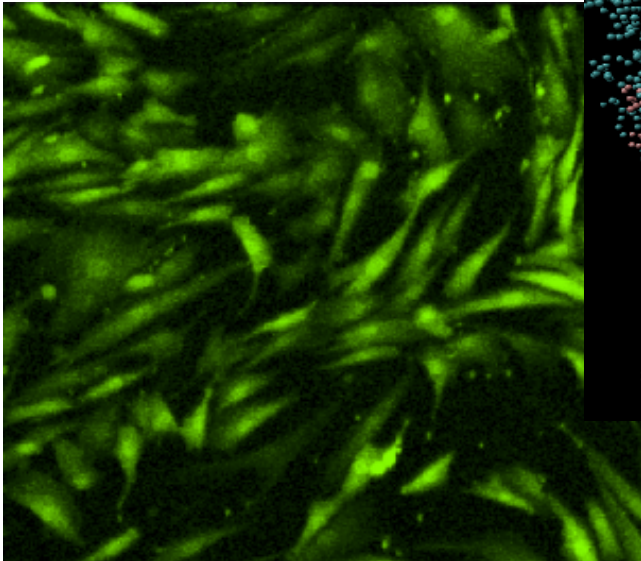
Optimizing Gelatin-Based Hydrogels for use in 3D Bioprinting of Human Dermal Fibroblasts

Elaine Chao[1], Eliana Millstone[2], Kenton Wu[3], Juyi Li[4], Miriam Rafailovich[4]

[1]Northwood High School, Irvine, CA 92620, [2]Stella K Abraham High School for Girls, Hewlett, NY, 11557 [3]The Wheatley School, Old Westbury, NY 11568 [4]Department of Materials Science and Chemical Engineering, Stony Brook University, NY 11794

Hydrogels are networks of polymers that are swollen with water and can be composed of natural or synthetic polymer chains. These biomaterials have several applications in tissue engineering and regenerative medicine as they are very biocompatible. Additionally, hydrogels can be crosslinked to create an entangled polymeric network that can be used to encapsulate cells and other compounds. Hydrogels can be crosslinked ionically through interactions between ions and polymer chains, enzymatically through the creation of covalent bonds, or through photopolymerization from exposure to UV radiation. The ease of modification and biocompatibility of hydrogels makes it an especially useful material in bioprinting[1].

Bioprinting is a revolutionary new 3D biofabrication technique used to precisely dispense biomaterials, including hydrogels and cell-laden mixtures. This study utilized a modified version of the Inkredible+ extrusion-based bioprinter, which prints using air pressure and has both heating and cooling capabilities for the cartridges, allowing for the printing of a wide array of materials. Specific advantages of extrusion-based bioprinters include high deposition and printing speed and its ability to print porous structures[2]. In this study, gelatin, Pluronic® F127, polymerized F127, alginate, crosslinked gelatin, and gelatin-F127 hydrogels were synthesized to optimize mechanical properties for bioprinting.

For the crosslinked gelatin and hybrid gelatin-F127 hydrogels, several different ratios of gelatin to microbial transglutaminase (mTG) and gelatin to F127 were synthesized. The printing process for each gel was optimized by finding the extrusion pressure, temperature, and speed that allowed for the extrusion of a single, continuous line. The crosslinked gelatin and hybrid gelatin-F127 hydrogels were also optimized to find the ratio that would most consistently and effectively print a single, continuous line. The optimized printing conditions were then used to attempt to print a 3D cylindrical structure. The 3D bioprinted designs were created in AutoCAD Fusion 360 and processed in Cellink Heartware to create gcode files for printing.

Rheological analysis was performed on the crosslinked gelatin hydrogels to determine the change in elastic modulus over time. This data was used to determine the best possible crosslinked gelatin hydrogel combination for use in bioprinting and determine ideal times for gelatin-mTG crosslinking before printing.

To analyze the effects of bioprinting on cell viability, sterile gels were mixed with human dermal fibroblast cells and printed at each gel's optimal printing condition [see figure 1]. The printed gels were then analyzed with fluorescence microscopy to determine cell viability during the printing process, which may be affected by sheer pressure, print speed, and nozzle gauge.

Future research will involve further analysis of embedded cells and culturing of cells from bioprinted gels. Additional tests need to be done to print mechanically stable 3D structure.
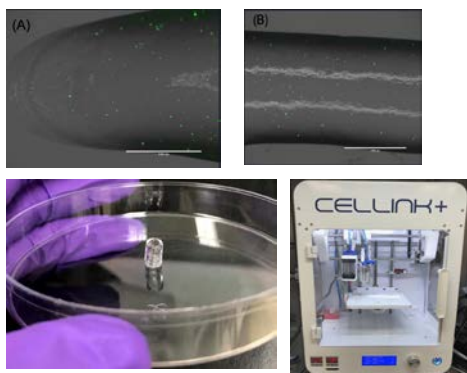
Figure 1. Fluorescent microscopy was performed after 20% Pluronic F127 was mixed with human dermal fibroblasts and shows significant cell viability after being printed at optimal pressure, temperature, and speed.

Figure 2. Successful blood vessel print test run was performed on 30% Pluornic F127 at optimal speed, temperature, and pressure.

Figure 3. Inkredible+ extrusion based bioprinter with heating and cooling capabilities.

[1] "Hydrogel: Preparation, Characterization, and Applications: A Review." *Egyptian Journal of Medical Human Genetics*, Elsevier, 18 July 2013.

[2] "Hydrogels for 3D Bioprinting Applications." *Egyptian Journal of Medical Human Genetics*, Elsevier, 24 July 2015.

Synthesizing and Characterizing Novel Gelatin and Poloxamer PF127, PF108, PF98 Hybrid Hydrogels

Erica Choi[1], Christina Tong[2], Juyi Li[3], Miriam Rafailovich[3]

[1]St. Paul's School, Concord, NH 03301, [2]Fairview High School, Boulder, CO 80305, [3]Department of Materials Science and Engineering, Stony Brook University, Stony Brook, NY 11794

Hydrogels are three dimensional cross-linked polymeric networks. They have been used largely for regenerative medicine and still continue to show very promising applications in the biomedical field due to its biocompatibility and unique properties. Gelatin, a protein derived from collagen in animal tissue, is widely used in the creation of hydrogels; it has excellent biocompatibility, non-immunogenicity, biodegradability, and is relatively low cost[1]. However, gelatin possesses poor mechanical strength and instability, especially under physiological conditions. Cross-linking gelatin with polymers has been shown to increase these properties. Poloxamers, tri-block copolymers composed of PEO_x-PPO_y-PEO_z chains, are being explored for their biomedical applications due to their unique thermo-gelling properties, biocompatibility, and self-assembling micelle structures[2]. This study had two major goals: synthesize and characterize hybrid gels using poloxamers PF127, PF108, and PF98 in order to evaluate their potency and characterize these new poloxamers.

Hybrid hydrogels gels were synthesized by mixing 15% w/v gelatin, 20% w/v poloxamer solution. 10% w/v Microbial transglutaminase (mTG) was added to crosslink the gelatin. Gel solutions were plated, incubated at 37°C, and swelled with 1.5 mL DI water in 30 minute intervals over 3 hours. Rheological analysis was done to evaluate the mechanical strength of these gels, revealing that PF108 had a significantly higher elastic modulus compared to the other gels [Fig 1]. The laser microscope imaging supported this result as the structure of the PF108 hybrid gel displayed branching fibers, while the structures of the other hybrid gels displayed gelatin mesh networks [Fig 1]. The significantly lower surface roughness of the PF108 hybrid gel is associated with decreasing cell attachment, thus, gelatin-PF108 hybrid gel may possess promising characteristics to serve as a cell barrier layer.
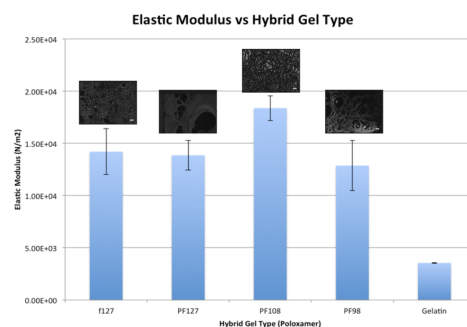
Figure 1: Elastic Modulus for hybrid poloxamer gels

To further characterize the poloxamers, a variety of tests were used on the solutions using the rheometer. The amplitude sweeps revealed important properties about each poloxamer regarding elastic and viscous modulus. Frequency sweeps were performed to determine the critical frequency at which G' (elastic modulus) = G'' (viscous modulus) [Fig 2]. At amplitude sweeps above such frequency, G'>G'' held true for each poloxamer, while below such frequency, PF108 and PF98 had G''>G'. This suggests that the top layers of collapse at low frequencies while all layers stay elastic at high frequencies [Fig 2]. Temperature sweeps utilized the critical frequency to determine the temperature at which each poloxamer solution transitions from liquid to gel [Fig 3].

Future research for hybrid hydrogels will include assessing the cell attachment and testing the clinical viability of the gels through in vivo studies and under physiological conditions. For the poloxamer gels, future research will include further determination of its structures.
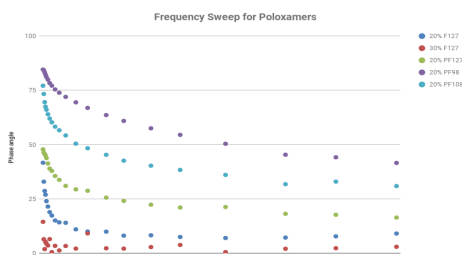
Figure 2: Phase angle vs. Frequency for poloxamer gels
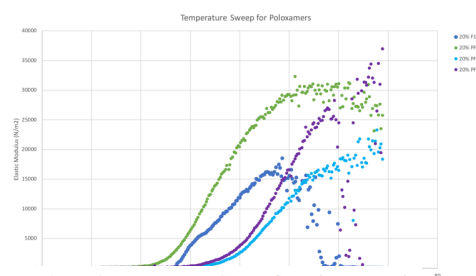
Figure 3: Temperature Sweep for poloxamer gels

[1]Ahmed, Enas M. "Hydrogel: Preparation, Characterization, and Applications: A Review." Journal of Advanced Research , vol. 6, no. 2, 2015, pp. 105–121., doi:https://doi.org/10.1016/j.jare.2013.07.006.

[2]Caló, E., & Khutoryanskiy, V. V. (2015). Biomedical applications of hydrogels: Areview of patents and commercial products. European Polymer Journal,65, 252-267.doi:10.1016/j.eurpolymj.2014.11.024

Analyzing the *In Vitro* Viability of Novel Gelatin-Pluronic® F127 Hybrid Hydrogels as Cell Barrier Membranes

Kevin Chen[1], Joon Young Lee[2], Aaron Sun[3], Juyi Li[4], Miriam Rafailovich[4]

[1] Mira Costa High School, Manhattan Beach, CA 90266, [2] Seoul International School, Seongnam City, South Korea 13113, [3] Ed. W Clark High School, Las Vegas, NV 89102, [4] Dept. Mat. Sci. and Eng., Stony Brook University, Stony Brook, NY 11790

Hydrogels are hydrophilic macromolecular natural or synthetic polymer networks that are crosslinked to produce an elastic, gel-like structure. They are biocompatible, can mimic the characteristics of naturally occurring gels, and can be engineered with desirable properties, creating potential for a variety of promising biomedical applications[1]. Gelatin is a natural polymer with high biocompatibility frequently used in hydrogel synthesis; however, it has poor mechanical strength. Pluronic® F127, a hydrophilic triblock copolymer, can be mixed with gelatin for increased mechanical strength and tunable biocompatibility; additionally, unlike gelatin hydrogels, F127 hydrogels have demonstrated decreased cell attachment[2]. The resulting potential for a novel Gelatin-Pluronic F127 hybrid hydrogel to possess tunable biocompatibility, high mechanical strength, and impermeability to cells makes it ideal for biomedical use as a cell barrier membrane; thus, this study focused on analysis of their *in vitro* viability.

Based on previous research at Stony Brook University that determined an optimal Gelatin-F127 hybrid mix, 15% w/v Gelatin-20% w/v F127 hybrid hydrogels were synthesized with 1%, 5%, 10%, and 15% w/v microbial transglutaminase (mTG), a cross-linking enzyme that synthesizes mesh networks from polymer strands. Characterizing hybrid hydrogels with rheological analysis demonstrated drastically increasing average elastic modulus with increasing mTG concentration (Figure 1). Further characterization using surface analysis with laser microscopy demonstrated decreasing surface roughness as mTG concentration increased.
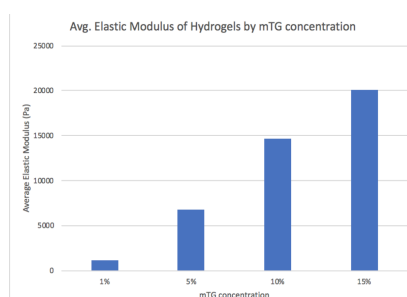
Figure 1: Average Elastic Modulus of Hybrid Hydrogels

Cell attachment was analyzed to determine the impermeability of the hybrid hydrogels to cells. Specifically, green fluorescent human dermal fibroblasts were plated on pure gelatin and hybrid hydrogel samples. Fluorescence imaging indicated a clear decrease in cell attachment with increased mTG concentration; for instance, while cells remained attached on highly crosslinked 15% gelatin, none remained attached on 15% hybrid hydrogels (Figure 2). Further analysis with confocal microscopy indicated similar results. To determine whether reduced cell attachment was due to barrier membrane capabilities or possible toxicity, cytotoxicity tests were conducted with fibroblasts plated in both hybrid gel cell mediums and in direct contact with hybrid gels. Similar fluorescence cell plate readings across the data for both tests indicated hybrid hydrogels are not toxic to cells and are biocompatible. *In vitro* membrane barrier testing was done with three-part gels plated in wells, with a control setup consisting of gelatin/gelatin/gelatin and an experimental setup of gelatin/hybrid/gelatin, with 5%, 10%, and 15% mTG concentrations for gels plated in the middle. Gelatin on the sides of the gels had a 10% mTG crosslinking density. Red and green fluorescent human dermal fibroblasts were plated on the side gelatin gels. Fluorescence readings revealed mixing of the fibroblasts in gelatin controls while the hybrid gels, particularly 15% mTG, prevented mixing of the fluorescent fibroblasts, demonstrating the *in vitro* effectiveness of the hybrid hydrogel as a cell membrane barrier.
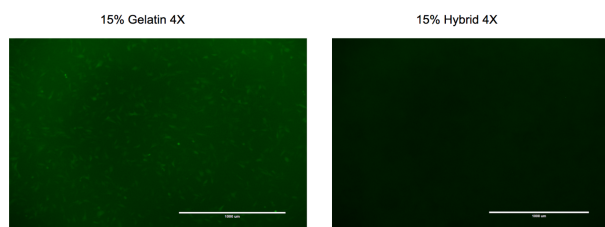
Figure 2: Imaging of Green Fluorescent Human Dermal Fibroblasts on 15% mTG Gelatin and Hybrid Hydrogels

Due to their non-cytotoxicity, cell impermeability, and high mechanical strength shown *in vitro*, hybrid hydrogels, particularly 15% mTG crosslinking density samples, have high potential for use as cell barrier membranes in guided bone regeneration following periodontitis, a disease that is the leading cause for tooth loss and affects nearly half of adults in the United States. They have further potential as burn wound dressings, as cell impermeability allows for both blocking of infections and easy changing of gel dressings with minimal patient pain. For further analysis of biomedical applicability, the ability of the synthesized gelatin-Pluronic® F127 hybrid hydrogels to entrap and release small hydrophobic drugs may be tested, as well as the clinical *in vivo* viability of the gels on animals with periodontitis or burn wounds.

[1] Ahmed, Enas M. "Hydrogel: Preparation, Characterization, and Applications: A Review." *Journal of Advanced Research*, vol. 6, no. 2, 2015, pp. 105–121., doi:https://doi.org/10.1016/j.jare.2013.07.006.

[2] Bhatnagar, D., Mehendru, N., Sun, Y., Nanda, J., & Mentor (2013). Rheological Characterization of Novel HA-Pluronic Thermoreversible Hydrogels. Journal of Chemical and Biological Interfaces,1 (2), 93-99. doi:10.1166/jcbi.2013.1015

Modeling the Diffusion of Drugs Through Hydrogels For Applications in Drug Delivery

Isha Puri[1], Zhining Shi[2], Dilip Gersappe[3] , Miriam Rafailovich[3]
[1] Horace Greeley High School, Chappaqua, NY 10514 [2] The Hockaday School, Dallas, TX 75229
[3] Department of Materials Science and Engineering, Stony Brook University, Stony Brook, NY 11794

In recent years, materials known as hydrogels, or hydrophilic networks of polymer chains, have been increasingly used to release medication slowly over time to a specific part of the body. Hydrogels have many physical properties that contribute to their utility for drug delivery; besides their highly porous structures which allow for straightforward loading and diffusion of drugs, hydrogels are easily controllable, highly biocompatible, and relatively flexible.[1] The goal of this research was to model how changes in the structure and behavior of hydrogels and various drugs would affect drug delivery via diffusion. The modeling throughout this study was done with LAMMPS (Large Scale Atomic/Molecular Massively Parallel Simulator), a molecular dynamics software that simulates particle movement.

Two types of physically associating gels were simulated in this study. We started with a simple system of 1000 telechelic polymers chains of length 20 segments (12.2% volume fraction)[2] and formed an organic gel via end group attractions. Then spherical nanofillers that had strong attraction to the end groups of the polymer chains were introduced to simulate an organic–inorganic network. To analyze the structures of the two gels, we examined the radial distribution functions for both and discovered that the gel with nanofillers had a significantly more uniform intercluster distance, suggesting that nanofillers facilitated the formation of ordered local structure.

Afterwards, we studied how drug particles of different sizes and shapes diffused through both gels. The drugs were first modeled as rigid solid spheres. To ensure that the diffusion coefficient only depended on the structure of the drug and the hydrogel, we minimized the concentration of drug particle. Mean squared displacement was measured over 500000 timesteps, and linear regression was performed to obtain the diffusion coefficient. The results (Figure 1) showed that the diffusion coefficient decreased as the size of the drug particles increased, and drug particles of the same size diffused at a slower rate in the nanocomposite gel due to higher crosslinking density. Then we used the same method to model drugs as 30 oligomers of length 5 segments, which also diffused at a slower rate in the nanocomposite gel.

The simulations provided information on how different parameters changed the diffusivity of solutes through hydrogels, which can lead to more effective uses of hydrogels in drug delivery therapies. For further study, we plan to study more parameters that can change the diffusivity, run the simulations on a bigger scale, and increase the complexity of the shapes of the drugs to better mirror drugs in the market.

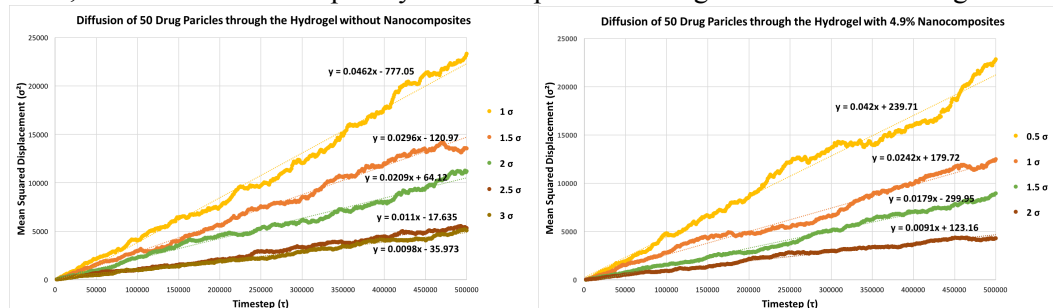Figure 1: graphs of mean squared displacement vs time for diffusion of drug particles through hydrogel without (left) and with nanofillers (right)

[1] Todd R. Hoare, Daniel S. Kohane, Hydrogels in drug delivery: Progress and challenges, Polymer, Volume 49, Issue 8, 2008, 1993-2007
[2] Xu, D., & Gersappe, D. (2017). Structure formation in nanocomposite hydrogels. *Soft Matter,* 2017, **13**, 1853.

Lattice Boltzmann Modeling of Fluid Flow Dynamics in Metal-Organic Frameworks

Shreyas Iyer[1], Hongyu Li[2], Dr. Dilip Gersappe[2], Dr. Miriam Rafailovich[2]

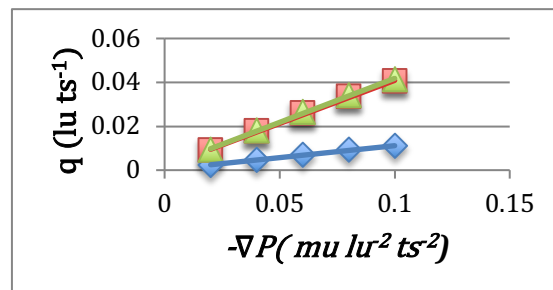[1]Munster High School, Munster, IN 46321

[2]Department of Materials Science and Chemical Engineering, Stony Brook University, Stony Brook, NY 11794

Metal-organic frameworks (MOFS) are large crystalline networks consisting of inorganic metallic ions bonded together by organic linkers. These structures have nanoscale pores, extremely high surface areas, and can be reused many more times than traditional materials. Thus, MOFs are emerging in various applications such as catalysis, sensing, gas storage, and gas separation [1]. Indeed, over 50% of industrial catalysts used today are MOFs [2]. Unfortunately, there are two main problems with the usage of MOFs. First is that the permeability of a MOF is hard to control or predict without experimentation or expensive laboratory testing. Second is that it is nearly impossible to create a perfect MOF without any defects [3].
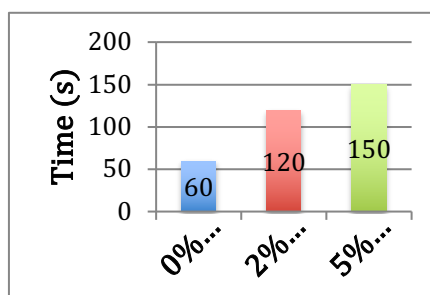
To address these issues, we used a Lattice Boltzmann model of fluid flow through a MOF-808 crystalline structure. Analyzing fluid flow is a necessary step toward understanding the mechanisms of their activities as catalysts, sensors, and filtration materials. The flow was initialized by creating a higher density at one side of the lattice and a lower density at the other, forcing the liquid to move through the pores of the MOF. Defects were introduced in the structure by creating a random number generator and constraining the outputs to certain probability values. Most MOFs have 2%-14% defects, so preliminary results were calculated for 0% defects, 2% defects, and 5% defects. The pressure gradient was tested at values of .02, .04, .06, .08, and .10. A surface integral was introduced into the code to calculate the flux of the fluid exiting the lattice.

Figure 1. Steady-state equilibrium flux versus negative pressure gradient for flow through MOFs with 0% defects (blue), 2% defects (red), and 5% defects (green). In Lattice Boltzmann modeling, the units of mass, length, and time are mass unit (mu), lattice unit (lu), and time step (ts),

The most relevant data existed at the points when the fluid flow had reached steady-state equilibrium. Flux versus negative pressure gradient was graphed and analyzed (Figure 1). Because effective permeability is directly proportional to the slope of the curve, this data was also yielded permeability values (Figure 2). To further contextualize these results, a simulation was done to determine the approximate amount of time that each lattice took to reach equilibrium (Figure 3). Velocity distributions were then characterized along a single, straight line using Paraview simulation software (Figure 4).

Figure 3. Time (seconds) to reach steady-state equilibrium in MOFs with 0% defects, 2% defects, and 5% defects.
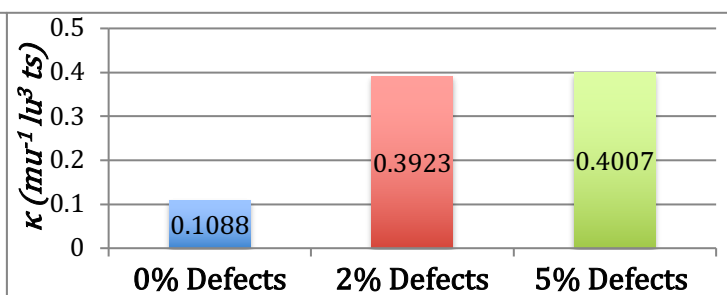
Figure 2. Steady-state equilibrium permeability in MOFs with 0% defects, 2% defects, and 5% defects. The permeability values were calculated by taking the slope of the lines of best fit from Figure 1.
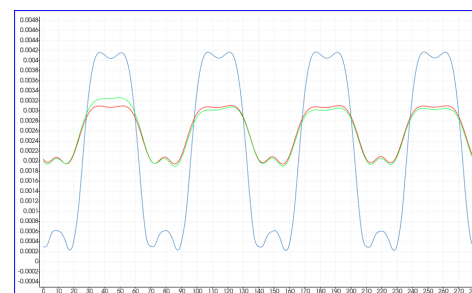
Figure 4. Steady-state equilibrium velocity distribution in MOFs with 0% defects (blue), 2% defects (red), and 5% defects (green). The values were taken across the x-axis of a cross section of the lattice.

The data indicate that the higher defect value lattices have increased permeability but take longer to reach equilibrium and have lower fluid velocities overall in this state, which is a novel result. This is likely due to the abnormal channels that are created when defects are introduced. In addition, these results are applicable to other anisotropic MOFs and suggest that MOFs can be designed with desired fluid permeabilities. Further development includes testing greater defect and pressure values, changing the defect locations on the lattices, and analyzing the channels created when defects are introduced.

[1] Maurin, G.; Serre, C.; Cooper, A.; Férey, G. The new age of MOFs and of their porous-related solids. Chem. Soc. Rev. 2017, 46 (11), 3104−3107.

[2] Yoon, M.; Srirambalaji, R.; Kim, K. Homochiral Metal−Organic Frameworks for Asymmetric Heterogeneous Catalysis. Chem. Rev. 2012, 112 (2), 1196−1231.

[3] Liu, Y.; Howarth, A. J.; Vermeulen, N. A.; Moon, S.-Y.; Hupp, J. T.; Farha, O. K. Catalytic degradation of chemical warfare agents and their simulants by metal-organic frameworks. Coord. Chem. Rev. 2017, 346, 101−111.

Session 3:
Cellular/Bacterial Interactions

Chairs:
Kao Li & Fan Yang

Characterization of Antibiofilm Activity of Silver Nanoparticles Deposited in situ on 3D Printed Polylactic Acid Implant Models

Anastasia Popova [1], Isha Brahmbhatt [2], Michael Cuiffo [3], Stephen Walker [4], Yuval Shmueli [3], Fan Yang [3], Miriam Rafailovich [3], Adriana Pinkas-Sarafova [3]

[1] Hackley School, Tarrytown NY, 10591, [2] Ardsley High School, Ardsley NY, 10502,
[3] Department of Material Science and Chemical Engineering, Stony Brook University, Stony Brook NY, 11790
[4] Department of Oral Biology and Pathology, Stony Brook University, Stony Brook NY, 11790

The formation of bacterial biofilms on implants is a great problem, because once formed they cannot be removed. Thus, there is a need of an approach to modify implant materials in order to prevent biofilm formation. There has been a lot of research done on the antimicrobial properties of silver nanoparticles [1]. However, when silver nanoparticles have been mixed with a polymer before implant preparation, it has been observed to be unable to release silver ions which carry the antimicrobial effect. Polylactic acid (PLA) is biodegradable and FDA-approved for use in the human body. The Brunst method has recently been patented for *in situ* synthesis of Ag nanoparticles coating PLA [2]. Thus silver nanoparticles, when incorporated on the PLA surface, will allow release of silver ions for an extended period of time, inhibiting biofilm formation. The efficiency of coating can differ based on $AgNO_3$ concentration used, and PLA filament content related to different 3D printers.
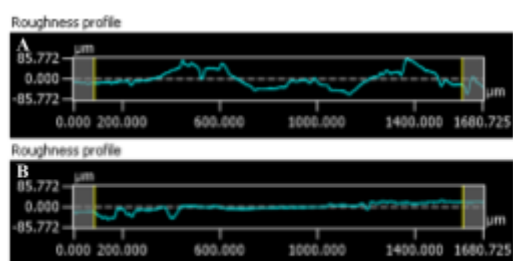

Figure 1: Roughness profiles of the Makerbot PLA samples (A) and the Ultimaker 2+ PLA samples (B)

We hypothesized that an increased concentration of silver nanoparticles would result in an increased ability to inhibit biofilm formation and will not be affected by the difference between the filaments.

PLA scaffolds were printed using two 3D printers, a Makerbot Replicator 2X and Ultimaker 2 Extended+, with corresponding filaments, and characterized with a laser microscope and FTIR. Two concentrations of $AgNO_3$ (0.1M and 0.01M) and 0.001M $NaBH_4$ were used with the Brunst method simultaneously, for both scaffolds. The *in situ* deposition of silver nanoparticles was observed with SEM. The PLA-$AgNO_3$ scaffolds were tested for ability to prevent biofilm formation against two strains of bacteria, *Staphylococcus aureus* (gram-positive) and *Escherichia coli* (gram-negative) in TSB media. Biofilm formation was identified by crystal violet staining, life/dead fluorescent stain, and confocal microscopy at 6, 24 and 48 hours. The PLA-$AgNO_3$ scaffolds were also tested for dental pulp stem cell (DPSC) adhesion. After plating, DPSCs were cultured in media (αMEM, 10% FBS, 0.002M Asc. acid, 0.01M β Glycerol phosphate). Alamar blue staining and EVOS FL microscope were used to monitor cell attachment and proliferation.

Figure 2: *E. coli* Biofilms stained with Crystal Violet 22 hours after plating on Ultimaker samples.
A: Control, B: 0.01M PLA-$AgNO_3$, C: 0.1M PLA-$AgNO_3$

Figure 3: *S. aureus* Biofilms stained with Crystal Violet 48 hours after plating on Ultimaker samples.
A: Control, B: 0.01M PLA-$AgNO_3$, C: 0.1M PLA-$AgNO_3$

Analyses of both types of scaffolds show significant differences in surface roughness (fig.1), and chemistry. These reflected the adhesion and biofilm formation of both bacterial strains, surprisingly more attracted to smoother scaffolds printed on Ultimaker 2 Extended+. PLA-$AgNO_3$ nanoparticle coated scaffolds at 22 and 48 hours after bacterial inoculation showed significantly smaller size of the biofilms on average for both *E. coli* (fig.2) and *S. aureus* (fig.3) with 0.1M than the one with 0.01M nanoparticles (fig.2, fig.3) as proposed. The DPSCs had the same correlation and attached significantly better to the Ultimaker samples in comparison to the Makerbot samples (fig.4). Future work will include observing DPSC attachment on PLA scaffolds coated with $AgNO_3$, as well as analyzing the live-dead ratio of bacteria in the biofilms.
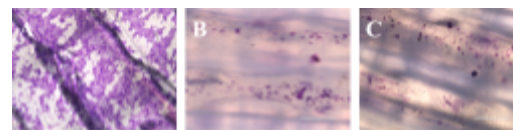
Figure 4: Cell growth 2 days after induction on the Control samples.
A: Makerbot Replicator 2X, B: Ultimaker 2 Extended+

[1] Mizajani, F., Ghassempour, A., Aliahmadi, A., & Esmaeili, M. A. (2011). Antibacterial effect of silver nanoparticles on Staphylococcus aureus. *Research in Microbiology,162*, 542-549. Retrieved August 5, 2018.

[2] Cuiffo, M. A., & Halada, G. (2013). *U.S. Patent No. R-8530*. Washington, DC: U.S. Patent and Trademark Office.

Characterization of Antibiofilm Activity of Silver Nanoparticles Deposited in situ on 3D Printed Polylactic Acid Implant Models

Anastasia Popova [1], Isha Brahmbhatt [2], Michael Cuiffo [3], Stephen Walker [4], Yuval Shmueli [3], Fan Yang [3], Miriam Rafailovich [3], Adriana Pinkas-Sarafova [3]

[1] Hackley School, Tarrytown NY, 10591, [2] Ardsley High School, Ardsley NY, 10502,
[3] Department of Material Science and Chemical Engineering, Stony Brook University, Stony Brook NY, 11790
[4] Department of Oral Biology and Pathology, Stony Brook University, Stony Brook NY, 11790

The formation of bacterial biofilms on implants is a great problem, because once formed they cannot be removed. Thus, there is a need of an approach to modify implant materials in order to prevent biofilm formation. There has been a lot of research done on the antimicrobial properties of silver nanoparticles [1]. However, when silver nanoparticles have been mixed with a polymer before implant preparation, it has been observed to be unable to release silver ions which carry the antimicrobial effect. Polylactic acid (PLA) is biodegradable and FDA-approved for use in the human body. The Brunst method has recently been patented for *in situ* synthesis of Ag nanoparticles coating PLA [2]. Thus silver nanoparticles, when incorporated on the PLA surface, will allow release of silver ions for an extended period of time, inhibiting biofilm formation. The efficiency of coating can differ based on $AgNO_3$ concentration used, and PLA filament content related to different 3D printers.

Figure 1: Roughness profiles of the Makerbot PLA samples (A) and the Ultimaker 2+ PLA samples (B)

We hypothesized that an increased concentration of silver nanoparticles would result in an increased ability to inhibit biofilm formation and will not be affected by the difference between the filaments.

PLA scaffolds were printed using two 3D printers, a Makerbot Replicator 2X and Ultimaker 2 Extended+, with corresponding filaments, and characterized with a laser microscope and FTIR. Two concentrations of $AgNO_3$ (0.1M and 0.01M) and 0.001M $NaBH_4$ were used with the Brunst method simultaneously, for both scaffolds. The *in situ* deposition of silver nanoparticles was observed with SEM. The PLA-$AgNO_3$ scaffolds were tested for ability to prevent biofilm formation against two strains of bacteria, *Staphylococcus aureus* (gram-positive) and *Escherichia coli* (gram-negative) in TSB media. Biofilm formation was identified by crystal violet staining, life/dead fluorescent stain, and confocal microscopy at 6, 24 and 48 hours. The PLA-$AgNO_3$ scaffolds were also tested for dental pulp stem cell (DPSC) adhesion. After plating, DPSCs were cultured in media (αMEM, 10% FBS, 0.002M Asc. acid, 0.01M β Glycerol phosphate). Alamar blue staining and EVOS FL microscope were used to monitor cell attachment and proliferation.

Figure 2: *E. coli* Biofilms stained with Crystal Violet 22 hours after plating on Ultimaker samples.
A: Control, B: 0.01M PLA-$AgNO_3$, C: 0.1M PLA-$AgNO_3$

Figure 3: *S. aureus* Biofilms stained with Crystal Violet 48 hours after plating on Ultimaker samples.
A: Control, B: 0.01M PLA-$AgNO_3$, C: 0.1M PLA-$AgNO_3$

Analyses of both types of scaffolds show significant differences in surface roughness (fig.1), and chemistry. These reflected the adhesion and biofilm formation of both bacterial strains, surprisingly more attracted to smoother scaffolds printed on Ultimaker 2 Extended+. PLA-$AgNO_3$ nanoparticle coated scaffolds at 22 and 48 hours after bacterial inoculation showed significantly smaller size of the biofilms on average for both *E. coli* (fig.2) and *S. aureus* (fig.3) with

Figure 4: Cell growth 2 days after induction on the Control samples.
A: Makerbot Replicator 2X, B: Ultimaker 2 Extended+

0.1M than the one with 0.01M nanoparticles (fig.2, fig.3) as proposed. The DPSCs had the same correlation and attached significantly better to the Ultimaker samples in comparison to the Makerbot samples (fig.4). Future work will include observing DPSC attachment on PLA scaffolds coated with $AgNO_3$, as well as analyzing the live-dead ratio of bacteria in the biofilms.
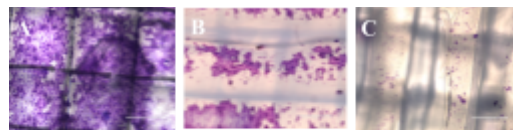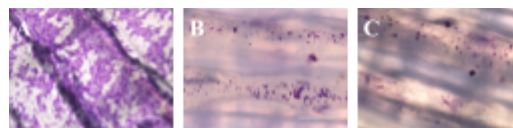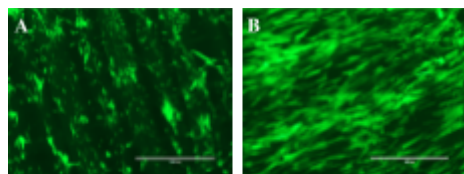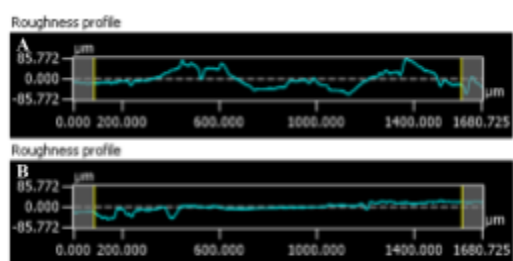
[1] Mizajani, F., Ghassempour, A., Aliahmadi, A., & Esmaeili, M. A. (2011). Antibacterial effect of silver nanoparticles on Staphylococcus aureus. *Research in Microbiology,162*, 542-549. Retrieved August 5, 2018.

[2] Cuiffo, M. A., & Halada, G. (2013). *U.S. Patent No. R-8530*. Washington, DC: U.S. Patent and Trademark Office.

Naturally Occuring Fibrinogen Chain Variant γ′ Associated with Decreased Risk for *Staphylococcus aureus* Bacteremia

Anson Zhou[1], Anyerlin Mora[2], Kao Li[3], Miriam Rafailovich[3], Dennis Galanakis[4]

[1]*Patchogue-Medford High School, Medford, NY 11763, [2]State University of New York at Stony Brook, Stony Brook, NY, 11794, [3]Department of Material Science and Engineering, State University of New York at Stony Brook, Stony Brook, NY, 11794, [4]Stony Brook Blood Bank, Stony Brook, NY, 11794*

Staphylococcus aureus bacteremia has become one of the most prevalent and difficult medical conditions to treat. Over time, the number of antibiotic-resistant *Staphylococcus aureus* strains has increased, posing a serious clinical challenge and public safety concern.[1] Bloodstream infections (BSI) is ranked as the 11th leading cause of death in the United States, accounting for almost 36,000 deaths in 2008 alone. It has been suggested however, that the number of BSI-related deaths in the United States is severely under-reported and actually numbers upwards of 70,000 given that in many cases bloodstream infections are overlooked as a cause of death amongst terminal conditions (eg. end-stage kidney disease, advanced malignancy) and underlying sources of infection.[2] With the viability of conventional treatments diminishing, naturally occurring therapies have become a target. Fibrinogen is the soluble blood precursor of the fibrin clot and plays crucial roles in mediating clot formation and wound healing.[3] Each molecule is symmetrical and consists of a set of three different chains termed Aα, Bβ, and γ. In approximately 10% of all fibrinogen, a natural variant called γ′ arises due to an alternative processing of the γ-mRNA.[4] *Staphylococcus aureus* has the ability to bind to fibrin(ogen) via membrane-bound bacterial virulence

Fig 1. Fibers from fibrin rich fibrinogen, 10X mag.

proteins, an important mechanism that contributes to bacteremia. However, studies in mice have shown that a higher incidence of mutant fibrinogen $\gamma^{\Delta 5}$ - which lacks certain bacterial binding motifs - actually significantly increases host survival rates from BSIs.[5] In this study, it was hypothesized that the human variant γ′ could possibly demonstrate a similar capacity to combat bacterial infections. Solutions of polystyrene (M_w=200k, monodispersed; M_w=400k, monodispersed; M_w=35k; M_w=280k) dissolved in toluene was created and silicon wafers were treated via piranha etching. The wafers were then treated with HF to turn the surface more hydrophobic and the polystyrene was spun cast on to the wafers for 30 seconds at 2500 RPMs and annealed overnight at 120°C. Two types of fibrinogen-fibrin solutions (rich in soluble fibrin and depleted in soluble fibrin) were deposited on the various polystyrene thin film samples. Fiber growth occurred overnight and was quantified using optical

Fig 2. Fiber quantification

microscopy (Fig. 1), identifying polystyrene (M_w=200k, monodispersed) to be the optimal type for fiber development (Fig. 2). *Staphylococcus aureus* was deposited on fibers grown in polystyrene (M_w=200k, monodispersed) and incubated at 37°C for 1 hour. A fluorescent live/dead stain was completed on the samples and observed with fluorescent microscopy. A subsequent trial was conducted; prior to bacterial deposition, the fibers were treated with anti-$\gamma^{(80-411)}$ to block a large portion of the gamma chain. A secondary anti-sheep antibody treatment was done after bacterial deposition to fluoresce the primary anti-$\gamma^{(80-411)}$ antibody. In future studies, anti-γ′ antibodies will be utilized and their impact on bacterial adhesion will be observed through AFM and SEM.

_____

[1]Wisplinghoff H, Bischoff T, Tallent SM, Seifert H, Wenzel RP, Edmond MB. Nosocomial bloodstream infections in US hospitals: analysis of 24,179 cases from a prospective nationwide surveillance study, *Clin Infect Dis* , 2004, vol. 39 (pg. 309-17)
[2]M. Goto, M.N. Al-Hasan, Overall burden of bloodstream infection and nosocomial bloodstream infection in North America and Europe, Clinical Microbiology and Infection, Volume 19, Issue 6, 2013, Pages 501-509
[3]Lovely RS, Falls LA, Al-Mondhiry HA, Chambers CE, Sexton GJ, Ni H, Farrell DH. Association of A/ fibrinogen levels and coronary artery disease. Thromb Haemost 2002;88:26 –31.
[4]M.W. Mosesson Fibrinogen functions and fibrin assembly, Fibrinolysis and Proteolysis, 14 (2000), pp. 182-186
[5]Flick, M. J., Du, X., Prasad, J. M., Raghu, H., Palumbo, J. S., Smeds, E., et al. (2013). Genetic elimination of the binding motif on fibrinogen for the *s. aureus* virulence factor clfa improves host survival in septicemia. *Blood* 121, 1783–1794. doi: 10.1182/blood-2012-09-453894

Investigating the Nanotoxicity of Titanium Dioxide via Fibroblast Growth and Infection with *Staphylococcus aureus*

Justin Zhou[1], Vincent Zhang[2], Jonathan Goldschlag[3], Ethan Winkler[3], Kaitlin Labiak[4], Fan Yang[5], Miriam Rafailovich[5]

[1]Patchogue-Medford High School, Medford, NY 11763; [2]Sachem High School East, Farmingville, NY 11738; [3]Hebrew Academy of the Five Towns and Rockaway, Cedarhusrt, NY 11516; [4]University of Michigan, Ann Arbor, MI 48109; [5]Department of Materials Sciences and Chemical Engineering, Stony Brook University, Stony Brook, NY 11794

Titanium dioxide (TiO_2) is commonly used in paints, toothpaste, sunscreen, cosmetics, pharmaceutics, cosmetics, and food additives. [1] While there has been an abundance of research on its anti-cancer and anti-bacterial applications with irradiation with UV light, there is little investigation on how TiO_2 may actually be harmful to cells. In a previous study, HeLa cells were exposed to TiO_2 nanoparticles, and it was concluded that exposure might significantly increase the risk of bacterial invasion. [2] Because of its wide array of applications, constant contact with these nanoparticles could be extremely harmful. In our study, we sought to corroborate the conclusions made by researching the effects of exposure of TiO_2 rutile nanoparticles on cell growth as well as bacterial infection behavior.
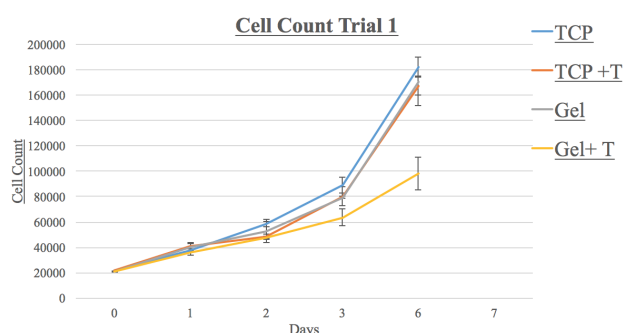
Figure 1. Cell count data shows significant decrease in Gel+TiO_2
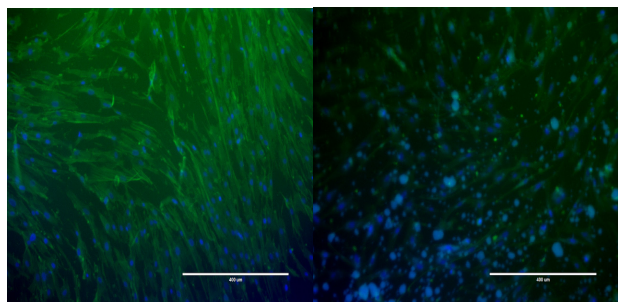
Figure 2. EVOS Microscopy shows unhealthy fibroblasts in the presence of TiO_2 (right image)

Human dermal fibroblasts and a gelatin hydrogel substrate were utilized. We sought to analyze how these cells would grow in four different conditions- normal tissue culture plate (TCP), TCP with TiO_2, Gel, and Gel with TiO_2. The titanium dioxide was characterized with X-ray diffraction, TEM, and UV-Vis spectrophotometry. We measured cell proliferation with the hemocytometer and correlated the doubling time calculated with EVOS and confocal microscopy.

In both our cell counting data and fluorescent microscopy images, it was apparent that there was little contrast between the TCP and TCP+TiO_2 samples, which may be due to the relatively low concentration of 0.1 TiO_2/mL. On the contrary, the Gel+TiO_2 samples showed a much lower cell count than the Gel samples (Figure 1). Moreover, the narrowness and clumping of fibroblast ends exposed to TiO_2 indicate cell deficiency (Figure 2). While we have not received bacterial colony formation units (CFU) data yet, it seemed that the bacteria are more clustered together with TiO_2.

From the data of the hemocytometer and the fluorescent microscopy, we can conclude that exposure to TiO_2 nanoparticles may potentially be toxic. Because a hydrogel substrate is meant to simulate physiological conditions, this provides compelling evidence that TiO_2 does decrease cell proliferation rate, while inhibiting some cellular mechanism to affect fibroblast morphology. Future research involves investigating why the fibroblast samples on a hydrogel substrate are more heavily affected than TCP samples, as well as the mechanisms behind different bacterial invasion behaviors.

[1]Ritesh K. Shukla, Vyom Sharma, Alok K. Pandey, Shashi Singh, Sarwat Sultana, Alok Dhawan, ROS-mediated genotoxicity induced by titanium dioxide nanoparticles in human epidermal cells, Toxicology in Vitro, Volume 25, Issue 1, 2011, Pages 231-241, ISSN 0887-2333

[2] Journal of Nanobiotechnology, 2016, Volume 14, Number 1, Page 1, Yan Xu, Ming-Tzo Wei, H. Daniel Ou-Yang, Stephen G. Walker, Hong Zhan Wang,Chris R. Gordon, Shoshana Guterman, Emma Zawacki, Eliana Applebaum, Peter R. Brink, Miriam Rafailovich, Tatsiana Mironava

Session 4: Fuel Cells

Chair:
Likun Wang
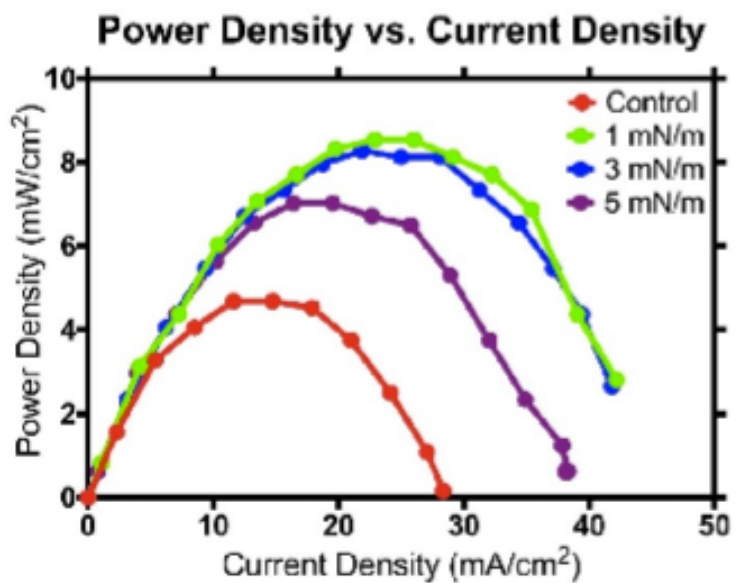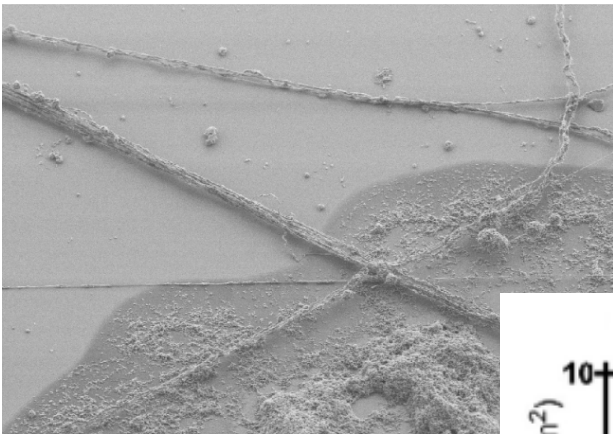
Coating Nafion 117 Membranes with Graphene Oxide using Various Surface Pressures to Increase Performance of Proton Exchange Membrane Fuel Cells

Lucia Lin[1], Kimberley Tran[2], Likun Wang[3], Miriam Rafailovich[3]
[1]Townsend Harris High School, Flushing, NY 11364
[2]Clayton High School, St. Louis, MO 63105
[3]Department of Materials Science and Engineering, Stony Brook University, Stony Brook, NY 11794

Proton exchange membrane fuel cells (PEMFCs) present a clean energy alternative to fossil fuels for generating electricity. In PEMFCs, hydrogen protons pass through the proton exchange membrane (PEM). To maximize performance, PEMs must have high proton conductivity and low gas permeability (Xue et al., 2014). Currently, Nafion, a perfluorosulfonic acid membrane, serves as the PEM in fuel cells. While Nafion has high proton conductivity, it is susceptible to hydrogen gas permeability which interferes with fuel cell performance (Francia et al., 2010). When coated on the PEM, graphene oxide (GO) can increase PEMFC performance due to oxygen-containing acidic functional groups which provide proton transport channels and smaller nanopores which decrease gas permeability (Farooqui et al., 2018; He et al., 2016).

The purpose of this research was to determine the effects of different surface pressures of a KSV Instruments Langmuir-Blodgett (LB) trough when coating Nafion 117 membranes with GO. 40 mL of GO solution was dropped onto the air-water interface using a syringe. The dipping mechanism of the LB trough was used to coat Nafion 117 membranes at 1 mN/m, 3 mN/m and 5 mN/m surface pressures.

Figure 1. Voltage vs. Current Density for Nafion 117 membranes coated in Graphene Oxide using the Langmuir Blodgett trough.

Figure 2. Power Density vs. Current Density for Nafion 117 membranes coated in Graphene Oxide using the Langmuir Blodgett trough.

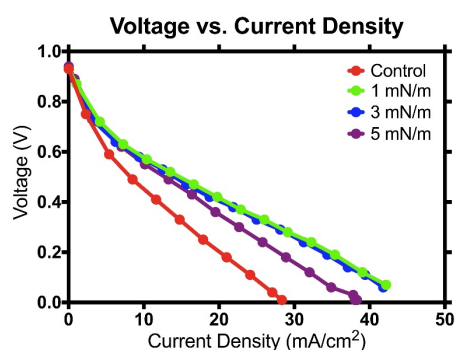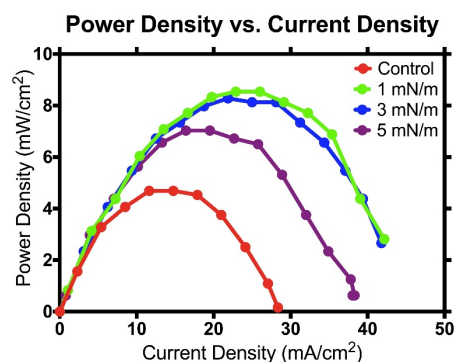The Nafion membranes were tested in a single-stack demonstration fuel cell kit from H-TEC. Four membranes were tested for fuel cell performance: an unmodified Nafion membrane as the control and Nafion membranes coated in GO at surface pressures of 1 mN/m, 3 mN/m, and 5 mN/m, respectively. The BK Precision 7601 DC Electronic Load controlled the resistance of the demonstration kit, and the BK 8600 Series Software recorded the current, voltage, and power. Current density and power density were later calculated.

The membranes coated with GO at surface pressures of 1 mN/m and 3 mN/m displayed similar decrease in voltage (Figure 1) and remained stable at the highest current densities (Figure 1 and 2). However, 1 mN/m showed the highest peak power density (Figure 2). When coating using the LB trough, the GO monolayer must be stable and homogeneous in order to best enhance the PEM's proton conductivity. From these results, it appears that within our experimental groups, 1 mN/m is an optimal surface pressure for coating Nafion with GO. Surface pressures higher than 3 mN/m can possibly cause the GO monolayer to collapse, which does not allow the LB trough to lay a fully homogeneous layer of GO onto Nafion. More tests will need to be conducted for surface pressures between 1 mN/m and 3 mN/m to determine the exact value for optimal surface pressure.

Further experimentation will be done to analyze the surface morphology and thickness of the GO layers when coated on Nafion 117 membranes with different surface pressures. Additionally, the effect of the optimal number of monolayers of GO on Nafion 117 can be determined to effectively enhance the performance of proton exchange membrane fuel cells.

Farooqui, U., Ahmad, A., & Hamid, N. (2018). Graphene oxide: A promising membrane material for fuel cells. *Renewable and Sustainable Energy Reviews, 82*, 714-733. doi:10.1016/j.rser.2017.09.081

Francia, C., Ijeri, V. S., Specchia, S., & Spinelli, P. (2011). Estimation of hydrogen crossover through Nafion® membranes in PEMFCs. *Journal of Power Sources, 196*(4), 1833-1839. doi:10.1016/j.jpowsour.2010.09.058

He, G., He, X., Wang, X., Chang, C., Zhao, J., Li, Z., . . . Jiang, Z. (2016). A highly proton-conducting, methanol-blocking Nafion composite membrane enabled by surface-coating crosslinked sulfonated graphene oxide. *Chemical Communications, 52*(10), 2173-2176. doi:10.1039/c5cc07406a

Xue, C., Zou, J., Sun, Z., Wang, F., Han, K., & Zhu, H. (2014). Graphite oxide/functionalized graphene oxide and polybenzimidazole composite membranes for high temperature proton exchange membrane fuel cells. *International Journal of Hydrogen Energy, 39*(15), 7931-7939. doi:10.1016/j.ijhydene.2014.03.061
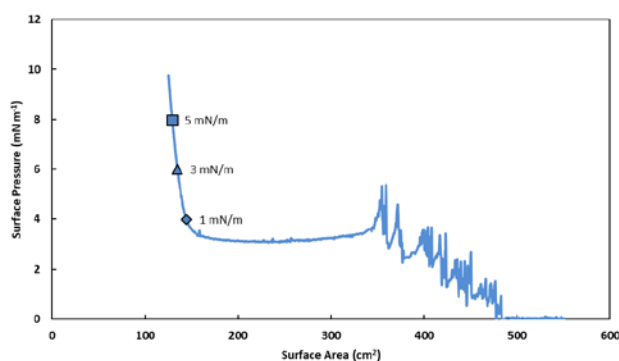
Alteration of the Surface Structure of the Nafion Membrane to Increase PEMFC Efficiency

Evan Lu[1], Brandon Oh[2], Matthew Qu[3], Michael Zhang[4], Kenneth Chan[5], Likun Wang[6], Miriam Rafailovich[6]

[1]Clear Lake High School, Houston TX [2]Seoul International School, Seoul ROK [3]Wayzata High School, Plymouth MN [4]Saratoga High School, Saratoga CA [5]Boston University, Boston MA [6]Department of Material Science and Engineering, State University of New York at Stony Brook, Stony Brook, NY

Proton-exchange membrane fuel cells (PEMFCs) have recently generated renewed scientific interest as a source of alternative energy due to their ability to generate electrical energy at a relatively low temperature and pressure without harmful by-products. Specifically, the polymer electrolyte membrane of PEMFCs remains a focus of current research, with Nafion being the most common polymer used in such membranes. However, the current efficiency of PEMFCs is well under the desired threshold to be widely used in a variety of applications[1]. With increased utilization efficiency of platinum content in PEM fuel cell[2], this research investigated the effects of the deposition of platinum nanowires onto the Nafion membrane at various surface pressures.

Platinum nanowires were synthesized by the Stony Brook Department of Chemistry and were sonicated in ethanol to create 1.0 mg/mL solutions. The resultant solution was used with a Langmuir-Blodgett (LB) trough (KSV 3000) to deposit a platinum nanowire monolayer onto the Nafion membranes at surface pressures of 1 mN m^{-1}, 3 mN m^{-1}, and 5 mN m^{-1} with respect to the baseline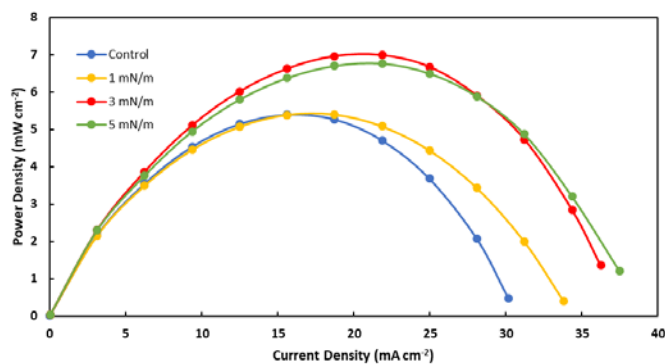 (Figure 1). All Nafion membranes were tested at the same fuel cell test station connected to a programmable DC electronic load (BK Precision 8601) with 4 cm x 4 cm electrodes of 0.1 g/cm^2 Pt/C. The hydrogen release rate was set to 80 cm^3 min^{-1}, and voltage and power outputs were measured starting from 0.000 A with a 0.050 A increase every 30 seconds.

Figure 1. LB trough-generated isothermal curve of platinum nanowire-ethanol solution

The isothermal curve has a baseline at around 3 mN m^{-1}; the irregularities of the curve past 350 cm^2 on the horizontal axis are due to the addition of platinum-ethanol solution disrupting the surface of the water bath. The baseline remains at approximately 3 mN m^{-1} because the ethanol has not yet evaporated and thus retains surface pressure on the water. Nevertheless, the abrupt spike in surface pressure confirms the presence of a platinum nanowire monolayer, and deposition occurred at the labelled points. Figure 2 displays the polarization curve of PEMFCs using an uncoated control in addition to the three membranes coated with platinum nanowires at the varying surface pressures. The control membrane performed the worst, as expected. Membranes coated with surface pressures of 3 mN m^{-1} and 5 mN m^{-1} returned similar results, so it is hypothesized that the optimal coating surface pressure lies between these two values.

Future work includes deposition of platinum nanowires at surface pressures between 3 mN m^{-1} and 5 mN m^{-1} to optimize the power output of the PEMFC. In addition, scanning electron microscopy can be used to detect differences between the various platinum nanowire-coated membranes and elucidate the properties of the coated Nafion membranes.

Figure 2. Polarization curves for an uncoated control membrane and three additional membranes coated with platinum nanowires at 1 mN m^{-1}, 3 mN m^{-1}, and 5 mN m^{-1}

[1] Lee, S., Mukerjee, S., Mcbreen, J., Rho, Y., Kho, Y., & Lee, T. (1998). Effects of Nafion impregnation on performances of PEMFC electrodes. *Electrochimica Acta*, *43*(24), 3693-3701. doi:10.1016/s0013-4686(98)00127-3

[2] Broka, K., & Ekdunge, P. (1997). Oxygen and hydrogen permeation properties and water uptake of Nafion® 117 membrane and recast film for PEM fuel cell. *Journal of Applied Electrochemistry*, *27*(2), 117-123. doi:10.1023/A:101846952056

Varying Graphene Oxide Deposition Mass in Polymer Electrolyte Membrane Fuel Cells to Optimize Fuel Cell Performance and Durability

Saajid Chowdhury[1], Kevin Xu[2], Matthew Moulton[3], Stoyan Bliznakov[4], Miriam Rafailovich[4]

[1]MacArthur High School, Levittown, NY, 11793; [2]Ward Melville High School, East Setauket, NY, 11733; [3]Cooper Union, New York, NY, 10003; [4] Department of Materials Science and Engineering, State University of New York at Stony Brook, Stony Brook, NY, 11794

While, in theory, Polymer Electrolyte Membrane Fuel Cells (PEMFCs) offer a clean and highly efficient form of alternative energy, there still remains several obstacles in their development that must be overcome to compete with traditional energy sources, including cost, power output and durability.[1] Studies have shown that GO has positive effects on both power density and durability of PEMFCs.[2] However, previous research involving GO deposition does not compare the effects of various mass loadings of GO on the electrodes or membrane to find the optimal amount needed to maximize efficiency. In this study, a calibration curve was created to correspond mass loading of GO with area below Raman spectroscopy peaks of different GO samples. Using this curve, the performance of various tested mass loadings of GO were compared to a control to observe differences in power output.

A GO solution of 5mL Isopropyl alcohol, 5mL DI water and 10mg of GO flakes was sonicated for two hours before being sprayed onto 1x1cm squares of aluminum sheets at masses of 2, 12, 27, 60, 98 μg per square centimeter. Raman spectroscopy was conducted on the individual samples with three scans of equal area size being taken of each sample. The areas below the spectroscopy peaks for each sample were recorded and a calibration curve was constructed, which correlates area below peaks with the mass loading of GO (Fig. 1).

Calibration Curve (GO mass vs. Area)
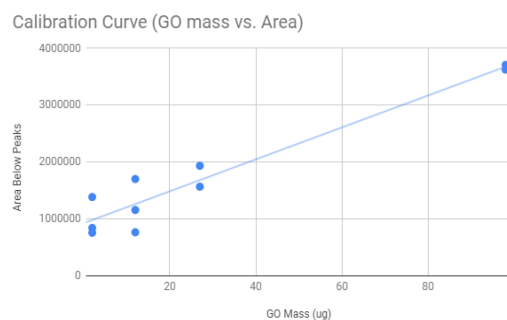
Four fuel cells were constructed with a platinum loading on the 5cm² electrodes of 2.6mg and 5.1mg for the anode and cathode, respectively. Two separate membrane electrode assemblies (MEAs) with 10μg and 20μg of GO solution sprayed on their electrodes were produced. Another MEA was also constructed with 1μg of GO solution spray-coated on the Nafion membrane. Each MEA was hot-pressed at 266°F and compared to a control cell that contained no GO.

Initial polarization curves and CV curves for each MEA were plotted at 60°C and 80°C, as well as after 5000 and 10000 cycles. As shown in Figure 2, both MEAs with the modified electrodes produced significantly lower power outputs than the control MEA. It is believed that the mass-loadings of GO may have been too high and were inhibiting electron movement within the fuel cell as evidenced by a high impedance spectrum. The MEA with 1μg of GO on its membrane, however, performed significantly better than the control fuel cell, validating that a lower mass loading than the other GO fuel cells would better optimize performance.
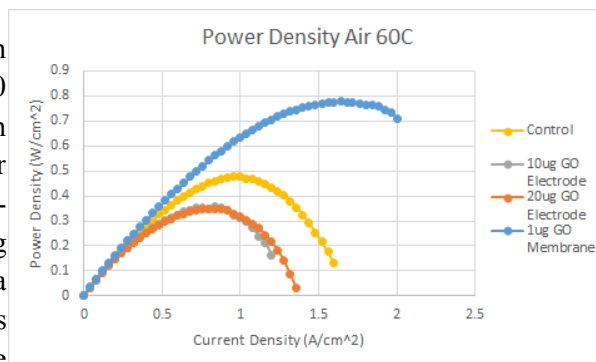
Figure 2. Power Curves for the 4 MEAs

Further work will be done to compare the reduction in active platinum catalytic area within the cells after running many cycles. More MEAs will also be produced to find the mass loading of GO on both the electrodes and the membrane that will have the greatest power output. Tests could also be run with gas feeds containing carbon monoxide to test GO's ability to prevent CO poisoning of the MEAs.

---

[1] Steele, B. C., & Heinzel, A. (2011). Materials for Sustainable Energy. Retrieved from https://www.worldscientific.com/doi/abs/10.1142/9789814317665_0031.

[2] Zarrin, H., Higgins, D., Jun, Y., Chen, Z., & Fowler, M., (2011). The Journal of Physical Chemistry, 115(42), 20774-20781. Retrieved from https://pubs.acs.org/doi/abs/10.1021/jp204610j.

Application of Electrospinning Deposition to Enhance Single and Triple MEA Performance in Polymer Electrolyte Membrane Fuel Cells

Zipei Liu[1], **Guan Hao Chen**[1], **Audrey Shine**[1], **Danielle Kelly**[1], **Likun Wang**[2], **Miriam Rafailovich**[2]
[1]Shenzhen Middle School, Shenzhen, China; [1]St. George's School, Vancouver, Canada; [1]Plainview Old-Bethpage JFK High School, Plainview, NY: [1]Friends Academy, Locust Valley, NY; [1]; [2]Department of Materials Science & Engineering, Stony Brook University, NY[5]

From the dawn of the industrial revolution, fossil fuels have remained the primary source of energy, threatening the fragile balance on our planet through ever-increasing carbon emissions. Standing at the cutting edge of material science, Polymer Electrolyte Membrane Fuel Cells (PEMFCs) provide an alternative source of clean energy through the reduction-oxidation reaction of hydrogen and oxygen gas. Although Langmuir-Blodgett through and air spraying techniques have served as the primary methods of catalyst ink deposition, this study applies electrospinning techniques to enhance electrical conduction across electrodes[1]. By producing 3D nanofiber structures, we aim to increase the surface area to volume ratio for catalysis, promote proton transport, and ultimately, optimize hydrogen fuel cell performance.

To accomplish this, different polymers were tested until (Poly(acrylic acid))[2] was chosen for its optimal viscosity and conductivity. When mixed in a 4:1 weight ratio with Nafion to create a base solution, fibers of consistent diameter (1 μm) were produced with Pt/C nanoparticles effectively attached, as demonstrated by SEM imaging (Fig. 1). The final solution consists of 4.10 wt % Pt/C, 8.73 wt % Nafion and 2.18 wt % PAA and was electrospun at a potential difference of 12.5 kV and a syringe pumping rate of 0.5 mL/hr onto microporous carbon electrodes, achieving a Pt loading of around 0.100 mg/cm^2.

Fig. 1: SEM of electrospun fibers from a 5.88% (polymer conc.) solution with Pt/C attached
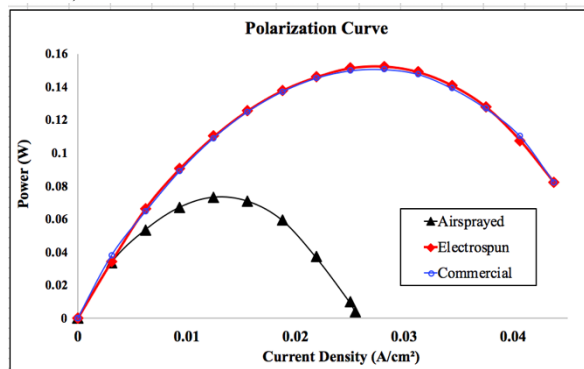
Fig. 2: Polarization Curve of airspray control MEA vs. electrospun MEA with same Pt loading and solute ratio

The electrospun electrodes, commercial electrodes, and airsprayed electrodes were then tested in an H-tech PEMFC kit in an open-air environment at the cathode with pure hydrogen being fed into the anode. The PEMFC tests indicate overall that electrospinning enhanced fuel cell efficiency. 0.1 mg/cm^2 Pt loading from electrospinning exhibited a 108% increase in max power output compared to 0.1 mg/cm^2 Pt loading from airspraying. Going forward, electrospinning solutions will be continually prepared to perfect the ratios of PAA, Nafion and Pt/C and optimize fiber formation. Polarization measurements will be recorded in pure air, 0.1% carbon monoxide, and triple MEA settings to determine if the fiber structure consistently enhances performance. Finally, Graphene Oxide and Au-Ag nanoparticles, which has previously been shown to mitigate CO poisoning, will be incorporated into the electrospinning solutions. We will proceed to compare the surface morphologies and performance of the fiber composites with the ultimate goal of identifying the most promising combination.

[1] Brodt M et al. Fabrication, In-Situ Performance, and Durability of Nanofiber Fuel Cell Electrodes. J. Electrochem. Soc. 2015; 162.

[2] Chen, H., Snyder, J. D., & Elabd, Y. A. (2008). Electrospinning and solution properties of Nafion and poly (acrylic acid). *Macromolecules*, *41*(1), 128-135.

Utilizing ALD-Coated Titanium Dioxide as a Gold Nanoparticle Catalyst Support in Electrodes to Increase Efficiency Proton Exchange Membrane Fuel Cells

Alice Fontaine[1], Allison Hsu[2], Anjali Singh[3], Kenneth Chan[4], Likun Wang[5], Miriam Rafailovich[5]
[1]Thomas Jefferson High School for Science and Technology, Alexandria, VA 22043, [2]Syosset High School, Syosset, NY 11791, [3]Novi High School, Novi, MI 48375, [4]Boston University, Boston, MA 02215, [5]Department of Materials Science and Engineering, Stony Brook University, Stony Brook, NY 11794

Proton exchange membrane fuel cells (PEMFCs) are increasingly being used for their lack of pollution and clean reactants and by products[1]. However, in real-life applications, the PEMFCs face carbon monoxide (CO) poisoning from hydrogen gas and atmospheric air impurities. The CO binds to the platinum at active catalyst sites of the electrodes, greatly lowering their electrochemical ability. Previous studies have found that gold nanoparticles (AuNPs) effectively catalyze the CO oxidation at low temperatures. Additionally, thin layers of titanium dioxide (TiO_2) are effective catalytic support[2]. In this study, our team investigated the effect of coating the electrodes with ALD-coated TiO_2 and AuNPs on the PEMFCs and the optimal number of layers of TiO_2 to allow the highest power output in the fuel cell.

Figure 1: Graph of polarization curves (Power density vs current density) of the control electrodes, as well as 1, 3, and 5 cycles of Titanium Dioxide, with and without gold

Atomic layer deposition (ALD) of TiO_2 was done on two 4cm x 4cm electrodes of 0.1 g/cm_2 Pt/C at 80°C using precursors of titanium tetraisopropoxide (TTIP) and water from 1 to 5 cy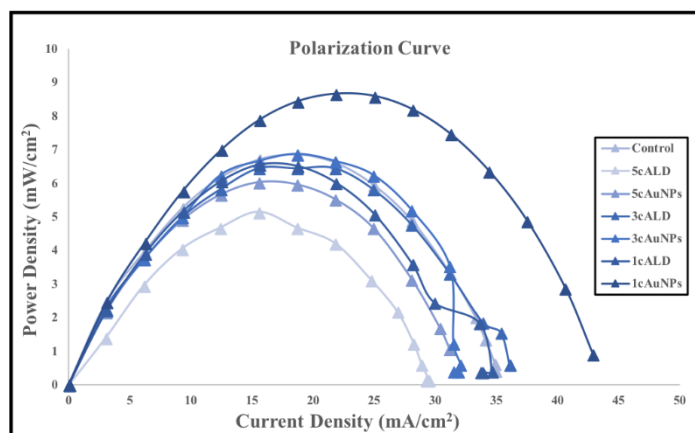cles. An AuNPs solution of 1mg/mL in toluene was created and synthesized through the Brust method. A Langmuir-Blodgett (LB) trough was used to coat a gold nanoparticle monolayer onto the TiO_2-coated electrodes. The electrodes were tested in a fuel cell test station (BK Precision 8601 DC Electronic Load single stack) with Nafion membrane. Tests were run with currents from 0.000A to 0.700A at 0.050A intervals timed at 30 seconds per interval to determine voltage and power output.

The power output of electrodes with a single layer of TiO_2 and AuNP coating had the highest power output of those tested, as shown in figure 1, with a peak of 0.1387 watts. This wattage is a 27% increase in power output in comparison to the power output of the control, which was found using uncoated electrodes. In general, the AuNP coat increased the power output for each amount of TiO_2. The trial with the worst power output, having a peak power output of 0.032 watts, 5 cycles of TiO_2 and no AuNPs confirms the previous research that TiO_2 is an effective catalyst support for AuNPs in the oxidation of CO, as TiO_2 alone blocks the flow of

Figure 2: TEM image of gold nanoparticles

protons through the PEM, but helps AuNPs catalyze CO. To confirm an even coat of AuNPs, photos were taken under a transmission electron microscope, as shown in figure 2, and analyzed using ImageJ. The average particle size was found to be 2.46 nanometers.

Further characterization tests such as ellipsometry to determine the thickness of TiO_2 and TEM imaging of the TiO_2 to find the distribution of particles will be done. Other future work includes testing the durability of the electrodes by running it through 33,000 cycles in the fuel cell test station, and CO will be cycled through the hydrogen fuel cell to test the effectiveness of the AuNPs.
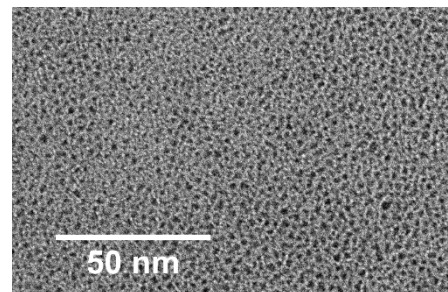
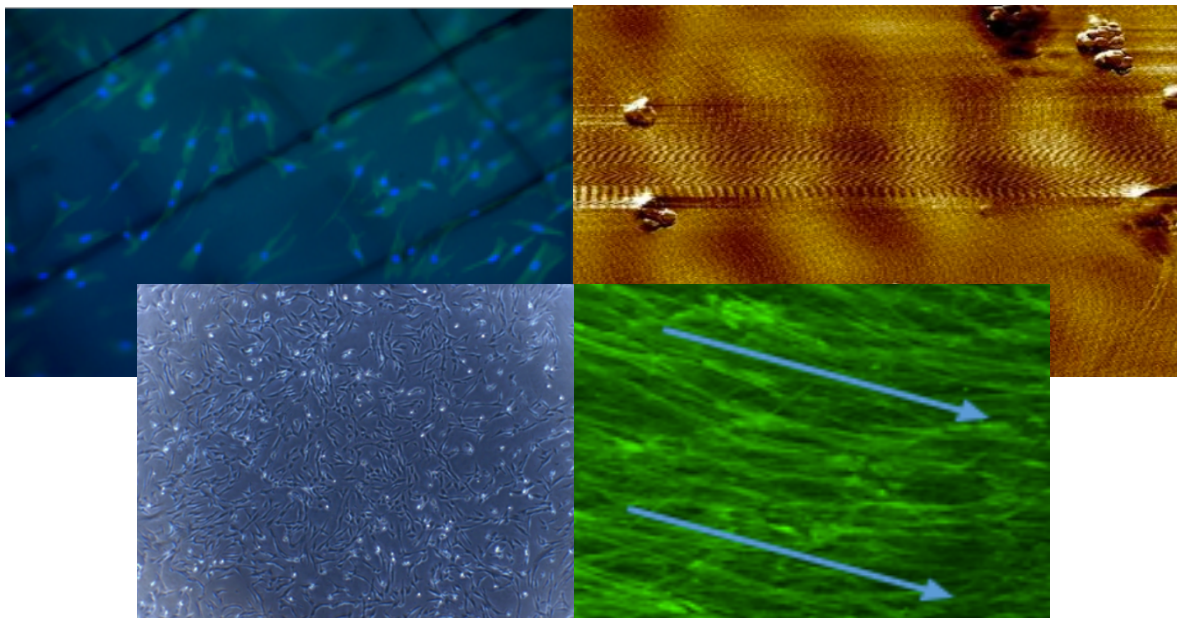[1]Cusick, Daniel. "Fossil Fuel Use Continues to Rise." Scientific American, Springer Nature. Web. 5 Oct. 2013.
[2]Haruta, M. "Nanoparticulate Gold Catalysts for Low-Temperature CO Oxidation."ChemInform, vol. 35, no. 48, 2004, doi:10.1002/chin.200448226

Session 5: Dental Pulp Stem Cells

Chairs:
Kuan-Che Feng, Linxi Zhang,
Ya-Chen Chuang, Xianghao Zuo,
Juyi Li

The Effect of the Surface Characteristics of 316L Stainless Steel on Cell-Substrate Interaction and its Implications for Biomedical Applications

Gemma Schneider [1], Michael Cuiffo [2], Xianghao Zuo [2], Juyi Li [2] , Miriam Rafailovich [2], Adriana Pinkas-Sarafova[2]

[1] Roslyn High School, Roslyn NY, 11576

[2] Department of Material Science and Chemical Engineering, Stony Brook University, Stony Brook NY, 11790

Despite myriad advances in materials, techniques, and implant design, implant failure remains a significant concern in the clinical world. In an effort to reduce implant failure rates, researchers have been investigating new ways to modify the surface of implants in order to promote implant-tissue integration, or osseointegration [1]. Many of these methods, such as an already FDA-approved laser rostering method, are expensive and time-consuming. We are thus looking at the potential of a novel, cost and time effective method to promote osseointegration: chemical etching using Vilella's Reagent. Commercially available 316L stainless steel (316L SS) is used for orthopedic implants due to its desirable structural properties, biocompatibility, and proven success in load bearing and fixation [2]. Because of its known benefits, we chose to utilize 316L SS in our study in which we investigated four prototypes: chemically etched wrought 316L SS, polished wrought 316L SS, chemically etched 3d-printed 316L SS, and polished 3d-printed 316L SS.

Each 316L SS sample was printed under identical conditions using a Renishaw AM250. Scanning electron microscopy (SEM) was used to assess the surface roughness (figure 1). All four prototypes were compared for ability to promote dental pulp stem cell (DPSC) attachment, proliferation, and differentiation. DPSCs were plated onto 3d printed and wrought 316L etched and non-etched samples and were cultured in the same medium (αMEM, 10% FBS, 0.002M Asc. acid, 0.01M β Glycerol phosphate). Alamar blue staining and EVOS FL imaging for fluorescence and transmitted light applications were used to monitor cell proliferation and cell-substrate interaction, respectively.
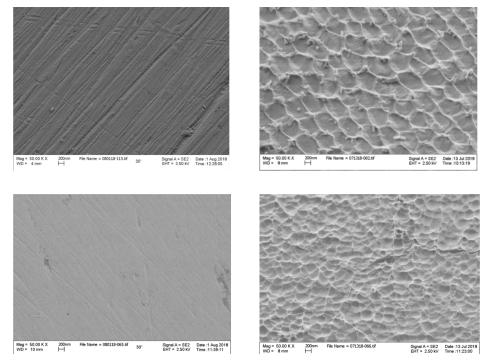
Figure 1. Pictured above are scanning electron microscope (SEM) images of the 3d printed 316L SS before (top left) and after (top right) etching with Vilella's Reagent and of wrought 316L SS before (bottom left) and after (bottom right) etching with Vilella's Reagent. All images were captured at a magnification of 50.00kx.

We performed x-ray photoelectron spectroscopy (XPS) on the 3d printed steel before and after etching in order to confirm that the etching process did not yield an unfavorable surface chemistry. The contact angle of each surface was then measured, which allowed us to confirm that the etching process increased the hydrophilicity of the surface. Thus far, our cellular study has suggested that the etched 3d printed 316L SS is the most favorable substrate in terms of cell growth (figure 2). Future work includes RT-PCR analysis of mRNA expression for DPSC differentiation, confocal imaging of actin-stained cells 24 hours after plating in order to assess cell adhesion, and a scratch test for evaluation of osseointegration.

Wrought polished 316L SS

Wrought etched 316L SS

3d printed polished 316L SS

3d printed etched 316L SS

Figure 2. Fluorescent imaging was performed 48 hours after induction. At this point, cells had grown and adhered to the substrate most effectively on the 3d printed etched 316L SS.

References:
[1] Kate MA, Palaskar S, Kapoor P. Implant failure: A dentist's nightmare. J Dent Implant 2016;6:51-6
[2] Disegi JA, Wyss H. Implant materials for fracture fixation: a clinical perspective. Orthopedics. 1989 Jan;12(1):75-9.

Investigating the Effects of ALD-Coated Titanium Dioxide on Dental Pulp Stem Cell Response to 3D-Printed PLA Scaffolds

Benjamin Chang[1], Antony Deluxe[2], Ethan Ho[3], Bhuvna Murthy[4], Rushi Patel[5], Wenqi Zhao[6], Nicholas Zumba[7], Kuan-che Feng[8], Dr. Miriam Rafailovich[8]

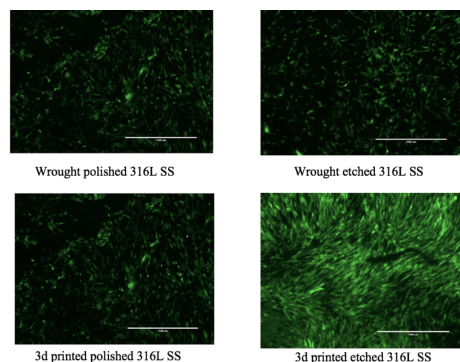[1]Woodbridge High School, Irvine, CA 92603; [2]Wheatley High School, Old Westbury, NY 11568; [3]Northfield Mount Hermon School, Gill, MA 01354; [4]Huron High School, Ann Arbor, MI 48105; [5]Herricks High School, New Hyde Park, NY 11040; [6]Milton Academy, Milton, MA 02186; [7]Columbia University, New York, NY 10027; [8]Department of Material Science and Engineering, Stony Brook University, Stony Brook, NY 11790

Poly-lactic acid (PLA), a synthetic biodegradable poly-lactone, is commonly used in the tissue engineering field for its suitable mechanical properties and biocompatibility[1]. In particular, its thermoplastic characteristics can be harvested by 3D-printing technology to create scaffolds for cell growth. However, the polyester surface is characterized by a suboptimal hydrophobicity for cell adhesion, which may limit its use[2].

In this study, 3D-printed PLA scaffolds are coated with a thin, uniform layer of titanium dioxide (TiO_2) through Atomic Layer Deposition (ALD) to create an environment for dental pulp stem cells (DPSCs) attachment, proliferation, and differentiation.

Figure 1 SEM analysis for uncoated (a) and TiO_2-coated (b) 3D-printed PLA scaffolds. Titanium peak is found on the coated scaffolds EDX image only, confirming the uniformity of ALD-coated TiO_2.

Circular disks of 12 mm in diameter and 2 mm in height were prepared using PLA filaments through 3D-printing at 50 mm/s and 230℃ as well as molding at 180℃ and 7 psi to compare the cell response on rough and smooth surfaces. ALD was performed at 85℃ for 50 cycles to produce a 5 nm layer of TiO_2 on the surface of the scaffolds. Scanning electron microscopy (SEM) was conducted on the scaffolds, and the results confirmed that ALD of TiO_2 was uniform (Fig. 1). The Atomic Force Microscopy (AFM) analysis revealed that the TiO_2-coated 3D-printed scaffolds have uniform, nanoscale roughness compared to the uncoated counterparts. DPSCs were plated on the scaffolds in Alpha MEM medium plus 10% Fetal Bovine Serum (FBS) at an initial 9×10^3 cell/mL. After day 1, the medium was changed every other day with Alpha MEM, 10%FBS, 200nM ascorbic acid and 10mM ß-glycerophosphate until the end of the experiment. Cells were counted and visualized on day 1, 4, and 7 through fluorescence staining and microscopy (Fig. 2). Cell number on day 1

Figure 2 Fluorescence microscopy images on Day 1 of 3D-printed ALD scaffolds (a), 3D-printed uncoated scaffolds (b), molded ALD scaffolds (c), and molded uncoated scaffolds (d). Scale bars represent 400µm.
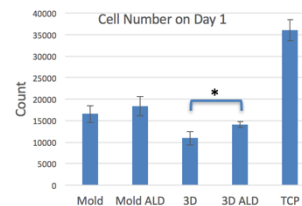
Figure 3 Average cell number on day 1 for different types of scaffolds and control (n=3). The asterisk represents significant difference between 3D and 3D ALD (p<0.05).
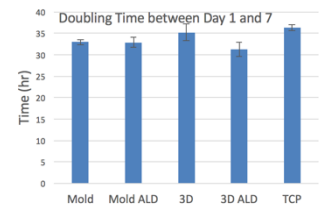
Figure 4 Average doubling time from day 1 to day 7 for different types of scaffolds and control (n=3). None of the treatment groups display significant difference from each other (p>0.05).

measured showed that on rough surfaces of the 3D-printed scaffolds, ALD coating significantly increased cell attachment (p<0.05) (Fig. 3). The calculated doubling time between day 1 and day 7 displayed no significant difference from each other regardless of scaffold type, signifying overall cell health (Fig. 4). Future research will be conducted on the differentiation through RT-PCR analysis and biomineralization of DPSCs through SEM analysis on Day 28 and 42.

1 Lopes MS, Jardini AL, Maciel R. Poly (lactic acid) production for tissue engineering applications. Chisa. 2012;42:1402–13.

2 Haddad, Tanit, et al. "Fabrication and Surface Modification of Poly Lactic Acid (PLA) Scaffolds with Epidermal Growth Factor for Neural Tissue Engineering." Biomatter, vol. 6, no. 1, 2016.

Evaluating the Effects of Graphene-Loaded Polylactic Acid Electrospun Fibers and Spun-cast Thin Films on the Proliferation and Differentiation of Dental Pulp Stem Cells

Sahith Vadada[1], Kavya Rao[2], Ashley Blatt[2], Diana Passariello[3], Kasim Waqar[4], Linxi Zhang[5], Miriam Rafailovich[5]

[1]Herricks High School, New Hyde Park, NY 11040; [2]Half Hollow Hills East, Dix Hills, NY 11746; [3]Columbia University, New York, NY 10027; [4]Binghamton University, Binghamton, NY 13902; [5]Department of Materials Science and Engineering, Stonybrook University, Stonybrook, NY 11790

As research in biomedical engineering continues to peak the interest of many scientists, studies utilizing dental pulp stem cells (DPSCs) have played a major role in the development of scaffolds. DPSCs are easily accessible and have a multilineage differentiation potential. The polymer scaffold we used is polylactic acid, rather than the more commonly used polystyrene(PS)-based tissue culture plastic. PLA is a biodegradable, bioabsorbable, and biocompatible polymer that has several applications in stem-cell based tissue engineering and drug delivery.[2] Adding a material like graphene, which holds many unique mechanical, chemical, and electrical properties, can have a powerful effect on how cells interact on biocompatible scaffolds.

The primary goal of our research was to test the effect of graphene in PLA electrospun scaffolds on the differentiation and proliferation of DPSCs. To initiate the experiment, we created four different solutions of varying concentrations of PLA and graphene. Two samples of 12.5% PLA/chloroform and 5 mg/ml PLA/chloroform solutions were created for electrospinning and spincasting. These solutions were reproduced with the addition of 3% graphene. PLA thin film substrates were spun-cast with and without graphene at 2500 rpm for 30 seconds each. Fibers were electrospun on silicon wafers and glass slides at 1 mL/hour and 20 kV. After electrospinning and spincasting were completed, DPSC cultures were prepared for a 28-day analysis to study cell proliferation and differentiation.

Scaffolds were characterized by SEM and AFM images. Graphene aggregations formed on thin films. After determining the diameter of the PLA fibers from Figure 1 SEM images, we discovered PLA/graphene fibers had a high dispersion rate. Cell counts showed that growth rates were similar for both fiber samples. Confocal microscopy was performed to view cell morphology, and 40x magnification images in Figure 2 displayed that cells grew linearly along electrospun fibers. PLA/graphene thin films inhibited the extension of some actin filaments. PLA and PLA/graphene fibers had low proliferation rates, as shown in Graph 1 , indicating a possible cell confluency on day 7. On days 7, 14, and 28, RT-PCR, SEM/EDX, and confocal microscopy will be conducted to measure differentiation and biomineralization of DPSCs. While microscopy will determine if the deposits and proteins display differentiation, RT-PCR will measure several differentiation gene markers, including osteocalcin and dentin sialophosphoprotein. These genes will indicate relative levels of osteogenic and odontogenic differentiation.
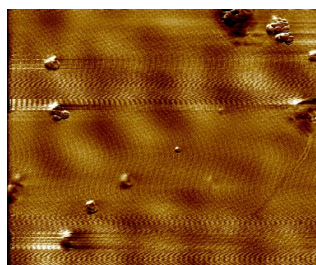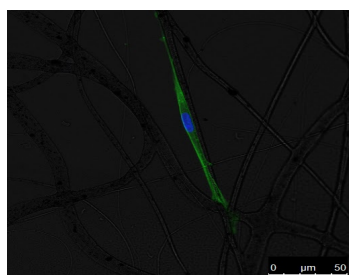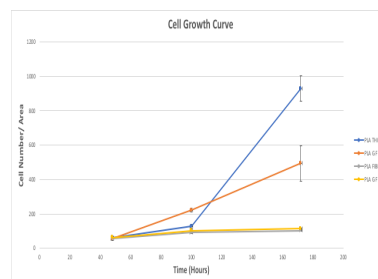
Figure 1: AFM characterization   **Figure 2: DPSCs are elongated on fibers**   **Graph 1: DPSC growth curve**

[1] Mabel M Cordeiro, Tomoatsu Kaneko, Zhihong Dong, Zhaocheng Zhang, Marta Miyazawa, Songtao Shi, Anthony J. Smith, Jacques E Nor. Dental Pulp Tissue Engineering with Stem Cells from Exfoliated Deciduous Teeth. Journal of Endodontics , Volume 34 , Issue 8 , 962 - 969.

[2] Lopes, M. Savioli, A. L. Jardini, and R. Maciel Filho. "Poly (lactic acid) production for tissue engineering applications." *Procedia Engineering* 42 (2012): 1402-1413.

Investigating the Effects of Substrate Mechanical Patterns on Proliferation and Differentiation of Dental Pulp Stem Cells

Albert Zhu[1], Grace Liu[2], Jessica Hofflich[3], Ya-Chen Chuang[3], Miriam Rafailovich[3], Marcia Simon[4]

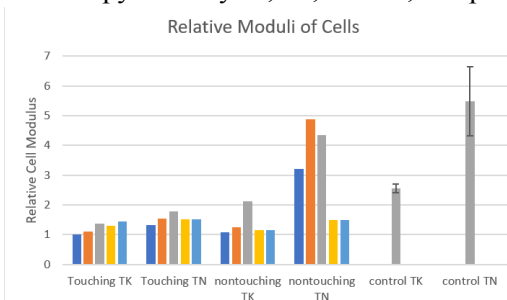[1] Our Lady of Lourdes High School, Poughkeepsie, New York, [2] Bayview Secondary School, Richmond Hill, Ontario, Canada, [3] Department of Materials Science and Chemical Engineering, Stony Brook University, Stony Brook, [4] Stony Brook University School of Dental Medicine, Stony Brook

Previously, stem cell differentiation control has relied heavily on chemical signals, but new research has demonstrated that it can be controlled by the mechanical properties of a cell's surroundings. Multipotent dental pulp stem cells (DPSCs) can differentiate into odontoblasts, osteoblasts, and adipocytes and are sensitive to the hardness of their substrate.[1] Odontogenesis is supported by hard thin spin-cast polybutadiene films and inhibited by soft thick films.[2] It is hypothesized that, during odontogenic differentiation, stem cells transmit signals that promote or inhibit differentiation. Hence, cells were plated in touching and non-touching conformations to determine whether these signals are transmitted physically or through the medium.

3 mg/mL and 20 mg/mL concentrations of polybutadiene/toluene were prepared and spun cast onto Si wafers to create 20nm and 200nm thin films. 2x2 cm wafers with thick or thin films were used as controls in isolated wells, and 4 1x1 cm wafers were placed with alternating thick and thin films so that they were all touching or all non-touching. Strain 13 DPSCs were plated at 5×10^3 cells/cm^2, fed every 2 days with osteogenic media of α-MEM, 10% FBS, Pen Strep, L-ascorbic acid, and β-glycerol phosphate and incubated at 37°C and 5% CO_2. On day 7, the relative moduli of the cells were measured using shear modulation force microscopy. On days 7, 14, and 28, samples were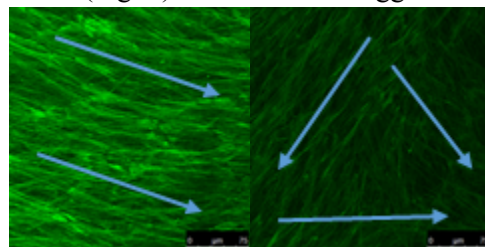 stained for confocal microscopy with AF488 and DAPI for F-actin and nuclei respectively and prepared for reverse transcription polymerase chain reaction (RT-PCR) using QIAzol Lysis Reagent.

Figure 1: Day 7 SMFM Cell Modulus Data

On day 7, the relative modulus was low for cells on thick films and high for cells on the thin film control. However, all cells on touching thin films and some on non-touching thin films had low relative modulus (Fig. 1). In confocal images, all cells had abundant amounts of actin and were therefore healthy[3]. However, actin on thin films tended to be randomly oriented while actin on thick films were oriented in one direction, which may explain the differences in moduli (Fig. 2). These results suggest that cells on thick films influenced differentiation of cells on thin films in co-cultures through media.

On day 28, biomineralized crystals will be characterized using Raman and scanning electron microscopy, and mRNA will be analyzed using RT-PCR to determine if odontogenic and osteogenic differentiation have occurred. This is identified by gene markers, specifically ALP, OCN, and DSPP. To produce more suitable *in vivo* conditions, microscale patterns will be created through laser etching, and nanoscale patterns by spin casting polybutadiene-polystyrene mixtures, which will phase-separate and create bumpy surfaces.

Figure 2: Day 14 thick vs thin film confocal images

[1]Chang, Chung-Chueng, et al. "Entangled Polymer Surface Confinement, an Alternative Method to Control Stem Cell Differentiation in the Absence of Chemical Mediators." *Advances in Materials Science and Engineering*, vol. 1, no. 3, 24 Sept. 2014, pp. 1-7.

[2]Even-Ram, Sharona, et al. "Matrix Control of Stem Cell Fate." *Cell*, vol. 126, no. 4, 25 Aug. 2006, pp. 645-47.

[3]Cooper, Geoffrey M. "Structure and Organization of Actin Filaments." *The Cell: A Molecular Approach*, 2nd ed., Sinauer Associates, 2000.

Utilization of P4VP and Graphene to control Dental Pulp Stem Cell Neurogenesis

John Chen[1], Zaiff Khan[1], Rebecca Isseroff[1], Linxi Zhang[2], Kuan Che Feng[2],
Dr. Marcia Simon[3], Dr. MiriamRafailovich[2]

[1]Lawrence High School, Cedarhurst, NY 11581
[2]Department of Material Science and Engineering, Stony Brook University, Stony Brook, NY, 11794
[3]Department of Oral Biology and Pathology, School of Dental Medicine, Stony Brook University, Stony Brook, NY 11794

Currently, the central nervous system is unable to heal effectively by itself, leading to a search for ways to regenerate or grow neurons for replacement. Dental Pulp Stem Cells (DPSCs) are multipotent stem cells that have exhibited the ability to differentiate into osteoblasts, cardiac cells, and neurons. Since DPSCs are easily acquired from extracted wisdom teeth and can provide cells in various areas resulting in an autologous implant, preventing rejection by the patient, DPSCs show a promising hope in biomedical research and engineering.[1] P4VP, a polymer shown to retain cell morphology, can help cells adhere to a substrate, potentially eliminating the need for polyornithine.[2] Graphene, known for its electrical conductivity, may prove useful in the differentiation of DPSCs into neurons, since neurons communicate through electrical impulses called synapses.[3] This experiment compares the effects of P4VP, graphene, polyornithine, and the presence of fibers, on DPSCs and their differentiation into neural cells. Cell functions will be monitored using microscopy and differentiation verified by Real-Time Polymerase Chain Reaction (RT-PCR) using primers for neurogenic markers (e.g., nestin, tubulin III, NF-M).

For spincasting, P4VP was dissolved in DMF at 7 mg/ml with or without 3% graphene by mass to P4VP). For electrospinning, P4VP at 25% by mass was dissolved in a 5:1 ratio of ethanol and DMF with or without 3% graphene by mass to P4VP. For evaluations of mRNA expression, 2x2 cm silicon (Si) wafers were used. These wafers were first cleaned using a 3:1:1 ratio of piranha solutions. Si wafers were spuncast at 2000 rpm for 30 sec along with glass coverslips, for optical microscopy, for 45 seconds. Half of the samples were also electrospun at 15k V and 3 mL/hr to create fibers (Figure 1). This experimental setup was replicated, one setup coated with polyornithine, the other without. All samples were treated with laminin (5 µg/mL) overnight. Glass coverslips were placed in 24 well plates and plated with 33,000 cells in 1 mL Growth Media (alpha MEM supplemented with 10% fetal bovine serum, 0.1 mM L-ascorbic acid 2-phosphate, 2 mM L-glutamine), and Si wafers were placed in 6 well plates, plated with 150,000 cells in 3 mL growth media. A positive control of tissue culture plastic was also plated. Cells were cultured in Growth Medium for 2 days, after which the media was replaced with neuronal growth media (Neurobasal A Medium, B27, 20 ug/ml EGF, 40 ug/mL FGF2), changing every 2-3 days for 21 days. During the first week there was no significant difference between the control and thin films. The cells growing in fiber samples tended to elongate and grow parallel to the fiber structures surrounding them with a higher confluency on P4VP fibers alone, compared to P4VP with graphene fibers (Figure 1). Future Work includes conducting confocal microscopy with F-actin staining and RT-PCR with early, middle, and late neurogenetic markers after 21 days of growth.
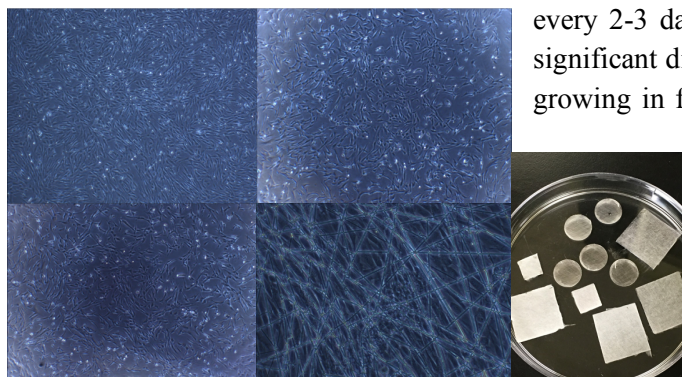
Figure 1: Control Tissue Culture Plastic (Top-Left), P4VP (Top-Right), P4VP + Graphene (Bottom-Left), P4VP Fiber (Bottom-Right), Electrospun Samples (Far-Right))

[1] Potdar, Pravin D, and Yogita D Jethmalani. "Human Dental Pulp Stem Cells: Applications in Future Regenerative Medicine." *World Journal of Stem Cells* 7.5 (2015): 839–851. *PMC*. Web. 5 Aug. 2018

[2]Comprehensive Review on the Use of Graphene-Based Substrates for Regenerative Medicine and Biomedical Devices , Sachin Kumar and Kaushik Chatterjee, ACS Applied Materials & Interfaces 8(40):26431-26457, 2016.

[3]Yihuan Tsai, Josh Cutts, Azuma Kimura, Divya Varun, David A. Brafman, A chemically defined substrate for the expansion and neuronal differentiation of human pluripotent stem cell-derived neural progenitor cells, Stem Cell Research, 15(1):75-87, 2015.

The Effects of TiO$_2$ Nanoparticles on the Proliferation and Differentiation of Dental Pulp Stem Cells

Mindy Li[1], Samantha Ying[2], Ya-chen Chuang[3], Delivrance Jenkins[4], Miriam Rafailovich[3]

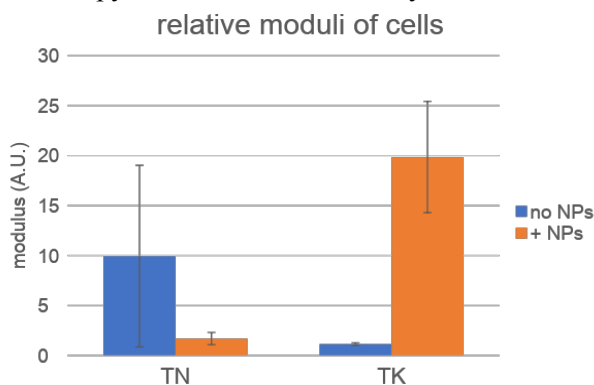[1]Princeton High School, Princeton, NJ 08540
[2]South Side High School, Rockville Centre, NY 11570
[3]Department of Materials Science and Engineering, Stony Brook University, Stony Brook, NY 11794
[4]Suffolk County Community College, Brentwood, NY 11717

The development of stem cell research has had a tremendous impact on the advancement of regenerative medicine, drug testing, and our understanding of the human body. Although stem cells were previously retrieved from embryos, several studies show that mesenchymal stem cells (MSC) have multipotency. Scientists have been investigating the abilities of dental pulp stem cells (DPSC), a type of MSC that can be found in the third molar[1]. DPSCs can be cryopreserved for future use and, when given the right environment, can develop into a myriad of different cells[2]. Titanium dioxide is most commonly used as a whitening agent in toothpastes and food products, with a small portion present in the form of nanoparticles (NPs). Recently, a study showed that the cellular uptake of TiO$_2$ NPs had adverse effects on the cell viability and growth of MSCs[3].

This study was conducted to further examine the effects of TiO$_2$ NPs on the proliferation as well as the differentiation of stem cells, specifically for osteogenesis and odontogenesis. To create a suitable substrate for the cells to attach to, thin (TN) and thick (TK) polybutadiene (PB) films were prepared by spin-casting 3 mg/mL and 20 mg/mL solutions on 1-by-1 and 2-by-2 cm^2 silicon wafers of Miller index [100]. After samples were annealed for five hours at 150°C at 2.0×10^{-7} torr, the PB films were determined to be ~20 nm thick and ~200 nm thick for TN and TK, respectively, through ellipsometry. The AV3 strain DPSCs were plated with a density of 5000 cells per cm^2, and rutile TiO$_2$ NPs were added at a concentration of 0.1 mg/mL the following day. Cell count was conducted on days 1, 3, and 6 with a hemocytometer. Atomic force microscopy (AFM) was used on day 5 to measure cell modulus (see Figure 1). A strange phenomenon was found where the addition of NPs made cells on the thick film harder and on the thin film softer. When the stained DPSCs were further examined with confocal microscopy (see Figure 2), the actin fiber growth supported the moduli data. Samples were collected for confocal microscopy and for real-time polymerase chain reaction (RT-PCR) on days 7, 14, and 28 and for scanning electron microscopy (SEM) on day 14 and 28. Confocal microscopy was used to examine actin fiber growth on day 14 (see Figure 2) as well as the nuclei of the DPSCs. SEM will allow us to examine the biomineralization on the films, and Raman microscopy to further confirm its crystal structure. Using RT-PCR, we can observe the mRNA expression for up-regulation of alkaline phosphatase, osteocalcin, and dentin sialophosphoprotein gene marker to monitor the differentiation pathways.

Figure 1. Relative moduli of cells measured on day 5 with AFM. TK/NPs saw a higher modulus than its control while TN/NPs had a lower modulus.
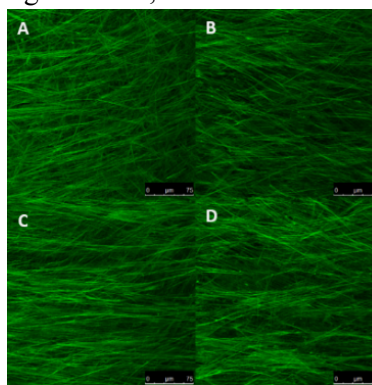
Figure 2. Confocal microscopy of actin stained with AF488 on day 14 samples for (A) TN (B) TN/NPs (C) TK (D) TK/NPs. Thick actin fibers are visible, indicating healthy cell growth.

[1] Atari, M., Gil-Recio, C., Fabregat, M., Garcia-Fernandez, D., Barajas, M., Carrasco, M. A., . . . Giner, L. (2012). Dental pulp of the third molar: A new source of pluripotent-like stem cells. *Development,139*(20). doi:10.1242/dev.089292

[2] Potdar, P. D., & Jethmalani, Y. D. (2015). Human dental pulp stem cells: Applications in future regenerative medicine. *World Journal of Stem Cells,7*(5), 839-851. doi:10.4252/wjsc.v7.i5.839

[3] Cai, K., Hou, Y., Li, J., Chen, X., Hu, Y., Luo, Z., . . . Lai, M. (2013). Effects of titanium nanoparticles on adhesion, migration, proliferation, and differentiation of mesenchymal stem cells. *International Journal of Nanomedicine,*3619-3630. doi:10.2147/ijn.s38992

Session 6: Environmental Protection

Chairs:
Yuan Xue & Xianghao Zuo

A Novel Fire Retardant Solution to Mitigate the Onset of Wildfires

Joshua Vilkas [1], Pik Hoi Lam [2], Nicole Jacobsen [3], Yuan Xue [4], Xianghao Zuo [4], Miriam Rafailovich [4*]

[1] Hebrew Academy of Nassau County High School, Uniondale, NY, USA, [2] Wilson Area High School, Easton, PA, USA, [3] Plainedge High School, Massapequa, NY, USA, [4] Department of Materials Science and Engineering, Stony Brook University, Stony Brook, NY, USA.

The dangers of wildfires have been brought to the public's attention recently as a Greek forest fire took the lives of nearly 91 innocent civilians[1]. The demand for a proper fire retardant to stop the spread of a blaze before it reaches residential areas is growing, and it is important to therefore ensure that the fire retardant is safe (non-toxic, etc.) for the environment and the organisms that inhabit it. The experiment's goal is to engineer an aqueous solution that can coat leaves and actively prevent the spread of wildfires. The leaf species used is *Cornus kousa*, a subspecies of the *Cornus,* or Dogwood family, and is freshly-picked from a local tree.

Table 1 Burning test of leaves

Solution	Time to self-extinguish fresh leaf	Time to self-extinguish dry leaf
Control	56.14 sec	6.94 sec
Solution A	<1 sec	<1 sec
Solution B	<1 sec	<1 sec
Solution C	<1 sec	<1 sec

The leaves are divided into three categories: fresh leaves, oven-dried leaves, and naturally fallen leaves. Fresh leaves are manually selected and used as a sample less than 24 hours after selection. Dried leaves are curated in a CIT Alcatel 2004A Vacuum Oven for 25 min at 90 Celcius and 400 mTorr. It is proven through burning tests that fallen leaves and oven dried leaves burn faster and easier than fresh leaves, due to the fact that fresh leaves contain 66.28% of water on average.

The research investigates the effects of solutions that consist of combinations of different concentrations of component m, component n, component o, and deionized water. The ingredients were hypothesized to form a fire retardant solution and in our current study, it is made into an aqueous solution that can be distributed onto leaves for application on live trees.

The effects of pyrolyzing the leaves are measured through the time required for self-extinguishing (Table. 1), charred area, and mass of leaves before and after burning (Figure 1). The ability of the solution to help yield char residue is analyzed through thermogravimetric analysis (TGA), shown in Figure 2. At 800°C, we could see that leaves coated with component m/DI water solution or component m/n/DI water solution yields more char than the the ones without coating. Contact angle tests are performed to determine the hydrophobicity of the solutions on the leaf surfaces, seen in Fig. 3.

In addition, a toxicity test on *Brassica rappa* (Wisconsin Fast Plants) in relation to seed germination and plant growth is performed to study the ramifications of the solutions on plants. It has been noted that varying concentrations of component m and n do not completely stop germination, but rather retard the progress of germination. Component n has been observed to retard germination the most.

Further studies are planned to test the toxicity of the solutions on animals living in the forested areas.
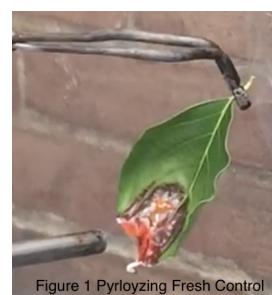

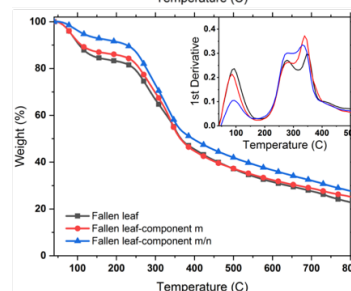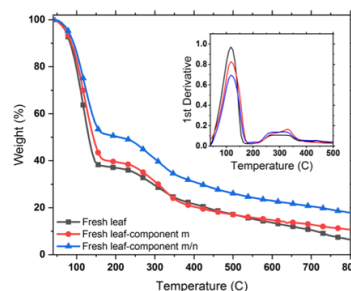Figure 1 Pyrloyzing Fresh Control

Figure 2 TGA results

Figure 3 contact angle measurements

[1] Kantouris, Costas, and Demetris Nellas. "Death Toll from Greek Wildfire Reaches 91 as Village Grieves." *USA Today*, Gannett Satellite Information Network, 29 July 2018, www.usatoday.com/story/news/world/2018/07/29/greek-wildfire-death-toll-climbs-village-mourns/860430002/.

[2] Shan He, Yichen Guo, Tehila Stone, Noah Davis, Dongwhan Kim, Taejin Kim, Miriam Rafailovich, "Biodegradable, flame retardant wood-plastic combination via in situ ring-opening polymerization of lactide monomers." The Japan Wood Research Society (2017) 154-160

The Effect of Graphene Oxide on Pheromone Evaporation in *Cimex lectularius* Traps

Bhawan Sandhu[1] , Tzipora Schein[2] , Rebecca Isseroff[1] , Harry Shan He[3], Miriam Rafailovich[3]
[1]Lawrence High School, Cedarhurst, NY 11516
[2]Hebrew Academy of the Five Towns and Rockaway, Cedarhurst, NY 11516
[3]Stony Brook University, Stony Brook, NY 11794

The infestation of *Cimex lectularius*, commonly known as bed bugs, has been plaguing homes for centuries. Rates of bed bug infestation have recently been on the rise due to resistance to the chemicals and toxins used for their extermination. A new tool against *C. lectularius* is the Fibertrap, which is considered to be more effective and less expensive than the chemicals currently used to eradicate the insects.[1]

Fibertrap incorporates fibers created by electrospinning to ensnare the fine leg hairs of *C. lectularius*. The insects are attracted to the traps because of the pheromones included, 1-Octen-3-ol and histamine. The problem with using the cost-effective pheromone 1-Octen-3-ol is that its evaporation rate is very fast, restricting the traps effectiveness to short periods of time. This research project examines using graphene oxide (GO) to prolong the effect of pheromones in *C. lectularius* traps.

Graphene oxide was first synthesised using a modified version of the Hummer's Method.[2] Graphite was dissolved using sulfuric acid (H_2SO_4) and was oxidized with potassium permanganate ($KMnO_4$) and sodium nitrate ($NaNO_3$). After oxidation, the GO was washed with distilled H_2O until the filtrate pH reached between 4 and 5. The GO was then dried in an oven at 50 degrees Celsius. Control concentrations of GO (10 mg/ml, 14 mg/ml, 20 mg/ml) were combined with H_2O. The same concentrations of GO were made with 1-Octen-3-ol. Another set was made with an additional pheromone of *C. lectularius*, histamine, along with 1-Octen-3-ol, the pheromone known to evaporate. A second set of samples was prepared using a solvent of 25% ethanol and 75% H_2O.

Fourier-transform infrared spectroscopy (FTIR) was used to identify the chemical bonds of the 1-Octen-3-ol in the 10 mg/ml solutions of GO. However, the solvents overpowered the FTIR data and no other bonds were visible. A new test was introduced to measure the decrease in mass over time of the 14 mg/ml solutions of the GO on a microgram scale, plotting the rate of evaporation for each sample. The results are shown in **Figure 1**. Future work will involve creating samples of pheromones without GO or ethanol solvent to compare the results of the mass lost and to test the bedbug's attraction to each sample .
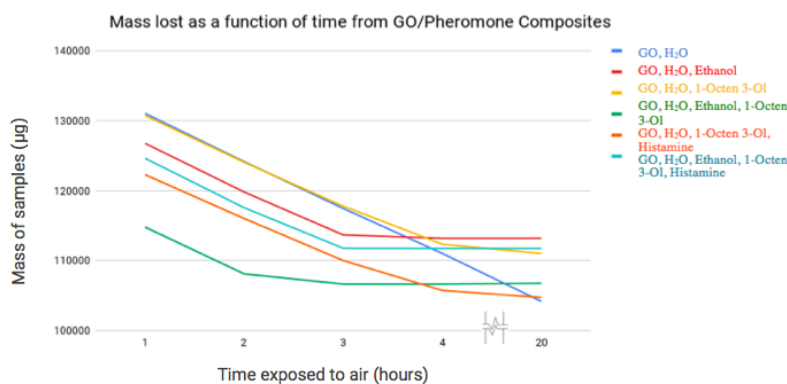
Figure 1: The mass of the 14 mg/m samples of GO and pheromones shown decreasing over time.

[1]Heitz, David. "Fibertrap Kills Bed Bugs Without Chemicals or Clean-up Crews." *Healthline*, Healthline Media, 4 June 2013, www.healthline.com/health-news/tech-new-microfiber-device-traps-and-kills-bed-bugs-06041
[2]Hummers, W. S., & Offeman, R. E. (1958, September 25). Preparation of Graphitic Oxide. J. Am. Chem. Soc. Journal of the American Chemical Society, 80(6), 1339-1339. doi:10.1021/ja01539a01

# Session 7: Nanocomposites

Chairs:
Xianghao Zuo & Yuan Xue
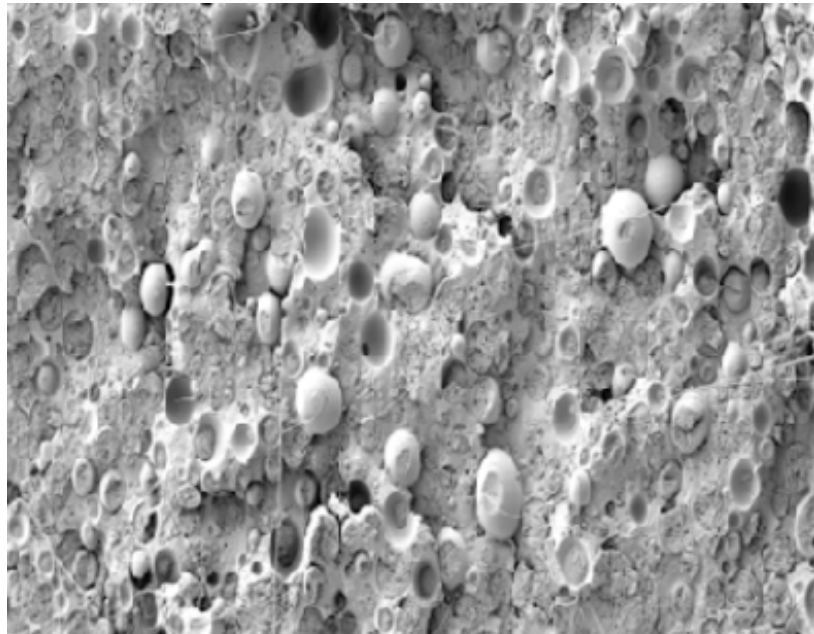
Enhancing Mechanical Properties of Biodegradable PLA using Ternary Polymer Blends

Ruilin Yin[1], Elena Urquiola[2], Xianghao Zuo[3], Yuan Xue[3], Miriam Rafailovich[3]

[1]St. Anthony's High School, South Huntington, NY 11747, [2]Hunter College High School, New York City, NY 10128, [3]Stony Brook University, Stony Brook, NY 11794

PLA is a 100% recyclable and biodegradable but weak polymer that has been used as an alternative to polystyrene in disposable cups, lids, and containers, and eating utensils. Commonly, binary blends including PLA and another polymer additive are created to enhance the mechanical properties of PLA, but this has found to be ineffective due to the high interface energy between the polymers.[1] We hypothesize that adding small concentrations of PMMA or SMMA as compatibilizers to the binary mixes will lower the interface energy between the polymers.

To create the ternary blends, the polymers were added to a C.W. Brabender and then molded into the tensile and impact test shapes using a Carver Hot Press. The blends were also run through an extruder to create filaments for 3D printing. The mechanical properties of these molded and printed ternary blends were tested using impact and tensile strength tests. We hypothesize that due to the acrylic and styrene group present in SMMA, it will act as a compatibilizer that is miscible with PLA and the styrene based polymers, lowering the interface energy and improving mechanical properties. Further analysis about the interfacial properties is done by SEM imaging.
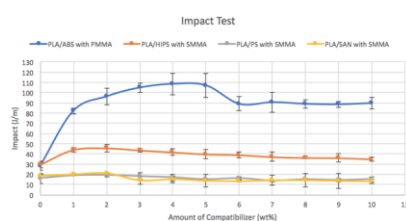

Figure 1| Impact test results for the 4 polymer blend vs compatibilizer weight

Each ternary blend contains 70% PLA and 30% styrenic polymer. The overall results of the impact test are shown in Figure 1. Among the materials we used, HIPS and ABS show a significant mechanical increase. The PLA/HIPS blend had maximum mechanical strength with 2wt% SMMA added, but as more SMMA was added, its mechanical strength weakened. A possible explanation for this is that the SMMA acts as compatibilizer and first gathers in the interface of the binary blend. As the amount of SMMA increases, the SMMA occupies the whole interface and forms a third polymer layer, because at high concentrations it is not totally miscible with either polymers.[2,3]

The SEM image of the PLA/HIPS blend with different SMMA concentrations confirmed these results, as shown in Figure 2. In Fig. 2a the blend with no SMMA shows the
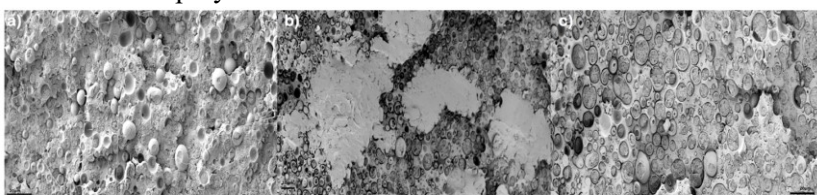
Figure 2| The SEM images of cryo-fractured surfaces: a) 70PLA30HIPS, b) 70PLA30HIPS2SMMA, and c) 70PLA30HIPS10SMMA

domain size of the HIPS matrix is ~11μm, in Fig. 2b the added 2wt% SMMA displays a significant decrease in size of the domain to ~5μm and the wrapping of HIPS by SMMA can be observed, in Fig 2c the domain size increased to ~9μm and the high concentration of SMMA formed an apparent layer around the HIPS, both contributing to the decrease of mechanical properties of the polymer blend at a high SMMA concentration. A 286% increase for the molded sample in the impact test was observed when 4wt% PMMA was used with the PLA/ABS blend. Figure 3 shows the significant improvement of impact strength for both the molded and 3D printed samples over the pure PLA and the binary PLA/ABS mix. It also shows that this ternary polymer material can maintain high mechanical properties when 3D printed.
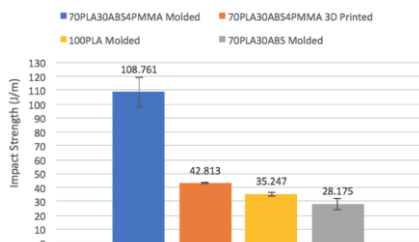
Figure 3| Impact strength test results comparison for different PMMA concentration and method

For future study, interfacial properties in the ternary blends could be investigated to reveal interactions that contribute to mechanical strength. This could be conducted using TEM and SIMS analysis.

Select References

1. Guo, Yichen, et al. "Enhancing Impact Resistance of Polymer Blends via Self-Assembled Nanoscale Interfacial Structures." *Macromolecules*, vol. 51, no. 11, 2018, pp. 3897–3910., doi:10.1021/acs.macromol.8b00297.
2. Israels, R.; Jasnow, D.; Balazs, A. C.; Guo, L.; Krausch, G.; Sokolov, J.; Rafailovich, M. Compatibilizing A/B blends with AB diblock copolymers: Effect of copolymer molecular weight. J. Chem. Phys. 1995, 102, 8149−8157.
3. Balazs, A. C.; Singh, C.; Zhulina, E. Modeling the Interactions between Polymers and Clay Surfaces through Self-Consistent Field Theory. Macromolecules 1998, 31, 8370−8381.

Enhancing Thermal Conductivity of Polylactic Acid and Polybutylene Adipate Terephthalate Blends with Boron Nitride and Graphene

Frederick Nitta[1], Vicki Xu[2], Yuan Xue[3], Xianghao Zuo[3], Miriam H. Rafailovich[3]

[1]Henry M. Gunn High School, Palo Alto, CA 94306, [2]Mission San Jose High School, Fremont, CA 94539, [3]Department of Materials Science and Engineering, State University of New York at Stony Brook, Stony Brook, NY 11794
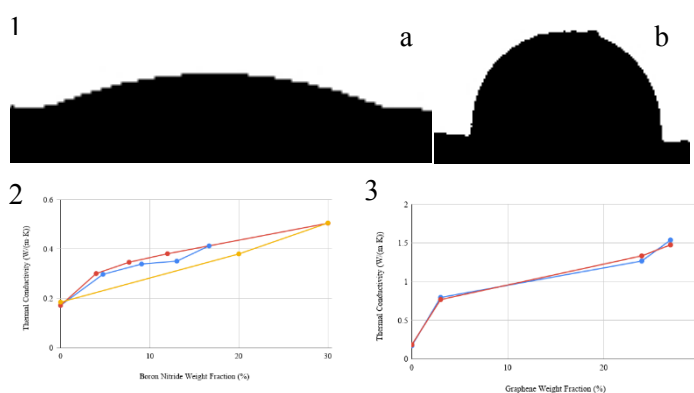
Thermal management is critical to the continually growing electronics industry to prevent devices from overheating and losing their functionality. As low-cost, lightweight, and highly versatile materials, polymers exhibit great potential for heat exchange applications, but their low thermal conductivity is a barrier to their effectiveness.[1] To overcome this obstacle, we can supplement polymers with thermally conductive fillers such as graphene and boron nitride.

In this project, we investigated the thermal conductivity of loading blends of PLA (polylactic acid) and PBAT (polybutylene adipate terephthalate) with graphene and hexagonal boron nitride (hBN). Graphene and hBN have thermal conductivities of approximately 5300 $W \cdot m^{-1} \cdot K^{-1}$ and 360 $W \cdot m^{-1} \cdot K^{-1}$, respectively.[2,3] We hypothesized that the thermal conductivity of the PLA/PBAT nanocomposite would be elevated compared to the thermal conductivity of the PLA/PBAT blend without the fillers. We also hypothesized that, since graphene had a greater thermal conductivity than hBN, the thermal conductivity would increase directly with the graphene-boron nitride ratio within the PLA/PBAT nanocomposite.

The CAM 200 Optical Contact Meter was first used to measure the contact angle between polymer droplets on hBN and graphene layers deposited on a silicon wafers to determine the polymers' relative affinities for the fillers. A twin-screw extruder (C.W. Brabender Intelli-Torque Plasti-Corder®) was used to melt-mix PLA (NatureWorks Ingeo™ Biopolymer 4043D) and PBAT (ecoflex® F Blend C1200) with varying concentrations of hBN powder (Sigma-Aldrich®, ~1 μm) and graphene nanoplatelets (xGnP®, Grade H, 5 μm). We first tested PLA/PBAT and PBAT blends with hBN alone. Seeing a slow increase in thermal conductivity with increasing weight fraction of hBN, we added the graphene to see if graphene-hBN interactions would lead to greater improvements in thermal conductivity. Then, the samples were molded with a hot press (Carver Model C) set at 180℃ and 7 psi. The thermal conductivities of the specimen were tested using the Anter Unitherm Model 2022 (ASTM E1530).

Fig. 1: Contact angle: (a) PBAT on hBN layer (b) PLA on hBN layer. PBAT had a 12.60° contact angle, and PLA had a 71.62° contact angle. PBAT also had a greater work of adhesion and thus a greater affinity for hBN.

Fig. 2: Plot of thermal conductivity versus hBN weight fraction in polymer nanocomposites (red: PLA/PBAT in a 1:3 ratio; blue: PLA/PBAT in a 7:3 ratio; yellow: PBAT only).

Fig. 3: Plot of thermal conductivity versus graphene weight fraction in polymer nanocomposites. Ratio of polymer to filler was held constant at 7:3. The ratio of PLA to PBAT was kept at 1:3 and the ratio of hBN to graphene varied from 1:9 to 9:1. 150 rpm, 200℃ for all. Thus, presence of graphene made a significant difference.

We discovered that adding the fillers did increase thermal conductivity. In addition, as the graphene content of the nanocomposite increased relative to the hBN content, the thermal conductivity increased as well.

For future research, we plan to conduct SEM and TEM imaging on our current samples to investigate how graphene and boron nitride interact within the PLA/PBAT blend. We also plan to investigate the mechanical properties of PLA/PBAT blends with graphene and boron nitride using impact and tensile strength tests. Ultimately, we hope to engineer a low-cost, biodegradable polymer nanocomposite with applications in the electronics industry.

[1] Huang, C., Qian, X., Yang, R. (2018). Thermal Conductivity of Polymers and Polymer Nanocomposites. *Materials Science*. Retrieved from journal URL.

[2] Balandin, A. A., et al. (2008). Superior Thermal Conductivity of Single-Layer Graphene. *Nano Lett.,* 8(3), pp. 902-907. DOI: 10.1021/nl0731872

[3]Jo, I. (2013). Thermal Conductivity and Phonon Transport in Suspended Few-Layer Hexagonal Boron Nitride. *Nano Lett.*, 13(2), pp. 550-554. DOI: 10.1021/nl304060

Creating Flame Retardant and Biodegradable Polymer Blends for Industrial Use

Albert Tian[1], Varun Jindal[1], Yuan Xue[2], Xianghao Zuo[2], Miriam Rafailovich[2]

1. Ward Melville High School, East Setauket, NY
2. Department of Material Science and Engineering, State University of New York at Stony Brook, Stony Brook, NY

White pollution remains an ever-present issue and points to the need for biodegradable polymers that can fit a variety of applications. PLA (Poly(lactic acid)) presents a solution: derived from renewable resources such as corn starch, cassava roots, and sugarcane, PLA has low production costs, exhibits biocompatibility and biodegradability, and still maintains comparable mechanical properties to other conventional polymers. However, due to its poor impact strength, PLA is not used for most industrial applications, but rather for packaging, bio-implants, and 3D printing. To increase impact strength, PLA is often mixed with flexible polymers such as PBAT[1] (polybutylene adipate terephthalate). To broaden its applications to electronics and automotive industries, PLA's flammability must be addressed.

We achieved V0 grade flame retardancy while maintaining and sometimes enhancing the mechanical properties of a PLA/PBAT blend using low RDP, APP and C-30B loading. Afterwards, we found the optimal settings for a 3D printer to maximize the mechanical properties.

As expected, the addition of PBAT to PLA enhanced the impact strength of the polymer blend (see Figure 1). However, addition of the flame retardants (APP, RDP) and compatibilizer (C-30B) reverted any mechanical advantage provided by the aforementioned PBAT addition. Alternatively, if the flame retardant blend is 3D printed with a vertical infill alignment, the impact strength increases by 15 J/m. We speculate the printing, as opposed to molding, creates a reinforced internal structure due to the directionality of the filament. Since the filament is aligned completely perpendicular to the direction of impact, there are no natural cleave lines in the sample.

Additionally, we notice while testing the tensile properties of our flame retardant blend, the printed samples tend to become fibrous under tension. However, the molded samples simply gain stretch marks and break cleanly. This can be easily seen through the tensile curves (see Figure 2 and 3). The printed sample has many jagged drops after the initial drop indicating how each large fiber breaks and passes on the stress to the next connecting fiber. In contrast, the molded sample has a much cleaner plastic deformation phase and breaks all at once.

Through the addition of PBAT, flame retardants (APP, RDP) and a compatibilizer (C-30B), the applications of PLA were successfully broadened. Not only is this blend flame retardant and thermoplastic, it is also biodegradable; it can be 3D printed and used in electronics all while representing a eco-friendly alternative to commercial plastics.
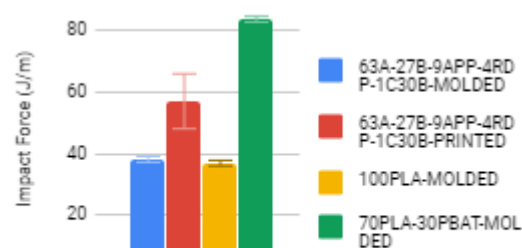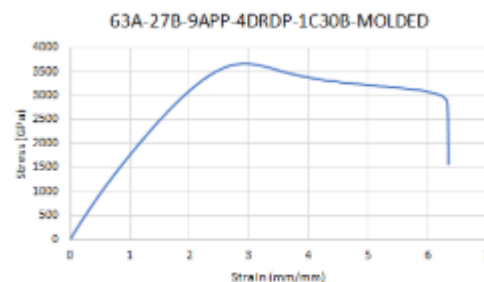

Figure 1: Comparison of Impact Strengths

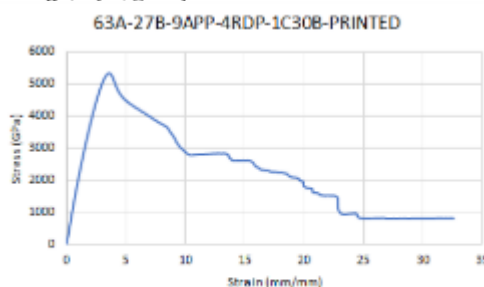Figure 2: Stress Vs. Strain graph for Molded Flame Retardant Sample

Figure 3: Stress Vs. Strain graph for Printed Flame Retardant Sample

1. Weng, Y.; Jin, Y.; Meng, Q.; Wang, L.; Zhang, M.; Wang, Y. Biodegradation Behavior of Poly(butylene dipate-coterephthalate) (PBAT), Poly(lactic acid) (PLA), and Their Blend Under Soil Conditions. Polym. Test. 2013,32,918−926

Session 8: Perovskite Solar Cells

Chairs:
Yuchen Zhou & Yifan Yin
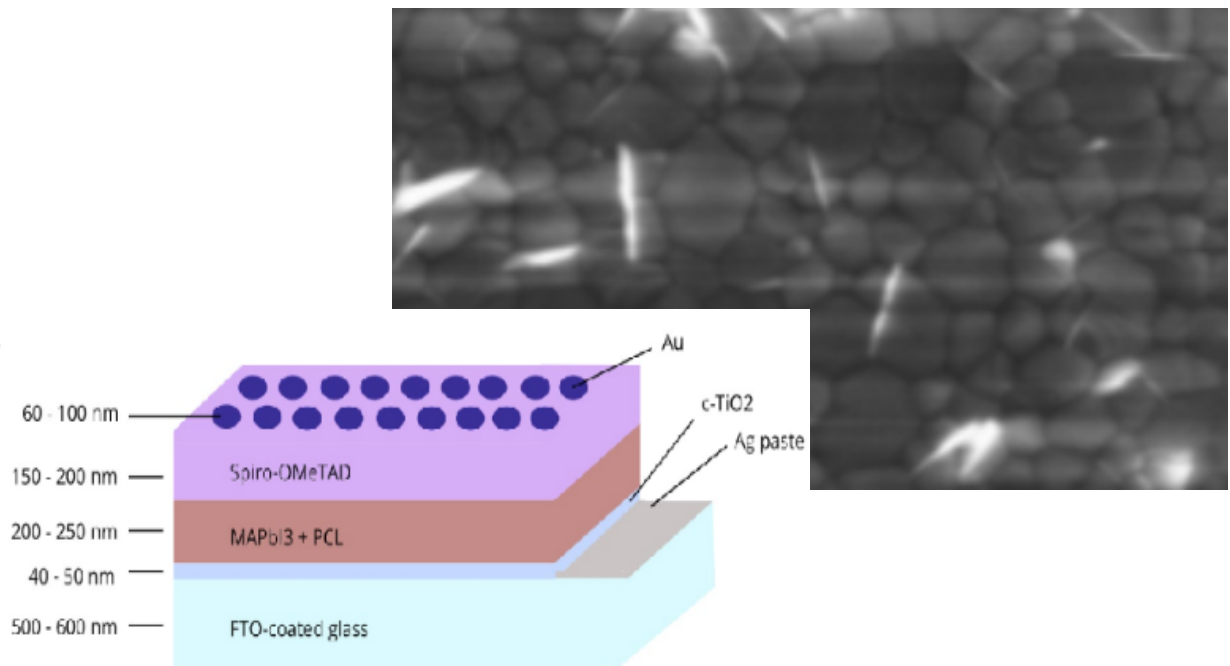
Optimization of Organic-Inorganic Halide Perovskite Solar Cells *via* a Novel Polycaprolactone Additive Pathway

Anisa Prasad[1], Sirina Prasad[1], Cecilia Orduña[2], Liana Lo[3], Yuchen Zhou[4], Yifan Yin[4], Miriam Rafailovich[4]

[1]Staples High School, Westport, CT 06880
[2]Columbia University, New York, NY 10027
[3]Cornell University, Ithaca, NY 14853
[4] Department of Materials Science and Engineering, Stony Brook University, Stony Brook, NY 11794

The recent global energy crisis has resulted in a push for the development and commercialization of renewable energy sources, most notably solar cells. In 2009, Kojima et. al. revolutionized the field of photovoltaics by synthesizing the first perovskite-based solar cell.[1] Perovskites are semiconducting materials with the crystal structure ABX_3 whose unique optoelectronic properties make them very suitable as the light-absorbing layer in photovoltaic devices. Previous research has shown that additives can optimize the perovskite crystallization rate, thus producing larger crystal grains and full coverage.[2] This results in a perovskite layer with fewer defects and a solar cell with a higher power conversion efficiency (PCE). This study investigates the effect of a biodegradable, environmentally-friendly polymer additive, polycaprolactone (PCL), on the performance of planar, thin-film methylammonium lead iodide ($MAPbI_3$) perovskite solar cells (PSCs).

Figure 1. Structure of PSCs fabricated in this study.

Planar, thin-film PSCs were fabricated with a FTO glass/TiO_2/PCL-doped $MAPbI_3$/spiro-OMeTAD/Au structure (Figure 1). The TiO_2, PCL-doped $MAPbI_3$, and spiro-OMeTAD layers were spin-coated, followed by PVD for the gold electrodes. To observe the effect of the additive on device performance, PCL/MAI/PbI_2 in dimethyl sulfoxide (DMSO)/γ-butyrolactone (GBL) precursor solutions were prepared with 5 different concentrations of PCL: 0.0, 0.1, 0.3, 0.6, and 1.0 mg/mL. UV-Visible Light (UV-Vis) spectrometry revealed comparable spectral shapes and absorption edges, indicating that doping PCL did not compromise the light-absorbing ability of the perovskite layer. Moreover, the PCL additive did not deform the crystal structure of the perovskite, as major peaks were seen in X-ray diffraction (XRD) graphs for all the samples.

The root mean square (RMS) values obtained from atomic force microscopy (AFM) data were much lower for higher concentrations of PCL, suggesting that the additive decreases surface roughness. To further characterize surface morphology, perovskite crystal sizes were compared using scanning electron microscopy (SEM) images. Distributions of grain size show that all films with the PCL additive exhibit much larger grain sizes, and thus fewer grain boundaries (GBs), than pure perovskite film (Figure 2). A smoother perovskite layer

	J_{sc} (mA/cm^2)	V_{oc} (V)	FF (%)	PCE (%)
$MAPbI_3$ without PCL	15.08	0.955	65.6	9.45
PCL, 0.1 mg/mL	18.25	1.015	57.7	10.7
PCL, 0.3 mg/mL	16.05	1.015	65.7	10.7
PCL, 0.6 mg/mL	14.10	1.015	63.1	9.03
PCL, 1.0 mg/mL	15.53	0.965	55.6	8.34

Table 1. J_{sc}, V_{oc}, FF, and PCE given by efficiency tests for each PSC device.

with fewer GBs facilitates the diffusion of excitons to their respective transport layers; thus, based on improved surface morphology, the PCL additive is expected to enhance PSC performance.

J-V curves and data from efficiency tests are shown in Figure 3 and Table 1, respectively. PSCs fabricated from perovskite precursor solutions with 0.1 and 0.3 mg/mL PCL exhibited the highest PCE of 10.7%. The peak in efficiency at lower concentrations of PCL and subsequent drop at higher concentrations suggest that while small amounts of additive enhance PCE, too much can decrease cell performance. The increase in PCE of cells with the novel PCL additive suggests its viability as a promising component of future, high-efficiency PSCs.
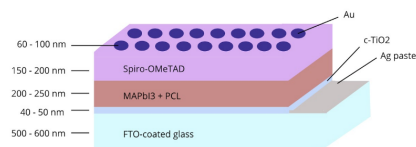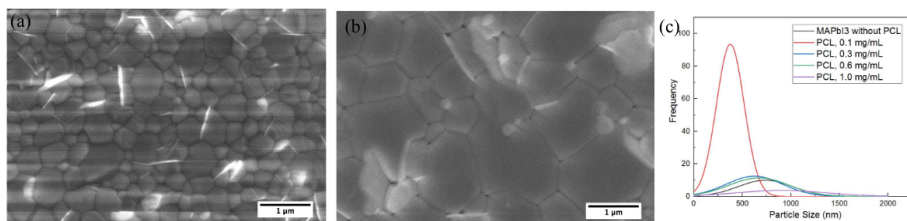

Figure 2. (a) SEM of pure $MAPbI_3$ layer. (b) SEM of $MAPbI_3$ film with 1.0 mg/mL PCL. (c) Distributions of particle sizes (nm) for $MAPbI_3$ films with different concentrations of PCL.
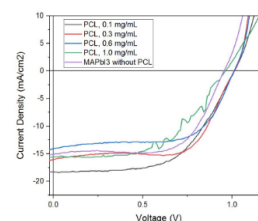
Figure 3. *J-V* curves for PSC devices fabricated.

[1] Kojima, A., Teshima, K., Shirai, Y., & Miyasaka, T. (2009). Organometal halide perovskites as visible-light sensitizers for photovoltaic cells. *Journal of the American Chemical Society*, *131*(17), 6050-6051. doi: 10.1021/ja809598r.

[2] Zuo, L., Guo, H., Jariwala, S., De Marco, N., Dong, S., DeBlock, R., ... & Yang, Y. (2017). Polymer-modified halide perovskite films for efficient and stable planar heterojunction solar cells. *Science advances*, *3*(8), e1700106.

Improvement of Perovskite Solar Cell Efficiency through Polylactic Acid Additive Induced Boundary Passivation

Thomas Chen[1], Aum Upadhyay[2], Byron Phan[3], Cecilia Orduña[4] , Liana Lo[5] , Yifan Yin[6] , Yuchen Zhou[6] , and Miriam Rafailovich[6]

[1]Mission San Jose High School, Fremont, CA USA [2]Interlake High School, Bellevue, WA USA [3]Hunter College High School, New York, NY USA [4] Columbia University, New York, NY USA [5] Cornell University, Ithaca, NY USA [6] Department of Materials Science and Engineering, Stony Brook University, Stony Brook, NY USA

In recent years, there has been an unprecedentedly large improvement the power conversion efficiency (PCE) of perovskite solar cells, which rivals that of established silicon and thin-film cells[1]. Perovskite solar cells have many advantages over established photovoltaic (PV) technologies, such as its low-cost, rapid manufacturing process and its exceptional optoelectronic properties: absorption, photoluminescence, & low charge-recombination rates[1, 2]. Perovskites are hybrid organic-inorganic metal halides with structural formula ABX_3, where A is an organic cation, B is an inorganic cation, and X is a halide anion[2].

In this research, polylactic acid (PLA) was added to the perovskite layer in hopes of improving PCE and perovskite film morphology. We hypothesize that its carbonyl functional groups will exhibit a weak interaction with ionic PbI_2 in solution. This would form a PLA-PbI_2 suspension which could lower the interfacial energy and passivate the crystal grain boundaries. By passivating the crystal grain boundaries the crystal areas could be increased, which reduces the defects in the perovskite layer and in turn increases the PCE.

The fluorine doped tin oxide glass was spin-coated with the TiO_2 precursor solution and then annealed. The perovskite solution was spin-coated in a 2 step process at 1000 and 5000 rpm. Chlorobenzene was added 3 to 4 seconds before the end of the perovskite spinning as an antisolvent to induce crystallization. The Spiro - OMeTAD was spin coated at a constant speed of 4000 rpm, and physical vapor deposition was used to add the gold electrodes. The final device is depicted in Figure 2. Scanning Electron Microscopy (SEM) was conducted to analyze the crystal grain sizes. The crystal sizes increased by up to 226% after the addition of PLA. Using a 2-sample T-test, both the 0.6 mg/mL 16K and 30K molecular weight PLA show a statistically significant increase in the crystal sizes at an alpha level 0.01 ($p < 0.00001$ for 16k, $p < 0.0001$ for 30k).
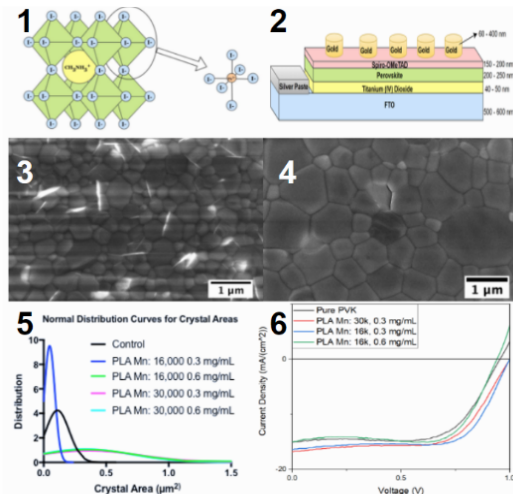
Since both molecular weights had a positive effect on the crystal size, the increase is likely due to an intrinsic chemical interaction between PLA and perovskite. Furthermore, bright spots on the SEM images, which indicate the presence of poor-conducting polymer-based aggregates, suggest an interaction at the interface of the crystals as seen in Figure 3. The increase in intensity of the peak at 15 degrees in the XRD data from the control indicates the presence of PbI_2 and PLA complexes. Finally, turbidness resulted in mixing the clear perovskite and PLA solutions, suggesting the formation of a complex. Yet, UV-Vis spectroscopy and XRD peaks at 14 degree and 28 degree indicate that the addition of PLA did not modify the crystal structure of the perovskite. This supports the hypothesis that the PLA-PbI_2 complexes may act as a surfactant between crystal grains. Furthermore, PLA additives significantly increased the PCE of the PV devices up to 17.5% using the 16K 0.3 mg/mL PLA additive. This is consistent with the unanimous increase in crystal sizes, which is correlated with improved efficiency as seen in Figures 4 and 5. The 16K 0.3 mg/mL devices showed the best PCE of 11.10%. This improvement is likely due to the increased charge transport caused by PLA-PbI_2 complexes passivations at the interfaces of crystal grains. The complexes passivate the crystal boundaries, decreasing exciton dissolution and trapping at the boundaries and redirecting exciton flow in the direction of the useful current. Finally, the improvement through adding PLA varies non monotonically with PLA concentration, suggesting that there is an optimal concentration to achieve maximum efficiency.

These results demonstrate that PLA additives are a promising method to improve the performance of the PV devices. They also give evidence for two mechanisms by which PLA achieves these positive effects: boundary passivation and crystal-interface surfactant.

Fig. 1 - Perovskite crystalline structure **Fig. 2 -** Solar cell architecture
Fig. 3 - SEM image of control **Fig. 4 -** SEM image of 30k 0.3 mg/mL
Fig. 5 - Normal distribution curve for crystal area **Fig. 6 -** J-V curves

[1] J.-P. Correa-Baena, A. Abate, M. Saliba, W. Tress, T. Jesper Jacobsson, M. Gratzel and A. Hagfeldt, Energy Environ. Sci., 2017, 10, 710–727

[2] Zhou, H., Chen, Q., Li, G., Luo, S., Song, T., Duan, H., . . . Yang, Y. (2014). Interface engineering of highly efficient perovskite solar cells. Science, 345(6196), 542-546. doi:10.1126/science.1254050

Session 9:
3D Printing

Chairs:
Yuval Shmueli & Zhuolin Xia
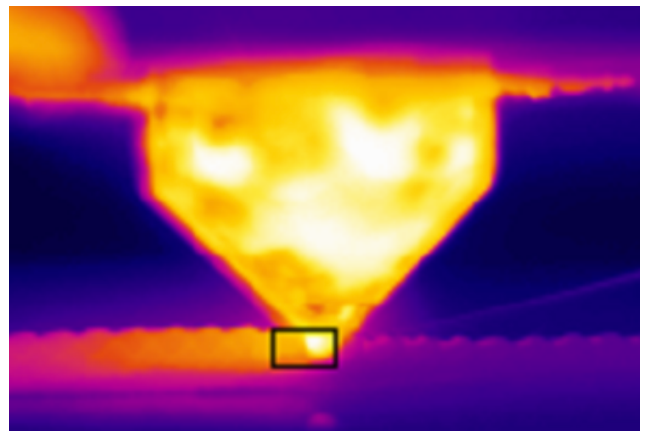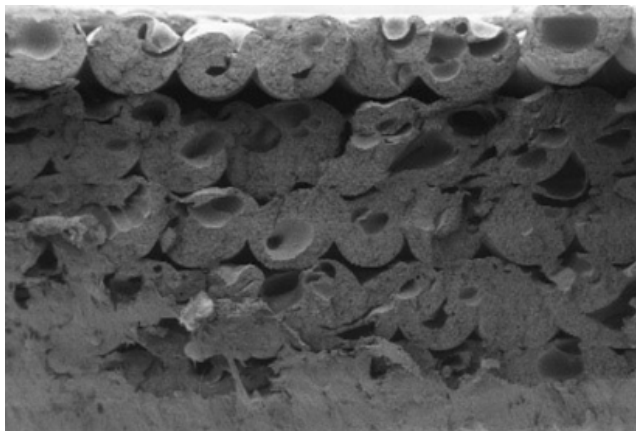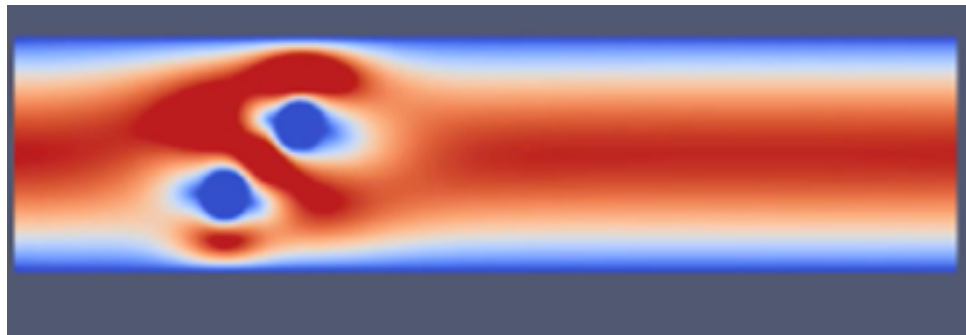
Characterization of Electrical and Mechanical Properties of Thermoplastic Poly(Lactic Acid) Filaments Infused with Graphene Nanoplatelets through Fused Deposition Modeling Techniques

Xiaoxin Wang[1], Steven Wu[2], Derek Zheng[3], Matthew York[4], Ahmed Shata[5], Yuval Shmueli[5], Miriam Rafailovich[5]

[1]Padua Franciscan High School, Parma, OH 44134; [2]Clear Lake High School, Houston, TX 77062; [3]Monta Vista High School, Cupertino, CA 95014; [4]Case Western Reserve University, Cleveland, OH 44106; [5]Department of Material Science and Engineering, State University of New York at Stony Brook, Stony Brook, NY 11794

Additive manufacturing through fused deposition modeling (FDM), the most common method of 3D printing, has become a significant manufacturing technology utilized in a wide variety of fields, from engineering to biomedicine. Current 3D printing filaments are commonly composed of poly(lactic acid) (PLA), a biodegradable material synthesized from plant matter that suffers from poor thermal diffusion [1], resulting in structurally weak prints. Recent studies on graphene have revealed its high mechanical strength and useful thermal and electrical conductivity properties. Graphene, when infused in 3D prints, can form an improved high tensile strength conductive polymer with increased structural integrity and application to modern electronics [2]. This study focuses on incorporating graphene nanoplatelets (GNP) within PLA filaments across various concentrations in order to characterize their effects on thermal diffusion, porosity, mechanical strength, and electrical conductivity, all of which can influence the structural integrity and characteristics of a 3D printed product.

To determine optimal conditions for thermal diffusion between filaments, rectangular lattice samples with concentrations of 0%-10% GNP were printed with interfilament widths (IFW) of 0.4 mm-0.5 mm with nozzle extrusion temperatures (NET) of 200°C-245°C on the Lulzbot Mini and Ultimaker 2 Extended+ FDM printers. A FLIR A300C thermal camera recorded thermal diffusion and cooling time to T_g (~65°C) during the printing process (Fig. 1), which was corroborated with Scanning Electron Microscope (SEM) imagery of lattice cross sections. Thermal diffusion was generally optimized at 230°C NET, 10% GNP, and 0.4 mm IFW (Fig. 2-4). 245°C NET tended to cool faster than 230°C due to the larger temperature disparity between the print and the surrounding air. SEM imagery revealed that the graphene platelets were oriented in the same direction as the printed filament, allowing heat to transfer quickly lengthwise within the core of the filament and retaining heat for a longer period of time, explaining why higher grap hene concentrations improved thermal diffusion. Smaller IFWs minimized voids, surface area for heat diffusion into air, and distances for diffusion between filaments.

Fig. 1. Thermal imagery of lattices during printing process

Future studies will utilize small angle X-ray scattering to further characterize the relationship between thermal diffusion and crystallinity of GNP lattices. Circuits of 10%-20% GNP will be printed to study electrical conductivity, and 3-point bending tests will be conducted on samples to study the effect of thermal diffusion and filament composition on mechanical strength. Experimentation will also be continued with boron nitride, another promising material similar in structure to graphene, infused as a nanocomposite with PLA to characterize its applications in 3D printing.
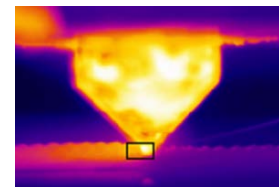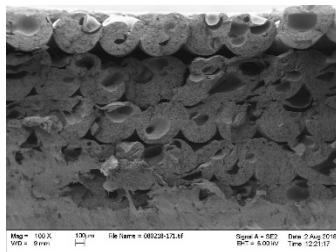

Fig. 2: SEM image of poor diffusion between filaments (0.5mm IFW/5% Graphene/230°C NET)
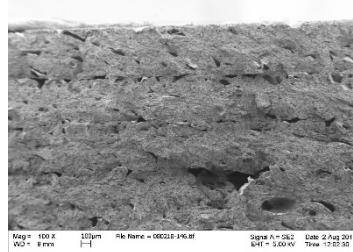

Fig. 3: SEM image of improved diffusion between filaments (0.4mm IFW/10% Graphene/230°C NET)
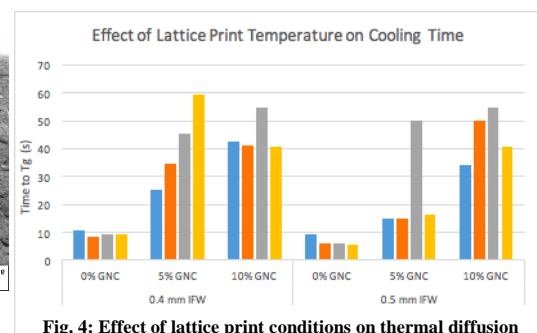

Fig. 4: Effect of lattice print conditions on thermal diffusion

[1] Garlotta, D. (2001). A Literature Review of Poly(Lactic Acid). *Journal of Polymers and the Environment,9*(2), 63-84. Retrieved August 5, 2018.

[2] "Graphene - Material Information." *Information about Nanomaterials and Their Safety Assessment,* www.nanopartikel.info/en/nanoinfo/materials/graphene/material-information#literatur. Accessed 5 Aug. 2018.

Evaluating the Effects of Material Composition on Molded and 3D Printed Samples

Vedant Singh[1], **Daniel Chao**[2], **Matthew York**[3], **Yuval Shmueli**[4], **Miriam Rafailovich**[4]

[1]The Wheatley School, Old Westbury, NY 11568, [2]Hunter College High School, New York, NY 10128, [3]Case Western Reserve University, Cleveland, OH 44106, [4]Department of Materials Science and Engineering, Stony Brook University, Stony Brook, NY 11790

Poly(propylene) is currently a topic of interest in the 3D printing world -- with better mechanical and thermal properties than the leading filament material, Poly(lactic acid), its difficulty to print due to its semi-crystalline nature holds it back from being used more often.[1] poly(propylene) is currently used in living hinges, chairs, electrical packaging, batteries, and textiles due to its chemical resistance, elasticity, and toughness, which further demonstrates its potential in 3D printing.

3D printing has shown to create well-defined structures that could be key in improving the thermal properties of a polymer relative to molded polymers, but a point of interest is improving the thermal, mechanical, and electrical properties of said structures to allow for easier and a greater range of uses. One property that might have an effect on these is the orientation of the filaments in 3D printed samples. With each of their proven abilities to conduct heat and electricity, graphene and boron nitride may also amplify the thermal and electrical conductivity or mechanical strength when mixed with poly(propylene), allowing for easier printing and more uses for 3D printed products.
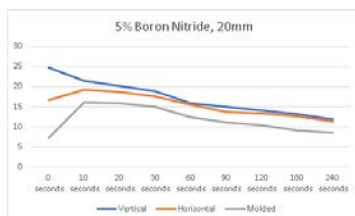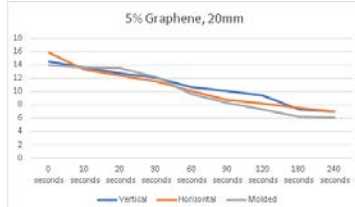

Figure 1) Temperature Difference for 5% B-N

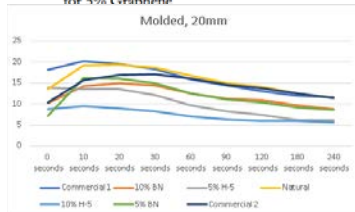Figure 2) Temperature Difference for 5% Graphene

Figure 3) Temperature Difference for Molded Samples

5% and 10% mixtures of graphene and boron nitride with polypropylene, as well as Ultimaker NFC manufactured polypropylene and pure poly(propylene) filaments were used to create samples. For each compositions, three differently-oriented samples were made: one with filaments running vertically through the sample, one with filaments running horizontally, and one that was molded. The Lulzbot Mini printer was used to create the 3D printed samples with a 10mm by 5mm base and a 10mm height with a .4mm filament. The hot press was used at 390°F and with 11,000 pounds of pressure to melt pellets of each material into a mold. The prisms were then placed onto a 100°C stage and recorded using a FLIR A300C thermal camera. The temperature was observed from 0 cm, 2 cm, and 4 cm from the bottom of the sample using the Research IR software. The difference was calculated between the 0 cm and 2 cm positions and the 0 cm and 4 cm positions to give a measurement of thermal conductivity.

In Figure 1, the different orientations of the 5% boron nitride affected the thermal conductivity of the samples. The printed versions of the sample had negative effects on the thermal conductivity, as it slowed down the transfer of heat to the top of the sample, leading to larger differences in temperature. Among the printed samples, horizontal samples allowed for quicker heat transfer than the vertical samples.

Similarly, in Figure 2, the 5% graphene samples follow a similar trend. All three samples began with similar temperature differences between the bottom and 20mm above the bottom, but by the end the molded sample had a noticeably smaller temperature difference, while the horizontally and vertically printed samples ended up with similar results.

Finally, Figure 3 shows a comparison of the thermal conductivity of different composites -- it can be seen that 10% graphene has a noticeably stable temperature difference, staying lower than all of the other samples at all times past the start. Following 10% graphene is 5% graphene, ending up with a slightly higher temperature difference, but getting there at a slower rate. 5% and 10% BN are shown to have better thermal conductivity than pure poly(propylene) -- both commercial and manufactured, but not be as conductive as graphene.

[1] Garlotta, D. (2001). A Literature Review of Poly(Lactic Acid). *Journal of Polymers and the Environment,9*(2), 63-84. Retrieved August 5, 2018.

[2] "Graphene - Material Information." *Information about Nanomaterials and Their Safety Assessment,* www.nanopartikel.info/en/nanoinfo/materials/graphene/material-information#literatur. Accessed 5 Aug. 2018.

Optimizing 3D Printing of PLA Filaments through Lattice-Boltzmann Modeling and Graphene Nanocomposite Integration

Lan Jiang[1], Caroline Zeng[2], Zhuolin Xia[3], Yuval Shmueli[3], Dilip Gersappe[3]

[1]University High School, Irvine, CA 92612

[2]Wayzata High School, Plymouth, MN 55446

[3]Department of Materials Science and Engineering, Stony Brook, NY 11790

As a rapidly expanding field, 3D-printing technology has several applications ranging from personal prototyping to industrial manufacturing. Optimal filament composition increases filament fusion, which creates stronger structures and decreases printing time[1]. Graphene nanocomposites are a promising material to incorporate in 3D printing due to high thermal conductivity and chemically stable configurations. In addition, modeling is more efficient than traditional lab techniques for running and visualizing combinations of various material compositions[2]. The objective of this study was to derive methodologies to determine optimal strength and efficiency in 3D printing fusion through modeling the effects of graphene molecules on heat diffusion and welding in the polylactic acid (PLA) filaments.
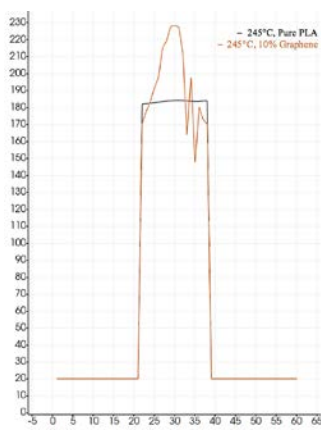

Figure 1: Advection density along position of simulated pure PLA and 10% graphene filament junctions at 245°C

Modeling techniques from Lattice Boltzmann, a class of computational fluid dynamics methods for fluid dynamics, were derived in the C++ based software Palabos v2.0 and visualized in Paraview. The general approach of this study was split into two phases: the first focused upon modeling graphene's effects on fusion through manipulating coded parameters only. In contrast to polypropylene, PLA has poor crystallization and melts/fuses with greater consistency, making modeling through parameter manipulation an accurate method. This approach is simple in that the graphene effects can be directly modeled through changing relaxation coefficients, thus resulting in faster simulation generation because of minimal requirements for computational power. Upon plotting the advection density of the pure PLA and 10% graphene simulations against the length of filament junctions, graphene incorporation proved to increase heat diffusion (Figure 1).

The second phase involved modeling graphene's effects through creating actual particles in the fluid flow simulation. This simulation is ultimately more accurate than phase one, but required novel coding techniques to create first simulation of multiple particles moving in a streamlined process through a fluid (Figure 2). Currently, the simulation is successful for two graphene particles, but in future directions, techniques for simulating more particles will be explored.
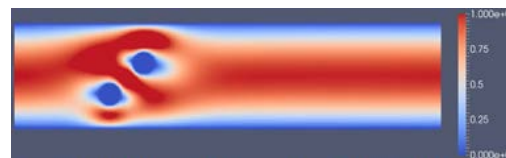

Figure 2: Simulation of multiple graphene particles in PLA filament

Ultimately, this study determined graphene is a promising material for improving filament fusion and created a novel technique in particle-fluid flow simulation through successful modeling of multiple 3D printing processes involving graphene nanocomposite incorporation.

---

[1] Seppala, J. E., & Migler, K. D. (2016). Infrared thermography of welding zones produced by polymer extrusion additive manufacturing. *Additive Manufacturing,12*, 71-76. doi:10.1016/j.addma.2016.06.007

[2] Thürey, N., & Rüde, U. (2005). Optimized free surface fluids on adaptive grids with the lattice Boltzmann method. *ACM SIGGRAPH 2005 Posters on - SIGGRAPH 05*. doi:10.1145/1186954.1187082

[1] Garlotta, D. (2001). A Literature Review of Poly(Lactic Acid). *Journal of Polymers and the Environment,9*(2), 63-84. Retrieved August 5, 2018.

[2] "Graphene - Material Information." *Information about Nanomaterials and Their Safety Assessment*, www.nanopartikel.info/en/nanoinfo/materials/graphene/material-information#literatur. Accessed 5 Aug. 2018.

Support from the Morin Foundation Trust and
the National Science Foundation is gratefully acknowledged